McGill University

Particle flow visualization in hydrocyclones using the Positron Emission Particle Tracking Technique

Jennifer Radman

260188597

Department of Mining and Materials Engineering

McGill University

Montréal, Québec

Canada

April 2014

A thesis submitted to McGill University

in partial fulfillment of the requirements of the degree of

Master of Engineering

Abstract

The technique of Positron Emission Particle Tracking (PEPT), developed at University of Birmingham in the late 1980s has become a powerful tool to track particles flowing in various industrial engineering applications. Hydrocyclones are extensively used in a widespread amount of applications for many industries, but are predominantly used in closed circuit grinding operations as classifiers in mineral processing. Many attempts have been made to capture the key relationships between hydrocyclone operating and geometrical variables in models, but hydrocyclone characterization is still heavily empirical and on a case-by-case basis. Due to their simplistic design, easy operation, low cost and maintenance, hydrocyclones have gained a widespread positive reputation for solid-liquid separations. Despite their wide use and long history in industry, the internal flow field of the hydrocyclone is complex in nature and remains a challenge to visualize under standard operating conditions. The work presented in this thesis project has looked at the feasibility and potential of PEPT to examine the flow in hydrocyclones. This study presents views of the real-time particle motion within small diameter hydrocyclones by PEPT. There is a need to develop a visualization method by which the velocity distributions can be quantified under realistic industrial conditions. Therefore, this thesis project will give an overview on current hydrocyclone flow field theory, and presents the experimental results of particle flow visualization inside two inch standard and stub hydrocyclones using PEPT under water and water-silica conditions.

Resumé

La technique de localisation des particules par l'émission de positons (PEPT), développée à l'université de Birmingham dans les années 1980s, est un outil puissant dans diverses applications de génie industriel. Les hydrocyclones sont largement utilisés dans une quantité répandue des applications pour de nombreuses industries, mais sont principalement utilisés dans les opérations de broyage en circuit fermé de classification dans le traitement des minerais. De nombreuses tentatives ont été faites pour capturer les relations clés entre hydrocyclone des variables géométriques et fonctionnement mais la caractérisation de l'hydrocyclone est encore largement empirique et au cas par cas. En raison de leur conception simpliste, l'opération facile et faible coût de maintenance, les hydrocyclones ont acquis une bonne réputation répandue pour les séparations solide-liquide. Malgré leur large utilisation et longue histoire dans l'industrie, le champ d'écoulement interne de l'hydrocyclone est de nature complexe et demeure un défi de visualiser dans des conditions d'utilisation normales. Les travaux présentés dans ce projet se sont penché sur la faisabilité et le potentiel de PEPT d'examiner le movement fluide des hydrocyclones. Cette étude présente le mouvement des particules en temps réel de petits hydrocyclones par PEPT. Il est nécessaire de développer une méthode de visualisation par lequel les distributions de vitesse peuvent être quantifiées dans des conditions industrielles réelles. Par conséquent, ce projet donnera un aperçu sur la théorie du champ d'écoulement de l'hydrocyclone actuel et présente les résultats expérimentaux de visualisation de movement de particules à l'intérieur de hydrocyclones en utilisant PEPT pour deux conditions : l'eau et la silice en suspension.

Thesis Contributions

The following work was presented at the Physical Separation 2013 conference in Falmouth, England:

1. J. Radman, R. Langlois, T. Leadbeater, J. Finch, N. A. Rowson, and K. Waters, "Particle flow visualization in silica slurry inside a hydrocyclone using the positron emission particle tracking technique," *Manuscript submitted for publication,* 2013.

In all the work presented in this thesis, the author has conducted all the analysis and characterization as well as prepared the manuscript drafts. In all studies, the University of Birmingham's School of Physics and Astronomy positron camera was used under the direction of Thomas Leadbeater and the University of Birmingham's School of Chemical Engineering hydrocyclone rig was used with the discretion of Prof. Neil Rowson. In the water study, the author has conducted all the experiments and materials production. In the silica slurry study, the author was assisted by Raymond Langlois for the positron emission particle tracking (PEPT) experiment and material production. Finally, comprehensive supervision was offered by the supervisor, Professor Kristian Waters, and co-supervisor, Professor James Finch.

Acknowledgements

I would like to thank Prof. Kristian Waters, my thesis project supervisor, for his professional guidance and valuable support and to Prof. James Finch, my graduate project supervisor, for his useful and constructive recommendations on this project.

I would like to express my very great appreciation to Raymond Langlois and Dr. Thomas Leadbeater for their valuable and constructive suggestions during the planning and development of this research work. Their willingness to give their time so generously has been very much appreciated.

Thanks to the University of Birmingham's School of Physics and Astronomy who allowed me the opportunity to use their positron camera and the University of Birmingham's School of Chemical Engineering who lent their hydrocyclone for testing.

Special thanks to the McGill Chair in Mineral Processing who funded through the Natural Sciences and Engineering Research Council of Canada Collaborative Research and Development grant sponsored by Vale, Teck, Xstrata Process Support, Barrick Gold, Shell Canada, Corem, SGS Lakefield Research and Flottec; and through the Natural Sciences and Engineering Research Council of Canada Collaborative Research and Development grant sponsored by the AMIRA P9N project made this research project possible.

I wish to acknowledge the support provided by McGill University's mineral processing group with special thanks to Sarah Jung who offered unending encouragement.

I would extend my gratitude to my graduate seminar presentation group; Matthew Bohan, Paul Carriere, Thomas Feldmann, Abu Syed Kabir and Shirin Kaboli, their support and constructive criticism helped refine my thesis seminar presentation.

Special thanks are extended to the support and administration staff of McGill University's Materials Engineering, in particular Barbara Hanely and Teresa Zatylny, for whom I am eternally grateful for making my leave of absence transition seamless.

Thanks to Annie Brongel, my physiotherapist, without her I wouldn't be able to walk today.

A final thanks to my mom, Patricia Finnerty, my sister, Elaine Radman, best friends, Rhoda Sollazzo, Edith Mak and Theresa Lambert, and Beverly Conrad for their encouragement and support throughout my graduate degree.

Table of Contents

List of Figures

List of Tables

Glossary of Abbreviations

CFD: computational fluid dynamics

EIT: electrical impedance tomography

LDV: laser Doppler velocimetry

LOR: line of response

LZVV: locus of zero vertical velocity

PEPT: positron emission particle tracking

PIV: particle image velocimetry

UST: ultrasound tomography

1. Introduction

Liquid-solid separation, used in a wide range of industrial engineering activities, can be quantified by a group of unit operations comprising of the separation and subsequent removal and collection of solid particles from a liquid suspension. The separation of solid particles from an aqueous medium is achieved by the utilization of mechanical forces to induce fluid flow in a complex media such that an intrinsic knowledge of fluid mechanics, particle mechanics and material properties is crucial. Liquid-solids separation can be divided into four unit operations: filtration, sedimentation, centrifugation and hydrocyclones. This thesis project focuses on hydrocyclones.

Hydrocyclones are extensively used in a wide variety of applications for many industries but are predominantly used in closed circuit grinding operations as classifiers in mineral processing. Many attempts have been made to capture the key relationships between hydrocyclone operating and geometrical variables in models but hydrocyclone characterization is still heavily empirical and on a case-by-case basis. Hydrocyclones are characterized by grade efficiency, pressure drop, flow split and cut-size. These four parameters quantify hydrocyclone performance. Since the first patent in 1891, hydrocyclones have been used in mineral processing industry for more than one hundred and twenty years (Bretney, 1891). Yet, there were very few commercial installations in the mineral processing industry until their rise to dominance in 1950s. Prior to this date, hydrocyclones were only used for dewatering or de-sliming operations (Lynch and Rowland, 2005). Due to their simplistic design, easy operation, low cost and maintenance, they have become ubiquitous in mineral processing plants. The internal flow field of the hydrocyclone is, however, complex in nature and remains a challenge to visualize under standard operating conditions.

The understanding of the separation mechanisms that govern hydrocyclones is inherently linked to the velocity field, particle and fluid flow within the system such that it is crucial to increase the knowledge base of classical hydrocyclone theory. There have been countless laboratory and pilot plant studies on hydrocyclones (Bergström and Vomhoff, 2007; Bradley, 1965; Bradley and Pulling, 1959; Concha, 2007; Dabir and Petty, 1986; Jirun et al., 1990; Knowles et al., 1973; Kraipech et al., 2006; Lim et al., 2010a; Marins et al., 2010; Plitt, 1976; Silva et al., 2009; Williams et al., 1999). The majority cover experimental testing to optimize performance through an understanding of operating parameters and geometry design. The internal flow field of the hydrocyclone has been investigated with less fervor with respect to those studies. The analysis of the fluid and particle flow inside a hydrocyclone is complex, and fundamental understanding of particle flow is essential to optimize the design and the performance of hydrocyclones. Typically, analysis is based on an experimental investigation that involves the direct measurement of

performance parameters (cut-size, pressure drop, flow rate and grade efficiency). Despite the valuable data obtained, they do not provide enough information to identify separation mechanisms and problematic regions that can cause performance reduction. In order to gain a fundamental understanding of first principles inside hydrocyclones, information on the structure of the flow itself is required (e.g. velocity distributions, fluid/particle trajectories, etc.). Measurement of these properties in opaque systems has been challenging with current measurement techniques. There is a need to develop a visualization method by which the velocity distributions can be quantified under realistic industrial conditions. Birmingham University developed a unique way of following particles and flows in opaque fluids using PEPT.

The scope of applications in PEPT is quite diverse and has come a long way since its inception where PEPT was initially developed to measure particle flow pattern in industrial apparatus and process equipment used in the pharmaceutical industry and has since been utilized to quantitatively map a wide array of industrial apparatus and process equipment (Parker et al., 1993). The internal flow of the hydrocyclone is complex and remains a challenge to visualize under practical, i.e., opaque, conditions. PEPT has been successfully used to visualize flow in a number of unit operations. These include: mixing vessels (Barigou, 2004; Marigo et al., 2013); fluidised beds (Van de Velden et al., 2008); tumbling mills (Bbosa et al., 2011; Volkwyn et al., 2011); and more recently in flotation cells (Cole et al., 2010; Fan et al., 2009; Waters et al., 2008) and spiral concentrators (Waters et al., 2012). The strength of PEPT is that opaque systems can be investigated whereas previous tracking methods require direct visualisation of particles (Dabir and Petty, 1984b; Fisher and Flack, 2002; Hsieh and Rajamani, 1988b; Jirun et al., 1990; Lim et al., 2010b; Marins et al., 2010; Monredon et al., 1992). It is interesting to note that the majority of applications to date are in gas-phase-continuous systems rather than liquid-phase-continuous systems. The main challenge with liquid-phase-continuous systems is finding a tracer than does not lose its activity due to leaching into the liquid (Seville et al., 2009). Particle flow patterns are difficult to model computationally as little is known about convection of particles within industrial apparatus and process equipment, especially in opaque liquids and enclosed devices. Tracking a particle within a piece of equipment using PEPT yields knowledge of the particle flow pattern, the fraction of time spent by a particle at each point in the system, the average velocity of the particle, the history of the particle inside a target volume and the residence time distribution of the particle. PEPT can validate computational models as predictive tools by allowing a comparison between the numerical simulations with experimental data.

The work presented in this paper looks at the feasibility and potential of PEPT to study the flow in hydrocyclones. Recently Chang *et al.* reported the underflow trajectory of a single particle inside a hydrocyclone using PEPT (Chang et al., 2011). Their study neglected natural flow in a closed system as the resin particles were injected into the stream via a syringe before the feed inlet. Their analysis of a

stationary resin bead standard deviation with respect to its immersion in water offers no correlation to a high speed moving resin particle, as relative count rate is subject to change due to the camera's resolution. Their paper offers no comparison to high speed resin particles of the same size class. It's not reflective of the standard deviation of a moving resin particle. There is no standard deviation given for a high speed particle moving in the system of study. Their initial testing was of a stationary resin bead and their scope of their experiment was of a high speed resin bead. The study then analyzed the lines of response of a stationary particle and contrasted it to the standard deviation but did not cite the initial activity of the resin beads. The data given with respect to standard deviation yields predictable results as the stationary resin bead can yield a lower standard deviation with respect to increasing the number of lines of response that are chosen during the analysis of the camera data and it is not reflective of the overall accuracy of the data collection. The number of lines of response is an independent variable. The standard deviation with respect to relative position in the field of view of the camera does not offer insight to the moving particle's error as it only demonstrates that a stationary particle has the best resolution if placed at the center of the camera head. This is characteristic of positron camera's standard operating procedures (Hawkesworth et al., 1986) therefore offers no new information towards the error in the study of a moving particle inside a hydrocyclone. Only two passes were offered by Chang *et al.* with no mention of standard deviation between passes or average speed and residence time of the resin particles. The difference of this study to Chang *et al.* is a more rigorous study of particles moving through a small diameter hydrocyclone. While Chang *et al.* injected a resin bead particle into the feed inlet of a hydrocyclone and recorded its trajectory with PEPT, this paper tracks a silica particle in a silica system under a closed loop system. The tracer particle is of the same type of material as the rest of the system and enters the feed inlet without any preferential orientation as opposed to Chang *et al.*'s experimental runs. This thesis project focuses on the examination of the underflow velocity profiles of particles in a hydrocyclone which was neglected by the previous PEPT study. This project summarizes noteworthy experimental methods that were used to visualize the internal flow field of hydrocyclones, as well as an overview of current hydrocyclone flow field theory and the experimental results of particle flow visualization inside a hydrocyclone using PEPT under water and water-particulate conditions.

2. Literature Review

2.1. Introduction

The meteoric rise to dominance of hydrocyclones in liquid-separation only began in the 1950s despite the principles and design being documented for more than fifty years (Bretney, 1891; Lynch and Rowland, 2005). Prior to this era, rake and spiral classifiers monopolized liquid-solid separation but as high-capacity wet-grinding circuits in the mineral processing industry increased in demand, hydrocyclones became an attractive alternative to conventional classifiers previously used in industry at the time (Lynch and Rowland, 2005). The growing use of hydrocyclones in industry spurred investigations into the performance and separation mechanisms that govern hydrocyclones in order to construct predictive models. Applications in industry are two phase separation with water being the suspending medium. The most frequent uses of hydrocyclones include liquid clarification, slurry thickening, solids washing, solids classification by particle size, solids sorting according to density or particle shape, particle size measurement, separation of two immiscible liquids and degassing of liquids (Svarovsky, 2001). The separation mechanisms are inherently linked to hydrocyclone performance and are dependent on understanding the velocity field, particle and fluid flow within the system such that it is crucial to increase the knowledge base of classical hydrocyclone theory. Hydrocyclones are the undervalued unit operation in mineral processing as there isn't a fundamental baseline for a unifying hydrocyclone theory especially in heavy particle loading. Emphasis on study has lent heavily on performance rather than particle and flow interaction. This section gives an overview of hydrocyclone theory, a critical assessment on imaging techniques used to visualize and characterize flow patterns inside hydrocyclones and PEPT theory. The imaging techniques elaborated upon in this section are pitot tubes, photography, laser Doppler velocimetry (LDV), particle image velocimetry (PIV), electrical impedance tomography (EIT), X-ray, ultrasound tomography (UST) and positron emission particle tracking (PEPT).

2.2. Hydrocyclones

2.2.1. Introduction

Classification is defined as the process of separating a mixture containing particles of different sizes into two streams, one containing coarse particles and the other containing fine particles. Screens and cyclones are both classifiers but are governed by different principles. The focus of this paper is hydrocyclones; a branch of cyclones that deal with a liquid media. A simple conceptual model can be used to understand the operation of a classifier, e.g. a cyclone, where it is viewed as a two-step process.

First, there is the classification step that produces the two streams, overflow and underflow, and then the bypass step where some of the overflow stream is sent to the underflow (Wills and Napier-Munn, 2006). In theory, a perfect classification would be that all the coarse particles report to one stream, the underflow, while the fine particles would leave with the overflow. This does not happen in practice such that understanding the mechanisms that govern cyclone classification are important. Despite being used in industry since the 1930s, little is known on the actual process of cyclones. Modeling has been done but it is based largely on assumptions and specific criteria of a certain system (Coelho and Medronho, 1992; Hsieh and Rajamani, 1988a; Plitt, 1976; Rajamani and Milin, 1992; Schubert, 2010; Silva et al., 2009).

2.2.2. Fundamental governing principles

The hydrocyclone is a classifier. Separation occurs due to the difference in settling rates of particles differing in weight and size. In the case of hydrocyclones, the feed to a cyclone is slurry of liquid and particles typical in mineral processing. Due to the prevalence of water being the fluid medium, the liquid cyclone has become known as the “hydraulic cyclone” which has been abbreviated to "hydrocyclone" (Bradley, 1965). This project will use "hydrocyclone" to specify cyclones handling water slurries. The main components of a hydrocyclone are as follows (Figure 1):

a) inlet - creates a circular motion and directs the feed into the cyclone.
b) vortex finder - collects the fine particles at the top of the cyclone, which is called the overflow and typically most of the water exits with the overflow. The vortex finder extends into the cylindrical section to prevent the feed from short-circuiting to the overflow.
c) cylindrical section - where classification take place.
d) conical section - guides the coarse particles towards the bottom of the cyclone.
e) apex - discharges the coarse or heavy particles, which is called the underflow.

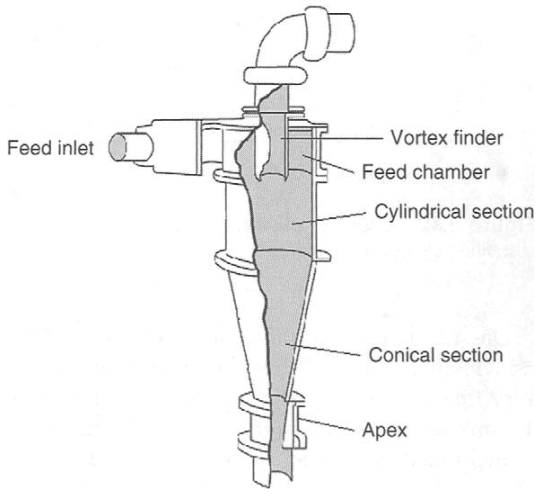

Figure 1: Hydrocyclone (Napier-Munn et al., 1996)

The hydrocyclone operates when water slurry under pressure enters tangentially from the inlet causing a swirling that generated a vortex in the cyclone itself. An air core develops along the axis of the cyclone (Bradley, 1965). A conventional hydrocyclone is a conically shaped vessel, open at its apex (or underflow) and is joined to a cylindrical section which has a tangential feed inlet. Hydrocyclones have the unique advantage over other classifiers as they have no moving internal parts. An external pump is required to transport the liquid suspension (slurry) to the hydrocyclone via the tangential feed inlet. The cylindrical section is closed off by a plate that has an axially mounted overflow pipe. The overflow pipe is extended into the cylindrical section by the vortex finder. The vortex finder mitigates the short-circuiting of the feed directly into the overflow. If the overflow is discharged at a point lower than the tangential feed inlet, a siphon can occur, causing a breakdown in the classification process itself, impairing the efficient operation of the hydrocyclone. In order to mitigate any siphon effect in the overflow, a vent pipe see Figure 2, is installed on top of the overflow pipe to open the system to atmospheric pressure (Trawinski, 1984).

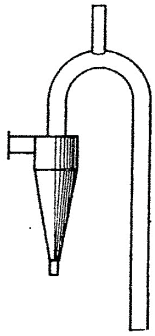

Figure 2: Overflow pipe elbow with vent pipe (Trawinski, 1984)

Liquid-solid separation in hydrocyclones relies on the principle that centrifugal force separates solids from the liquid medium by differences in density, shape and particle size. The feed enters tangentially to the hydrocyclone from the feed inlet under pressure with rotational motion setting up the primary outer vortex which flows downwards towards the apex. A secondary vortex is set up simultaneously rotating upwards into the overflow via the vortex finder. These two vortices make up the main flow pattern, see Figure 3.

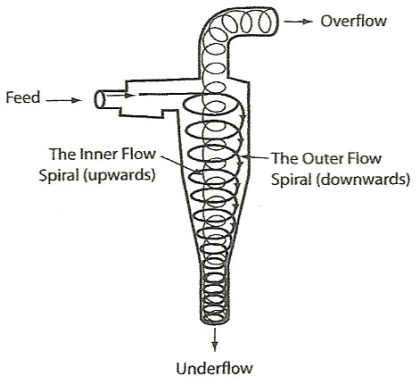

Figure 3: Schematic representation of the vortex flow inside a hydrocyclone (Napier-Munn et al., 1996)

The classical theory of hydrocyclone states that orbiting particles within the flow pattern are subjected to two opposing forces – an outward centrifugal force and an inward drag force, see Figure 4. The centrifugal force accelerates the settling rate or the particles such that it separates particles according to size, shape and density.

Figure 4: Forces acting on an orbiting particle in the hydrocyclone (Wills and Napier-Munn, 2006)

Faster settling particles will move towards the outer wall of the hydrocyclone where the velocity is lower and exit via the apex, while slower settling particles succumb to the action of the drag force which moves the particles towards the zone of low pressure along the hydrocyclone axis, and are carried up via the secondary vortex towards the vortex finder and subsequently the overflow pipe. The primary vortex then takes coarse particles to the underflow while the secondary vortex takes fine particles to the overflow where there is a continuous feed and two continuous discharges at or near atmospheric pressure.

2.2.3. Flow pattern

Knowledge of the flow pattern is essential for understanding functionality and optimizing performance and design. A short account of the flow pattern in cases of low solid concentrations is given in the following section. Classically, the hydrocyclone has a primary flow pattern comprising of an inner and outer region. The inner region is a forced vortex while the free vortex region is the outer region. The flow pattern in a hydrocyclone has a circular symmetry with the exception of the cylindrical region

surrounding the tangential feed inlet and overflow pipe (Svarovsky, 2001). The velocity of flow can be resolved into three components: the tangential velocity, the radial velocity and the axial velocity. It should be noted that the following is only a brief qualitative account to velocity profiles. The definitions of the three velocity components are derivatives of the accepted fundamental theories governing hydrocyclone flow. It would be remise not to note that hydrocyclone flow patterns are complex and still remains a source of great debate among experts. It may be incorrect to assume that hydrocyclones operating with varying geometry and higher slurry concentrations follow similar flow patterns. Measurement of the velocity distribution in a hydrocyclone is the primary step to predict the flow pattern.

Tangential velocity is responsible for creating the centrifugal force acting on particles inside the slurry inside a hydrocyclone. This is the foundation of hydrocyclone classification theory. The tangential velocity is responsible for the centrifugal force acting on particles. The radial velocity is low compared to tangential velocity. It is still debated whether the radial flow acts uniformly over the length of the hydrocyclone (from the feed inlet to the apex) or simply around the vortex finder (Bergström and Vomhoff, 2007). The axial velocity spans the entire length or the hydrocyclone from feed inlet to apex. Centrifugal force causes a net flow of solids towards the outer wall of the hydrocyclone, predominantly coarse particles compared to a net flow of liquid and fines towards the axis such that knowing the difference between these flows is important. The axial velocity shows the effect of both vortices, the primary one that reports to underflow and the secondary one that reports to the overflow. Understanding these axial flows can provide insight on separation mechanisms inside the hydrocyclone. Since there is an axial flow upwards and downwards, there must be a shear plane where there is no net velocity in the axial direction. In three dimensions, this shear plane becomes a Locus of Zero Vertical Velocity (LZVV) with respect to Cartesian coordinates, see Figure 5 (Holdich, 2002). The particles lying on the locus will be subjected to equal and opposing centrifugal and drag forces making them have an equal chance of reporting either to the underflow or overflow (Wills and Napier-Munn, 2006).

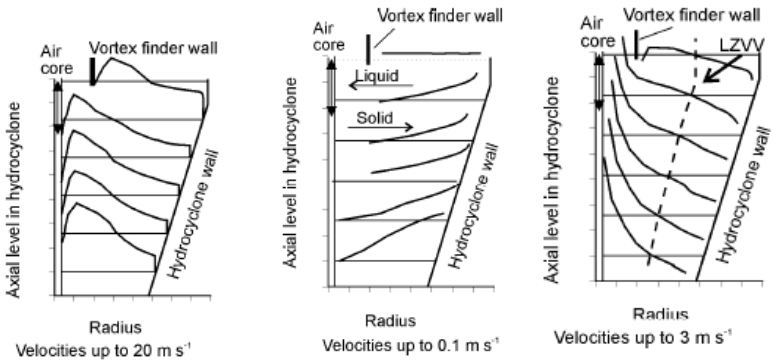

Figure 5: Velocities within the hydrocyclone (left to right: tangential, radial and axial) (Holdich, 2002)

2.2.3.1. Tangential velocity

The most frequently studied velocity component is the tangential velocity. Hydrocyclone theory supports the assumption that tangential velocity flow increases with a decrease in hydrocyclone radius. This can be expressed by the following empirical relationship

$$VR^n = \text{constant}$$

where V (m/s) is the tangential velocity, R (m) is the radius and n the empirical component (typically between 0.5 and 0.9) (Chiang et al., 2003). Tangential velocity and radius are proportional until the cylindrical air column (air core). Air cores form when a hydrocyclone discharges at atmospheric pressure (Svarovsky, 2001).

2.2.3.2. Axial velocity

The axial velocity is a strong downward flow in hydrocyclones operating vertically. This downward flow along the cylindrical and conical sections is paramount for hydrocyclone operation. The downward flow is counterbalanced by an upward flow in the air core region. The locus of zero vertical velocities is well documented inside the profile of the hydrocyclone (Svarovsky, 2001).

2.2.3.3. Radial velocity

The radial velocity is the smallest contributing velocity component. It is the most challenging to measure. Radial velocity is an inward flow towards the center of the hydrocyclone. It is at a maximum near the outer wall of the hydrocyclone and becomes negligible at the center near the air core as the radius decreases (Chiang et al., 2003). The location of zero radial velocity is unknown (Svarovsky, 2001).

2.2.3.4. Eddy flow

Near the rim of the vortex finder before it discharges to the overflow pipe towards the flat plate of the hydrocyclone, there are outward re-circulating eddy flows. These flows are characterized by strong inward radial velocities directed towards the vortex finder. This leads to a secondary flow pattern inside the hydrocyclone, the short circuit flow where the flow travels directly to the overflow (Svarovsky, 2001). Wall friction effects can give rise to non-tangential motion that causes other flow phenomena inside the hydrocyclone. At the top plate of the hydrocyclone surrounding the vortex finder, friction causes the tangential flow to slow down locally such that lower tangential velocities paired with the higher pressure far out in the hydrocyclone causes the short circuit flow. The short circuit flow will then pass from the feed inlet directly to the vortex finder. The re-circulating eddy flow can exist also on the outer radius of the vortex finder wall, see Figure 6 (Bradley, 1965). This impedes the separation efficiency of the hydrocyclone as the short circuit flow can account to 15% of the total feed flow (Chiang et al., 2003), this is somewhat mitigated by the overflow pipe.

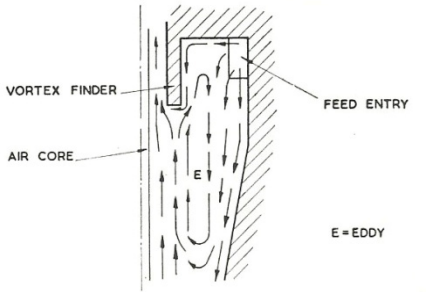

Figure 6: Depiction of the short circuit and eddy flows (Bradley and Pulling, 1959)

2.2.3.5. Natural vortex length

The primary outer vortex flow weakens and changes its direction at a certain axial distance from the vortex finder. This axial magnitude has been called the "natural vortex length" of the hydrocyclone, and the axial position is referred to as the "end of vortex". Below the natural vortex, particle separation and transport are less efficient (Alexander, 1949). Hydrocyclone designs with a natural length equal to or greater than the physical length of the hydrocyclone cyclone are advised as a rule of thumb for design considerations. Despite the natural vortex length having a relevant effect on overall hydrocyclone efficiency, there has been very little experimental work on the natural vortex length (Abrahamson and Allen, 1986; Qian and Zhang, 2005; Stairmand, 1951).

2.2.3.6. End of vortex

An interesting phenomenon of the flow has previously been observed near the apex of the hydrocyclone where the natural vortex would end before the apex. In 1949, work began on understanding this end of vortex phenomenon by investigating the natural length of the vortex inside gas cyclones (Alexander, 1949). The spontaneous end of the natural vortex flow inside has two possible explanations:

1) *vortex precession*: There is a change in the rotational axis of the core of the vortex causing it to bend towards the wall of the hydrocyclone and the end turns around the wall.
2) *vortex breakdown*: An expression of an axisymmetric phenomenon where flow reverses.

Despite the natural vortex ending, through precessing around the hydrocyclone wall or breakdown towards the apex, the axial vortex motion is not halted but the primary vortex actually induces a secondary vortex downstream of it. This is a type of fluid coupling. This downstream secondary vortex is not the same as the secondary vortex going to the vortex finder that we find at the top of the hydrocyclone. The induction of the secondary downstream vortex is probably related to the precession of the primary vortex. This precession is always in the same rotational sense as the swirl in the bulk of the vortex before exiting through the apex (Hoffmann and Stein, 2008). Alexander states that there would be a stagnant zone between the "end of vortex" and the apex as there is no direct expulsive force on the

separated particles which would cause settling of particles in the cone and thereby block the apex (Alexander, 1949).

2.2.4. Key operating factors affecting cyclone performance

The variables that affect the performance of the cyclone can be divided into two main groups: operations variables (feed percent solids, feed rate, feed pressure and the number of cyclones in operation) and design variables (apex size, vortex finder size, body size and inlet size). The following section will examine the four key operating factors that affect cyclone performance: cut-size, flow split, grade efficiency and pressure drop.

2.2.4.1. Cut-size

The most accepted method to represent cyclone efficiency is the partition curve (Figure 7). The partition curve relates the weight fraction of each particle size in the feed to the particle size distribution. The cut-size, d_{50}, is the point which 50% of the particles of this particular size will have an equal probability of going to the overflow or underflow. The sharper the curve, the higher the efficiency of the hydrocyclone (Wills and Napier-Munn, 2006).

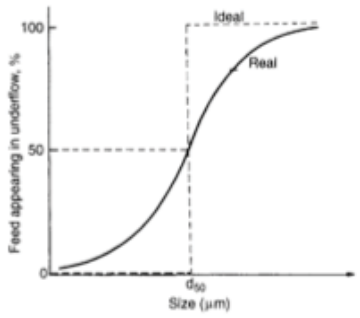

Figure 7: Partition curve for a hydrocyclone (Wills and Napier-Munn, 2006)

2.2.4.2. Flow split

Flow split, S, is the ratio of underflow to overflow. Flow split of water to the underflow will increase with larger apex sizes, smaller vortex-finders, increasing feed solids concentration and/or viscosity (Wills and Napier-Munn, 2006). It is hard to predict the actual flow of the hydrocyclones and it is often approximated leading to poor results of bad performance (Romero et al., 2004).

2.2.4.3. Grade efficiency

Grade efficiency is a function of particle size and defined as

$$G(x) = E\ dF_{su}(x)/dF_{sf}(x)$$

where $F_{su}(x)$ and $F_{sf}(x)$ are particle size distribution in underflow and particle size distribution in feed, respectively. E is the total efficiency, which is defined by

$$E = M_u/M_f$$

where M_u is the mass flow rate of particles in the underflow and M_f is the mass flow rate of particles in feed. In practice $F_{su}(x)$ and $F_{sf}(x)$ are unknown such that the actual functions are experimentally determined. Reduced grade efficiency is defined as

$$G'(x) = G(x) - R / 1 - R$$

where R is the underflow/feed ratio. This takes into account the fact that if no separation occurs, the efficiency will be zero. This is the effect of flow split (Figure 8). It has been observed that grade efficiency will increase with appropriate hydrocyclone size selection, limiting the water to the underflow and decrease with feed solids concentration and/or viscosity (Svarovsky, 1992; van Esch, 1991).

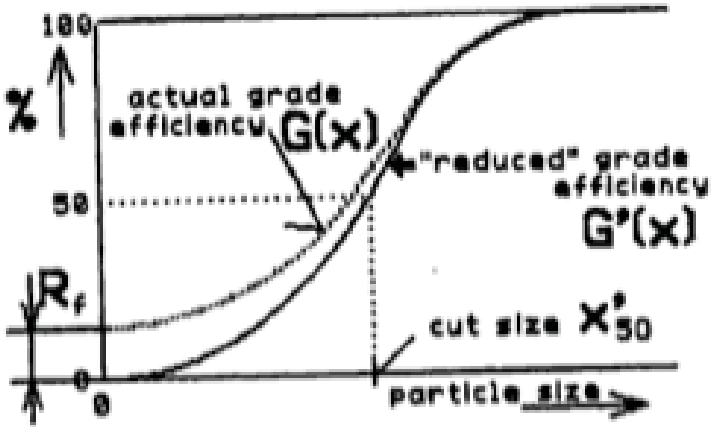

Figure 8: Grade efficiency curves for a hydrocyclone (Svarovsky, 1992)

2.2.4.4. Pressure drop

Pressure drop is defined as

$$C = \Delta P_u / \Delta P_d$$

which is the ratio between ΔP_u, upflow pressure drop and ΔP_d, downflow pressure (Jiang et al., 1998). It is an important factor as it the capacity of a hydrocyclone can be measured in terms of throughput which is dependent on pressure drop (Ortega-Rivas, 2000). Pressure drop is due to the tangential velocity as it drives the feed into suspension (Ortega-Rivas, 2000; Svarovsky, 1992).

2.2.5. Cyclone models

Empirical models are the main tool for cyclone design and optimization. A predictive model must incorporate all design and operating variables as well as engineering quantities (cut-size, efficiency, pressure drop and flow split) (Chen et al., 2000). Most models used to handle hydrocyclones are empirical

in nature and there are limitations such that there has been a great interest developing computational fluid dynamics (CFD) (Ba and Wang, 2006). Predictions using CFD have yielded comparable results with laboratory testing obtained using Laser Doppler Velocimetry (LDV) (Rajamani and Milin, 1992). As of yet there is no one model which comprehensively describes the operation of the hydrocyclone. A good model must involve the calculation of pressure drop, cut-size, grade efficiency and flow split. Most empirical models used are a combination of models, which describe a facet of cyclone operation. It is possible to select a combination of parameters that suit a particular hydrocyclone but will not be applicable to hydrocyclones in general or even one other hydrocyclone operation (Chen et al., 2000).

2.2.5.1. Empirical models

It is difficult to have a single standard model, however the models developed yield information allowing the estimation of hydrocyclone performance. The early modeling approaches were based on the assumption that cut-size was determined by the balance between centrifugal force and fluid drag (Napier-Munn et al., 1996). This assumption is known as the equilibrium orbit hypothesis and is not typically used in practice but allows a better visualization of the main effects in the hydrocyclone operation. The Lynch and Rao model was the first widely used empirical model (Coelho and Medronho, 1992; Napier-Munn et al., 1996; Svarovsky, 2001). All the models have empirical parameters such that they generally work well under a range of conditions in which the parameters were estimated. In industry, the models undergo calibration to fit a new operation. Feed properties (solids concentration and size distribution) can substantially affect hydrocyclone performance (cut-size). A successful empirical model is based on experience as most models are developed over a limited size range for hydrocyclones (Napier-Munn et al., 1996).

2.2.5.2. CFD modeling

CFD is a technique that is used to simulate the fluid flow in various flow modules, including hydrocyclones (Hwang et al., 2008). CFD modeling has been developed for certain types of cyclones as the flow can be calculated using commercial software which numerically solves the continuity and momentum equations of flows (Chu et al., 2009; Spelter and Nirschl, 2010). Modeling using CFD has become increasingly successful despite some variations between experimental data but it still remains a case-by-case model, which is reliant on experimental data.

2.2.6. Conclusions

The internal flow of the hydrocyclone is complex and remains a challenge to visualize under practical, i.e., opaque, conditions. Understanding the separation mechanism is inherently linked to the velocity field and particle and fluid flow within the hydrocyclone. Non-invasive real time imaging of particle flow inside the hydrocyclone that will resolve the flow patterns is required.

2.3. Flow imaging techniques

2.3.1. Introduction

When the velocity profiles in the hydrocyclone can be directly measured, more accurate predictive flow models can be developed from the extrapolated data. Flow imaging techniques should not be considered novel, as they have existed throughout history (Bradley and Pulling, 1959; Dabir and Petty, 1984a; Hsieh and Rajamani, 1988a; Jirun et al., 1990; Kelsall, 1952; Knowles et al., 1973). A comparison between the numerical simulations and experimental data is required, such that flow imaging techniques are used as tools to validate computational models. This section briefly introduces the current traditional methods that are being used to track flow patterns. In order to attain a better understanding, design and operation of engineering processes, visualization of the system is required. This becomes an issue in opaque systems. It is important to note that there is a fundamental distinction between (i) projection-imaging techniques, which the image is obtained by conventional photography, (ii) tomographic techniques, which the image is obtained of a slice through an object and (iii) particle tracking techniques, using radioactive tracers.

2.3.2. Pitot tubes

The pitot tube technique is based on the principle that when a flow is directed against an obstacle, it will be deflected towards the sides such that the flow pressure at the obstacle's tip will rise above the ambient pressure. Measuring this pressure difference, the flow velocity can be calculated using a simplified Bernoulli Equation (Mavros, 2001). Bergström et al. (Bergström et al., 2007) measured the tangential velocity flow field in a conical hydrocyclone operating with a unrefined bleached softwood kraft pulp fiber suspension using a self-cleaning pitometer (Figure 9), at different levels within the hydrocyclone (Figure 10).

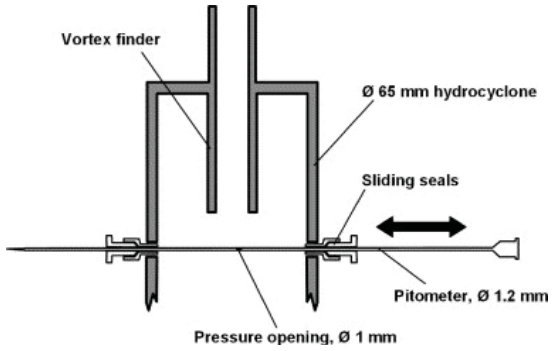

Figure 9: Pitometer in the 65 mm diameter hydrocyclone for fiber suspension testing (Bergström et al., 2007)

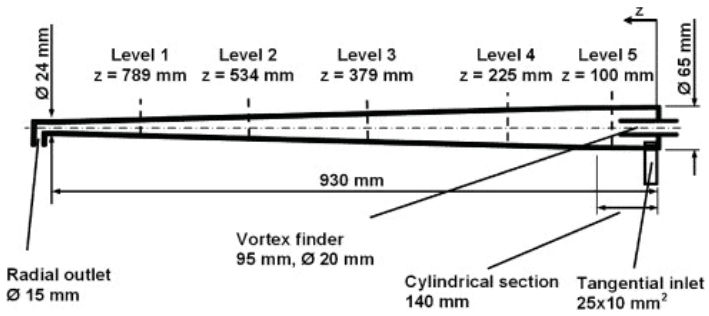

Figure 10: Measurement levels for 65 mm diameter hydrocyclone with pitometer (Bergström et al., 2007)

Figure 11 and Figure 12 show tangential velocity profile measurements obtained by the pitometer. Fibers had a strong influence on the velocity field such that it can be inferred that poor efficiencies seen in hydrocyclones at higher mass concentrations are caused by fibers influencing the velocity field by reducing centrifugal acceleration (Bergström et al., 2007). The radial acceleration profile and tangential rate-of-strain profile were determined as well. It is important to note that pitot tubes are intrusive to overall hydrocyclone operation, and while they offer a way to extrapolate velocity profiles they do alter the system they are used to investigate.

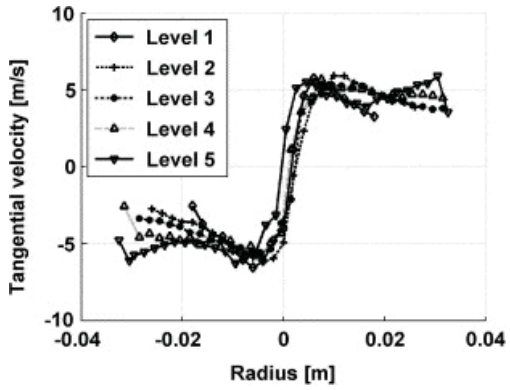

Figure 11: Tangential velocity profile measurements with pitometer of water (Bergström et al., 2007)

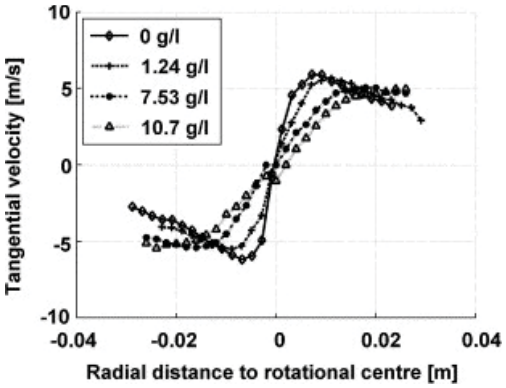

Figure 12: Tangential velocity profile measurements at 534 mm with varying solid concentrations (Bergström et al., 2007)

2.3.3. Photography

Photography encompasses methods using not only still frame imaging but also cinephotography where high speed cameras were used to investigate fluid and particle flow inside hydrocyclones. Cinephotography, as the name suggests is a catchall for techniques taking pictures of the vessel in question and mapping out circulation patterns. An improvement of this technique is streak lines where neutrally buoyant particles are dispersed into the liquid such that when still pictures are taken, their movement is seen as streamlines (Mavros, 2001). Kelsall used an optical method where ultramicroscope illumination and a microscope fitted with rotating objectives tracked the tangential velocity components of fine aluminium particles in the field of view surrounding the feed inlet and vortex finder of a 3 inch diameter hydrocyclone with varying tangential feed inlet diameters (Kelsall, 1952).

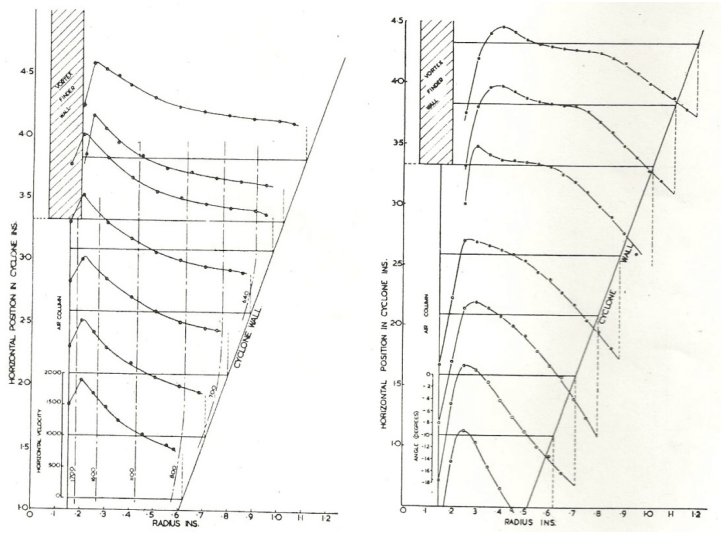

Figure 13: From left to right: Particle horizontal velocity vs. radius and particle axial velocity vs. radius all to underflow

Axial velocity components for the same tangential velocity components were obtained by measuring the angle of inclination between the horizontal and the particle tracks (Figure 13). Radial

velocity components were calculated for continuity but were not optically measured. Bradley and Pulling (Bradley and Pulling, 1959) took a sequence of photographs of dye injections into water flowing in transparent 3 inch diameter hydrocyclones to illustrate the water flow patterns inside (Figure 14).

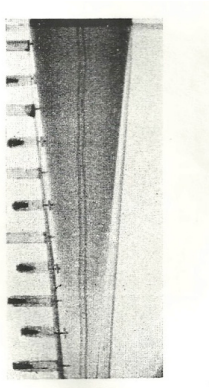

Figure 14: Dye injection in a 3 inch hydrocyclone illustrating the downward outer vortex (Bradley and Pulling, 1959)

Knowles recorded with a film camera the movement of anisole droplets in water (Knowles et al., 1973). Velocity profiles depicting the flow patterns near the vortex finder in a 3 inch glass hydrocyclone operating without an air core were generated from the testing. Figure 15 shows an undulating profile under the vortex finder can be attributed to re-circulating eddy flow in the cylindrical section of the hydrocyclone.

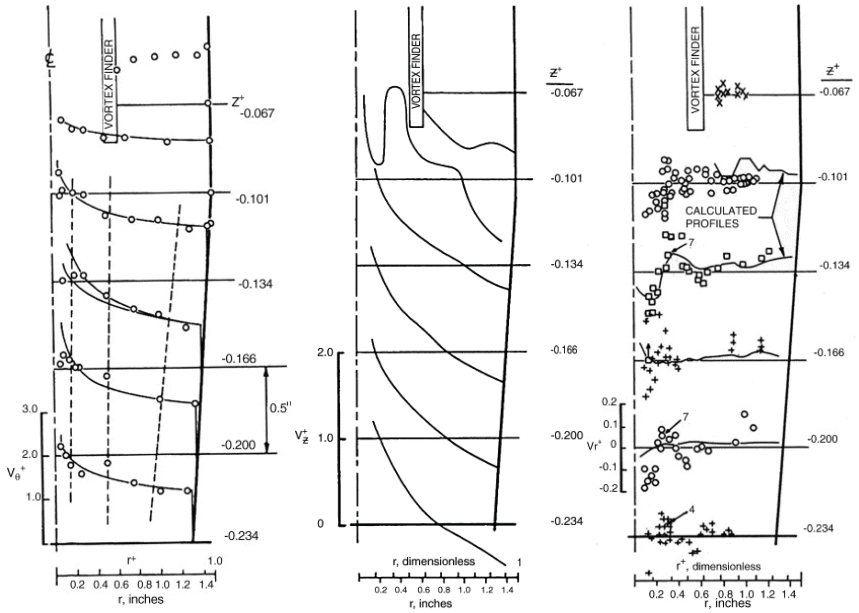

Figure 15: Velocity profiles of anisole droplets in a 3 inch hydrocyclone operating without an air core, from left to right: tangential, axial and calculated radial velocity components (Knowles et al., 1973)

2.3.4. Laser Doppler Anemometry

Laser Doppler Anemometry (LDA) synonymous with Laser Doppler Velocimetry (LDV) is a technique that does not interfere with the flow pattern as the probe lies outside the vessel being studied. A laser beam is split and the two resulting coherent beams are crossed at some point inside the vessel being studied such that in the intersection volume, parallel interference fringes are formed. When a particle crosses this volume, light is scattered and subsequently caught by a photodetector. Analysis of the change in the intensity fluctuations on the photodetector allows the velocity of the particle crossing the intersection volume to be determined (Mavros, 2001; Wang et al., 2006). LDA facilitates rapid investigation of the tangential velocity distribution of different hydrocyclone geometries. Dabir and Petty measured the tangential and axial velocity components of water in a 3 inch hydrocyclone using LDA operating without an air core (Dabir and Petty, 1984b; Dabir and Petty, 1986) (Figure 16).

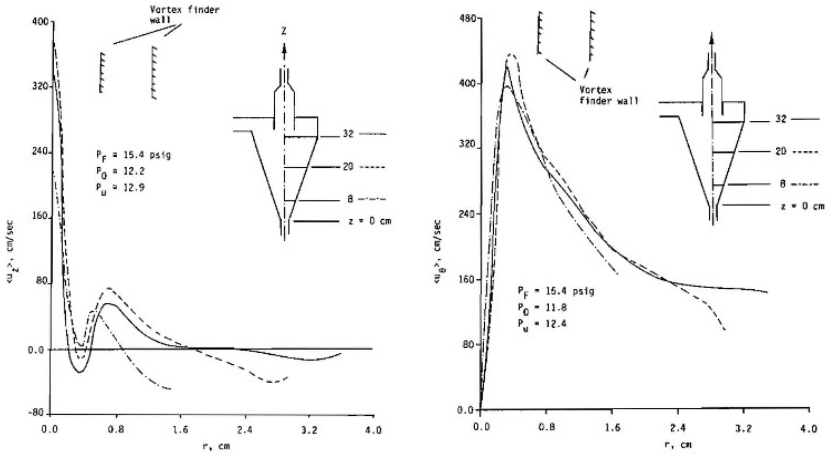

Figure 16: From left to right: Mean axial velocity profiles and mean tangential velocity profiles for 3 inch hydrocyclone (Dabir and Petty, 1986)

It is important to note that laser beam cannot directly pass through the air core to directly measure velocity as the laser beam is restricted to one medium for testing purposes. Therefore calibration is necessary or tests conducted without an air core (Fanglu and Wenzhen, 1987). Flow visualization by dye injection confirmed LDA measurements are shown in Figure 17.

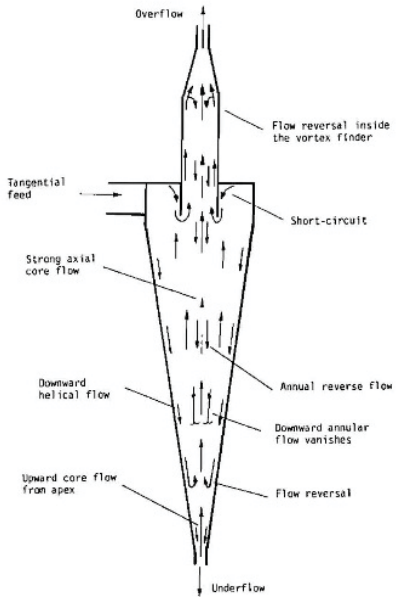

Figure 17: Flow patterns observed in 3 inch hydrocyclone using dye injection (Dabir and Petty, 1986)

Further studies were conducted to measure the tangential and axial velocity components by Fanglu and Wenzhen for water (Fanglu and Wenzhen, 1987), and by Monredon et al. for water and limestone suspensions (Monredon et al., 1992). Hsieh and Rajamani used 75 mm glass hydrocyclone to obtain axial and tangential velocity measurements with LDV in a water suspension with small silicon carbide powder to enrich the optics for data collection (Hsieh and Rajamani, 1988b). Radial velocity was calculated by solving continuity equations as the re-circulating eddy flows were too turbulent for direct calculations using LDV (Hsieh and Rajamani, 1988b).

2.3.5. Particle Image Velocimetry

Particle Image Velocimetry (PIV) is an extension of comparing two frames of the photographic recording of streaks of particles in a vessel. In the case of PIV, pictures of a plane cutting through a vessel are taken at short intervals with high light source illuminating the background. This requires a transparent liquid system. The displacement of each particle is recorded between shutter openings and yields a two-dimensional velocity (Mavros, 2001). Lim et al. used PIV to characterize the air core structure formation, pressure and velocity distributions of lightly seeded starch suspension, with an average particle diameter was about 47.4 micrometers (Lim et al., 2010b). Figure 18 highlights comparison of velocity vector fields obtained by PIV with those from computational fluid dynamic calculations.

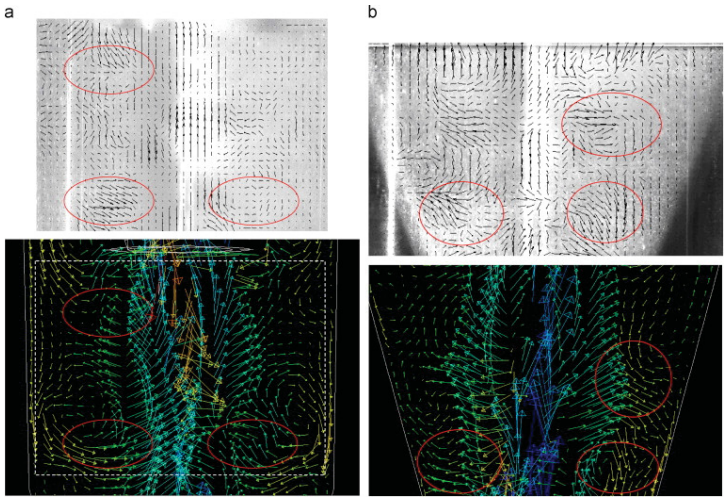

Figure 18: From top to bottom: comparisons of velocity vector fields from PIV measurements to computational fluid dynamics simulations for (a) cylindrical and (b) conical sections of a 45 mm diameter hydrocyclone (Lim et al., 2010b)

2.3.6. Electrical Impedance Tomography

Electrical Impedance Tomography (EIT) investigates a vessel's internal flow by using the differences in electrical resistivity between phases in a liquid suspension to map their instantaneous distribution in the vessel's cross section. Electrodes are placed on the outside of the vessel walls and their signals are computed through an algorithm that yields a resistivity profile of a two dimensional cross-section (Dickin et al., 1993). EIT testing by Gutiérreza et al. simultaneously measured the air core size and solids concentration profiles within the hydrocyclone with varying concentrations of calcium silicate particles, see Figure 19 (Gutiérrez et al., 2000). EIT imaging allowed the air core diameter to be predicted as a function of apex diameter and inlet feed pressure.

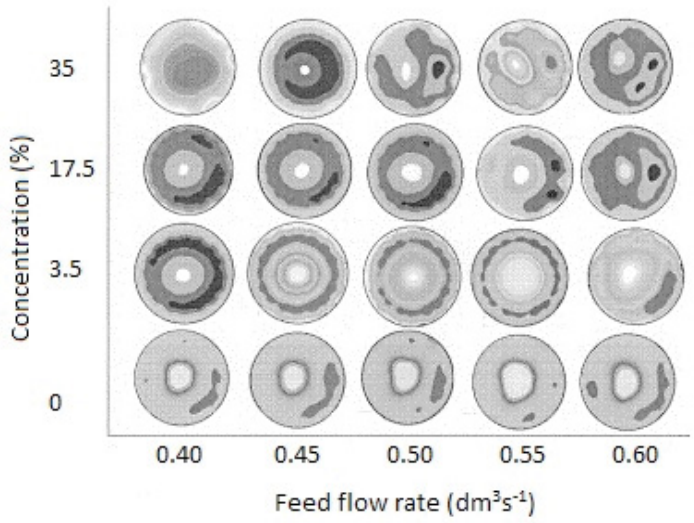

Figure 19: EIT sequence of resistivity images of hydrocyclone cross section at varying feed flow rates and concentrations (Gutiérrez et al., 2000)

2.3.7. X-Ray Tomography

X-ray tomography measures the proportion between the intensity of an x-ray beam emerging from the vessel of interest compared with the intensity of the original x-ray beam. This proportionality is equal to the summation of the x-ray attenuation coefficients of the vessel at each point along the incident line. A cross-sectional image is reconstructed allowing the creation of a two dimensional density map (Miller et al., 1993). Galvin and Smitham used x-ray computed tomography to infer the concentration distribution of magnetite particles at various elevations inside a glass hydrocyclone (Galvin and Smitham, 1994). This study concluded that specific gravity increased as the cross-sectional radius of the hydrocyclone decreased. The testing operated at a higher particle concentration than previous studies as the study wanted to demystify the solids concentration distribution within hydrocyclones, and provide a more thorough knowledge base into the nature of the hydrocyclone cut point. X-ray computed tomography has limitations near the walls of the hydrocyclone as image density data has large errors in magnitude of the concentration of the slurry (i.e. blurring at boundaries) as the path length of x-rays approach zero near the hydrocyclone walls caused by finite resolution. Contrast sensitivity poses another limitation as it is a measure of how well a feature can be distinguished from the surrounding background. Dopants can be added to increase contrast sensitivity but not all features have sufficiently large attenuation contrasts. X-ray tomography is best applied to thin vessel walls, and

Table 1 summarizes the range of x-ray tomography applicability when using a 160 keV constant potential x-ray source.

Table 1: X-ray tomography applicability thickness range (ASTM Standard, 2009)

Material	Practical thickness range
Steel	3 mm (1/8 in.)
Aluminum	25 mm (1 in.)
Aerospace composites	50 mm (2 in.)
Polyurethane Foam	300 mm (12 in.)

2.3.8. Ultrasound Tomography

Ultrasound tomography (UST) is a non-intrusive technique where an ultrasound pulse is reflected by the particles moving in the liquid. The fluid velocity is determined by the change in frequency of the ultrasonic wave that was emitted and subsequently reflected. By emitting a series of pulses and catching the echoes, the fluid velocity can be determined (Mavros, 2001). Schlaberg et al. measured the size and position of the air core of a hydrocyclone with UST (Schlaberg et al., 2000), see Figure 20.

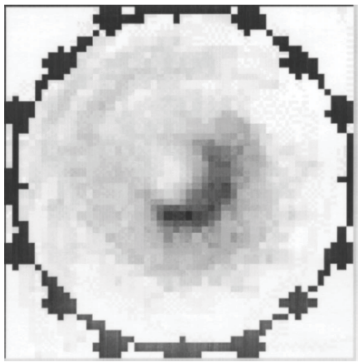

Figure 20: UST cross section image of 50 mm hydrocyclone operating with only water (Schlaberg et al., 2000)

2.3.9. Positron Emission Particle Tracking

Positron Emission Particle Tracking (PEPT) was developed at Birmingham University in the late 1980s as a powerful tool for in-situ and non-invasive characterization and visualization of particle flow within industrial engineering applications (Hawkesworth et al., 1986; Parker et al., 1993; Parker et al., 2002). The PEPT technique is relatively new compared to the pre-existing visualization techniques summarized in this section. PEPT is a variant of Positron Emission Tomography (PET) and uses a tracer particle that is labeled with a radionuclide, such as ^{18}F. Current PEPT scanners used were originally PET scanners. PEPT is a nuclear imaging technique that uses the unique decay characteristics of the radionuclide for imaging. The radionuclide undergoes beta decay – a proton is converted to a neutron accompanied by a release of a positron. Following its emission, the positron will slow down over a small stopping distance and will then annihilate with a neighboring electron. Each annihilation results in an emission of a pair of 511 keV gamma rays which in order to conserve momentum are emitted back-to-back, a hundred and eighty degrees. Detection of coincident pairs of gamma photons on the camera's two detectors provides a straight line along which the particle lies and lines generated by subsequent pairs will intercept at the source enabling determination of the particle position's by geometric triangulation (Parker et al., 2002). The primary methods used to irradiate a particle in order to produce a tracer have been direct irradiation and ion exchange (Fan et al., 2006b). Further information on these labeling techniques for PEPT can be found in previously published work by Fan *et al.* (Fan et al., 2006a, b).

Chan *et al.* tracked particle trajectories in circulating fluidized bed cyclones as a function of solids loading (Chan et al., 2009). This was the first time a particle was tracked in-situ inside a cyclone in real time. Although this work was on a gas/solid system rather than the water/solid system seen in hydrocyclones, the results still offer insight to hydrocyclone PEPT imaging. Testing was undertaken with two cyclone geometries, 95 and 200 mm diameters respectively, at variable solids concentration of sand with a wide particle distribution between 0 and 150 micrometers. Sand tracer particles approximately 100

micrometer in diameter were labeled with the ion-exchange technique. The tangential and axial velocity components and the residence time of the tracer particles were obtained along with the thickness of the boundary layer in the cylindrical section and the dense wall layer in the conical section of the cyclone. Figure 21 highlights the typical particle motion of the tracer particles at various values of solid concentration (C_s), axial gas velocity (v_c) and cyclone diameter (D_c). The particle motion inside the cyclone is dependent on solids loading. At low solid loading, tracer particles exhibit a vortex trajectory downwards to the apex while at higher solids loading, the particles are drawn into a dense wall layer that moves downwards towards the apex. High solids loading also increased the residency time of the particle as the tracer particle becomes trapped in a dense wall layer. These gas/solid cyclone observations are interesting to keep in mind when investigating hydrocyclones.

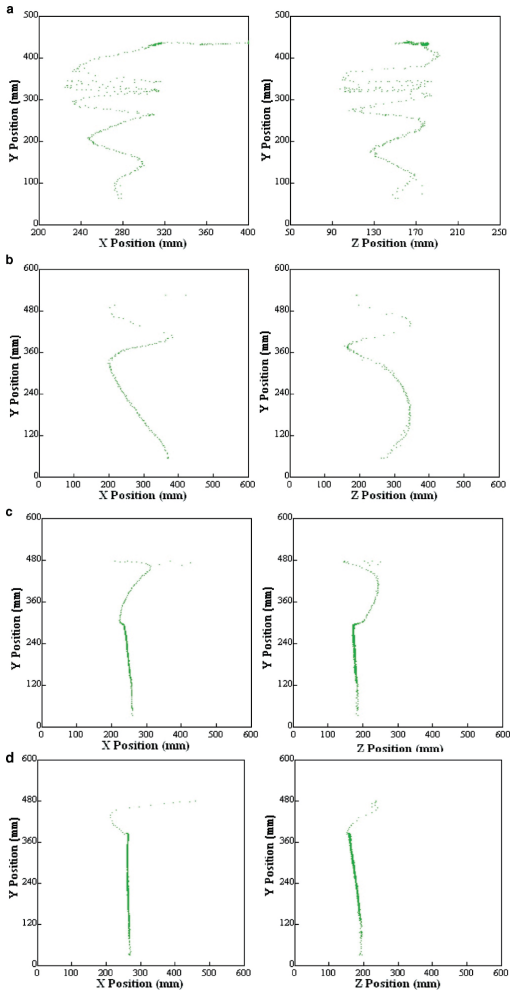

Figure 21: Motion of particle tracked using PEPT at varying values of Cs, vc and Dc: (a) Cs = 0.07 kg/kg, vc = 1.4 m/s, and Dc = 0.095 m; (b) Cs = 0.84 kg/kg, vc = 0.4 m/s, and Dc = 0.2 m; (c) Cs = 3.3 kg/kg, vc = 2.2 m/s, and Dc = 0.095 m; and (d) Cs = 10 kg/kg, vc = 0.88 m/s, and Dc = 0.095 m (Chan et al., 2009)

Chang *et al.* studied the flow of a strong-base anion exchange resin bead inside a 40 mm diameter hydrocyclone using the PEPT technique (Chang et al., 2011). The resin beads used were between 390 to 700 micrometers in diameter and were activated using the ion-exchange technique. The investigation injected the activated particle under a controlled system with a particle injector rather than have it enter the system via the pump downstream. Figure 22 shows the trajectory of one resin bead from 108 milliseconds when it enters the hydrocyclone to 247 milliseconds where the tracer particle exits via the apex. The progression is shown in a series of four snapshots.

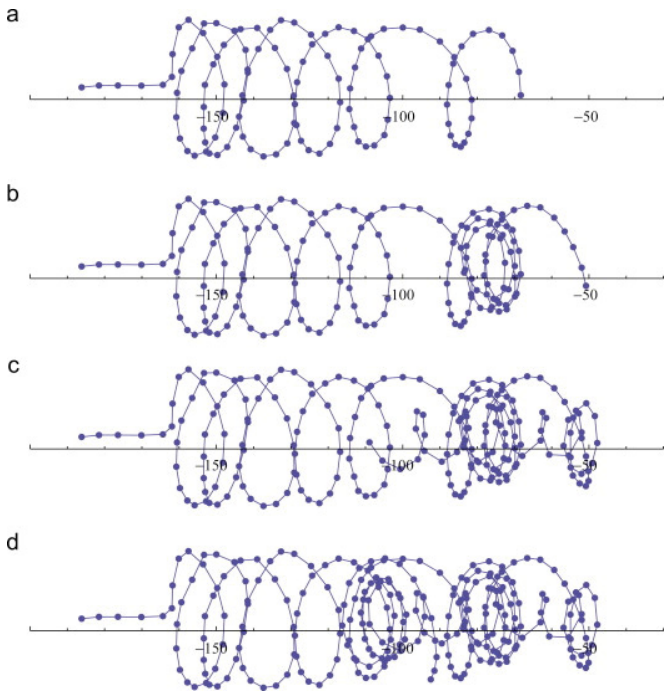

Figure 22: Trajectory of an activated strong-base anion exchange resin bead inside a 40 mm diameter hydrocyclone using the PEPT technique from 108 ms (a) to 247 ms (d) (Chang et al., 2011)

However, it is still very challenging to gain new experimental insights into the hydrodynamics of dense solid–liquid flows. In so far, image testing has not been conducted with hydrocyclones at high solid concentrations to track particle movement.

2.3.10. Conclusions

It is interesting to note that since the initial imaging in the early 1960s, very little theoretical imaging and velocity mapping was done until the 1980s, and all experimental studies mentioned in this literature review are in pure or lightly seeded water. Due to experimental limitations, there are very few experimental investigations on the flow field under high particle loading. These experimental limitations are often the nature of the engineering process itself; opaque process slurries, thick metal walled vessels, enclosed and large cumbersome equipment. Particle flow patterns are difficult to model computationally

as little is known about movement of particles within industrial apparatus and process equipment, especially in opaque liquids and enclosed devices. In order to have a better understanding, design and operation of engineering processes, visualization of the system is required. The average size for hydrocyclone image testing has been 3 inch in diameter or smaller due to limitations of testing equipment overall for larger scale ups. Opaque systems are also an issue. PEPT is unique in flow visualization terms as it is capable of probing opaque systems and examining flow phenomena in three dimensions that could not be observed as effectively by using other imaging techniques. PEPT is particularly suited to study of solid–liquid flows by mapping the flow of fluids and the flow of particles, as liquid flows can be mapped using a neutrally buoyant solid tracer. LDV cannot be used for image of hydrocyclones with an air core nor with high concentrations such that realistic industrial conditions cannot be tested with LDV. In order to optimize hydrocyclone performance CFD models must use experimental data that uses industrial conditions, rather than water or lightly seeded concentrations. These results are not indicative of realistic performance. Choosing an imaging technique is dependent on what component of the hydrocyclone needs to be studied. UST and EIT are reliable for air core sizing while PEPT is a good technique for real time particle tracking throughout the hydrocyclone. Otherwise, pitot tubes are intrusive to the flow pattern and LDV and PIV cannot function in opaque slurries that are common in most industrial applications using hydrocyclones. X-ray is limited to vessel thickness and has errors with boundary conditions and image density.

2.4. Positron Emission Particle Tracking

2.4.1. Introduction

This section introduces PEPT which is a variant of Positron Emission Tomography (PET), which was developed at University of Birmingham in the late 1980s (Hawkesworth et al., 1986; Parker et al., 1993; Parker et al., 2002). This imaging technique uses a tracer particle that is labeled with a radionuclide, such as ^{18}F, to investigate a system of interest with a positron camera. The radionuclide labeled tracer undergoes beta decay which is when a proton is converted to a neutron. This conversion is accompanied by the release of a positron which will annihilate with a neighboring electron. Each annihilation results in a pair of 511 keV gamma rays. To conserve momentum, these gamma rays are emitted back-to-back. A PEPT capable camera detects coincident pairs of gamma rays which provide a straight line along which the tracer particle lies. When at least three lines of response are detected by the camera, the location of the tracer particle can be detected by geometric triangulation (Parker et al., 2002).

2.4.2. Origins of Positron Emission Particle Tracking

The origins of PEPT are synonymous to the origins of PET, which date back 80 years (Anderson and Price, 2000). Its origins can be divided into three time periods: (i) the application in physiological

studies from the early 1930s towards the late 1940s of positron emitting radionuclides; (ii) the recognition that positron emitting radionuclides exhibit properties that are useful in nuclear medicine during the mid 1950s towards the early 1970s; and finally from the late 1970s to present day (iii) the combined use of positron-emitting radionuclides with the coincidence detection of the annihilation radiation and the tomographic reconstruction process from projections (Ter-Pogossian, 1992).

PET began in 1928, where the theoretical physicist Paul Dirac (1902-1984) postulated the existence of positive electrons based on the equations of quantum mechanics and Einstein's theory of relativity. Carl Anderson (1905-1991) proved his theory in 1932, when he observed experimentally that cosmic rays include particles with the mass of electrons, but with a positive charge (positrons). This work led to the development of larger cyclotrons that were able to produce large quantities of artificial radioisotopes, which are now the backbone of medical PET imaging. In the 1940s, a system for external measurement of radiotracers was developed and led to the evolution of the today's PET scanner and by consequence the PEPT scanner. Hand-held Geiger–Muller counters were initially used but soon evolved to an automated system of detector movement by which produced the first PET scanner. It was not long before PET was used to produce nuclear images. Multidetector systems were then developed culminating in the ring detector systems, which are used in PET imaging today (Anderson and Price, 2000). Over the last 20 years, PET has become the most powerful functional imaging modality in medicine (Sadrmomtaz et al., 2007). However, since the 1970s, its use has increased exponentially in the medical fields. In the mid 1980s, PET was developed into a functional imaging modality for engineering applications called the positron emission particle tracking at University of Birmingham in England (Bemrose et al., 1988; Parker et al., 1997; Parker et al., 1994).

2.4.3. Physics of positron emission and annihilation

This section consists of a review of the basic physics that govern PEPT and the detector technology used in modern PET scanners and intuitively PEPT scanners. To begin, the nucleus of an atom consists of two different types of nucleons, protons and neutrons. While similar in mass they differ in charge, a proton has a positive charge whereas a neutron is uncharged. Surrounding the nucleus is a cloud of negatively charged electrons. Atoms with the same number of protons, i.e. atomic number, but differ in the total number of nucleons, i.e. mass number, are known as isotopes of the element corresponding to the same atomic number. To illustrate, ^{18}F is an isotope of fluorine and consists of 9 protons, as it is fluorine, and 9 neutrons (Phelps, 2004).

The nucleus is held together by two opposing forces: the attractive force between nucleons and the repulsive Coulomb force between the positively charged protons. If a nucleus has either an excess of protons or neutrons, the nucleus is unstable and therefore prone to radioactive decay such that the overall

number of nucleons changes to suit a more stable configuration. Nuclei that decay are known as radionuclides. For an element that has isotopes that are unstable thus prone to radioactive decay, they are known as radioisotopes of that element (Serway and Beichner, 1999).

Radioactive decay is a process where the protons and neutrons are configured into a lower energy state. The transition to stable configuration may involve levels of the same nucleus or levels of different nucleus. Each different process is known as a decay mode. The scope of this paper will only discuss the positron emission decay mode, where if nuclei have an excess of protons. This decay mode is also known as beta-plus decay. Positron emission is essentially when a protons in the nucleus of the atom is converted into a neutron (η) and a positron (e^+) (Brookhaven National Laboratory, 2005).

A positron is the anti-particle to the electron having the same mass but opposite charge. During positron emission, the positron is ejected from the nucleus along with the undetected neutrino (υ). A good example of a radionuclide that decays by positron emission is ^{18}F:

$$^{18}F = {}^{18}O + e^+ + \upsilon$$

The net energy released is shared between the daughter nucleus, ^{18}O, the positron and the neutrino. PET imaging is based on positron emission decay. Decay by positron emission is dominant when dealing with low atomic number nuclei, higher atomic numbers lead to competition with another radioactive decay mode, electron capture decay. It is not within the scope of this paper to discuss electron capture decay. Radionuclides, which dominantly decay via the positron emission route, are preferred for PET imaging and by extension, PEPT. Half-life is the time required for half of the atoms of a sample of identical radioactive atoms to decay. Activity is measured in units of the number of disintergrations per second (1 bequerel (Bq) = 1 disintegration per second). Traditional units of the curie (Ci) and millicurie (1mCi = 10^{-3}Ci) are still used where 1 mCi = $37x10^6$ Bq = 37 MBq and 1MBq = $27x10^{-6}$ Ci = 27 μCi (Phelps, 2004).

Positrons ejected following beta-plus decay have relatively short lifetimes. This is due to the fact that they will rapidly lose their kinetic energy in inelastic interactions with atomic electrons in the material. Once most of the energy has dissipated, it will combine with an electron to form a hydrogen-like state, positronium. Using hydrogen for illustrative purposes, the proton that forms in the nucleus is substituted by a positron. The lifetime of this state is short before annihilation occurs. Annihilation is where the mass of the electron and the positron are converted into electromagnetic energy. The energy released can be calculated from Einstein's mass-energy equivalence in the following equation:

$$E = mc^2 = m_e c^2 + m_p c^2$$

where m_e is the mass of the electron, m_p is the mass of the positron and c is the speed of light. As both the positron and electron are almost at rest, the energy released comes largely from the mass of the particles. The released energy is in the form of high-energy photons with the net momentum near zero as both electron and positron are near rest when the annihilation happens. Using Einstein's mass-energy equivalence, the energy released is 1.022 MeV. Due to conservation of momentum and energy, annihilation does not typically result in the emission of a single photon but rather two photons are emitted simultaneously in opposite directions, 180˚ apart, and carrying energy equal to half of 1.022 MeV i.e. 511 keV, thus conserving energy and momentum. Thus, regardless of the element involved, there will be an emission of two back-to-back 511 keV photons, see Figure 23. There is the possibility that higher order annihilation can occur where more than two photons are emitted but the likelihood is about 0.003%. It is the detection of these back-to-back gamma rays that allow the position of a particle to be determined.

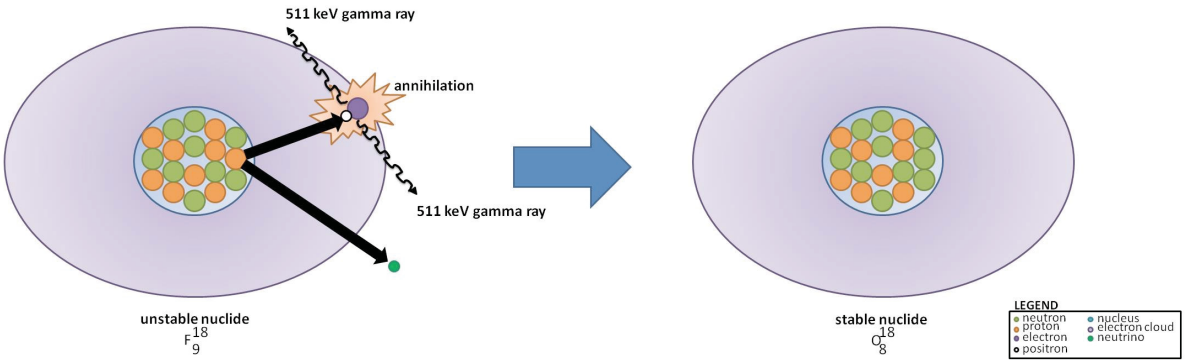

Figure 23: Beta-plus decay of fluorine-18

Annihilation photons are very energetic, in the region of gamma rays in the electromagnetic spectrum, and are detected by PEPT imaging. Due to the geometric relationship of the photons being emitted, 180˚ apart, if the photons can be detected and localized externally, the line drawn between both detected locations will pass directly through the point of annihilation. This property of the annihilation process was originally coined as electronic collimation. Since the point of annihilation is relatively close to that of positron emission, electronic collimation gives a good indication on where the radioactive atom was in the system of study. Comparing this with radioactive decay schemes results in the emission of a single photon. Yet the direction of the photon is determined by using absorptive collimation, which enables photons that are emitted in a certain direction to be impinged on the detector.

Since annihilation photons are in the gamma ray region of the electromagnetic spectrum, photons and gamma rays are used interchangeably to refer to annihilation photons. It is important to note that the properties are identical despite their difference in origin. Annihilation is the basis of PEPT imaging. A

PEPT scanner is designed to detect and localize back-to-back annihilation photons, which are emitted when a radionuclide decays via positron emission.

2.4.4. Data collection

PEPT uses coincidence detection, which consists of a pair of detectors along with associated electronics and a coincidence circuit. If annihilation occurs between the detectors, it is likely that a coincidence will be recorded. Since annihilation photons are emitted approximately 180˚ apart, a recorded coincidence is indicative of that annihilation has occurred along the line connecting the two detectors. The line is referred to as a LOR (Line Of Response). Under ideal conditions, two detectors along with associated circuitry will generate a coincidence.

2.4.5. Types of events

PEPT detectors are limited to the point that the type of coincidences that are detected are contaminated with undesirable events rather than only true coincidences where the events detected are solely the two annihilation photons from the same radioactive decay. Undesirable events are random, scattered and multiple coincidences. Another problem is that a vast majority of photons that are detected are single events where only one of the two annihilation photons is detected. Single events are not accepted by PEPT scanners but are responsible for random and multiple coincidence events. Figure 24 illustrates the four different kinds of events that can be detected by a PEPT scanner.

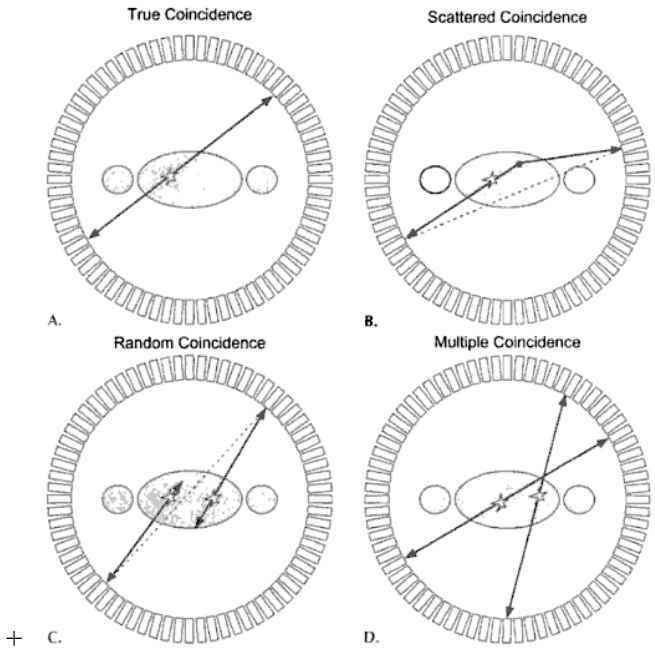

Figure 24: Schematic representation of the four main coincidence event types (Phelps, 2004)

In simple terms, a true coincidence is when both annihilation photons escape the vessel of study and are recorded by a pair of detectors while a scattered coincidence is when one or both of the two annihilation photons interact in the vessel before detection which results in a misposition of the event. Random coincidences are when a coincidence is created by two photons, which have spawned from two separate annihilations. These need to be subtracted from the overall data. Finally, multiple coincidences are when three or more photons are detected simultaneously. These are normally discarded (Phelps, 2004). The accuracy of the technique has been validated in two ways: PEPT measurements can be compared to with visual observations or concomitantly with another tracking technique such as Electrical Resonance Tomography (ERT) (Cole et al., 2010).

2.4.6. Sources of error

PEPT imaging has two effects, position range and noncolinearity, which can lead to sources of error when determining the line along which a positron-emitting radionuclide is to be located. Positron range is the distance from the positron emission site to the site of annihilation. PEPT scanners detect line to which the annihilation photons are located not the decaying atom location. The perpendicular distance between the emission site to the line defined by the annihilation photons that can cause mispositioning. Position range limits the resolution obtained by PEPT. Noncolinearity is due to the fact that the positron and the electron are not at complete rest when they annihilate such that the annihilation photons will be exactly at 180˚. PEPT assumes that the emission was exactly back-to-back which results in a small error in locating the line of annihilation. The blurring effect due to noncolinearity of the final location can be estimated as; $\Delta nc=0.0022xD$, where D is the diameter of the PEPT scanner. The error will increase linearly are the diameter of the scanner increases. It is important to note that the effect is relatively small and not a major limiting factor (Phelps, 2004). See Figure 25 for a schematic representation of both sources of error.

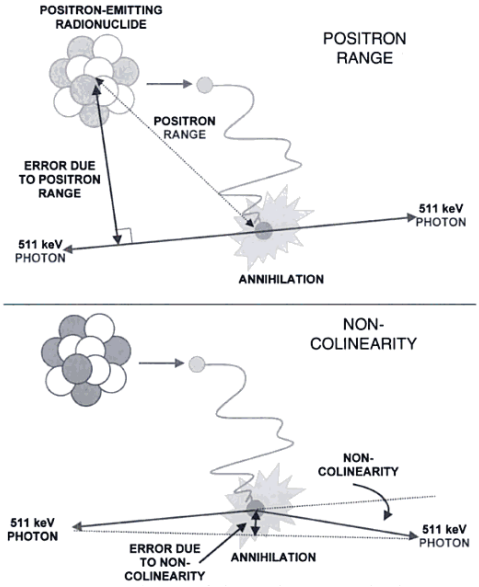

Figure 25: Schematic representation of the error in determining the location of the emitting nucleus due to position range (top) and noncolinearity (bottom) (Phelps, 2004)

2.4.7. Tracers

PEPT tracks a single radioactively labeled particle, therefore, suitable labeled tracer particles play a crucial role in PEPT. The optimum activity for a PEPT tracer is between 300 and 1000 μCi (Fan et al., 2006b). A large number of radioisotopes can be potentially used to label a single particle for PEPT but the half-life of the radioisotope should be short enough to avoid persistent radioactivity and long enough to enable detection over the timescale of the experiment. The radioisotopes used in this study is ^{18}F, in the form of fluoride ions because of its convenient half-life (110 mins) (Fan et al., 2006a), and it decays entirely by positron emission (Phelps, 2004). It is important in PEPT that the tracer's size and composition be identical to the bulk yet the radioactivity by which a single particle is labeled is dependent the particle composition and size and the labeling technique used. The primary methods used to irradiate a particle in order to produce a tracer have been direct irradiation and ion exchange. In direct activation, particles are directly bombarded using a 33 MeV ^{3}He beam (Fan et al., 2006a). A few of the oxygen atoms in the particles are then converted into ^{18}F radioisotope.

2.4.7.1. Ion exchange labeling technique

Ion exchange labeling technique (Fan et al., 2006a, b) is when an ion exchange material, typically a polymer resin, exchanges an ion with a dissolved species in a surrounding aqueous medium. In ion-exchange, only the functional groups near the surface of the resin can have ions dissolve in the surrounding aqueous phase such that ion exchange only involves functional groups on the surface. Ion exchange can be described by the following interaction on the surface of an anionic resin:

$$RA + B^- \Leftrightarrow RB + A^-$$

where A and B are ions and R is the functional group. Ion exchange resins are insoluble cross-linked polymers that have fixed functional groups with reversibly fixed ions. Ion exchange is when a solid embraces a dissolved species in the surrounding aqueous medium. The ions are stoichiometrically exchanged for other ions of the same sign. The functional groups are chemically active and can exchange ions with surrounding media. These functional groups can be acidic or basic. The charge of each group is normally compensated by an exchangeable ion. This thesis deals with anion resins which have positively charged fixed functional groups and carry exchangeable negatively charged counterions (Zagorodni, 2007). The ion exchange resin particles in this experiment are labeled with a radionuclide, ^{18}F, using ion exchange. The ion-exchange technique is used to label smaller resin particles between 60 to 1000 μm.

2.4.7.2. Direct activation labeling technique

Direct activation labeling technique (Fan et al., 2006a, b) is typically used to label a particle within the size range of 1 to 10 mm. The ion-exchange technique is used to label smaller resin particles between 60 to 1000 μm. For a single resin bead, the radioactivity is controlled by ion-exchange properties of the resin material, anions present in the radioactive water and processing time (Fan et al., 2006b). The main challenge with liquid-phase-continuous systems is finding a tracer than does not lose its activity due to leaching into the liquid. Direct activation is typically used to label a particle within the size range of 1 to 10 mm.

Direct activation labeling technique is when the particle is bombarded with a 33MeV ^3He beam. Some of the oxygen atoms in the particle are converted into the radionuclide ^{18}F. The ^{18}F in the particle exists as a structural element within a layer approximately 0.3 mm from the particle's surface. Further information on the direct activation labeling technique for PEPT can be found in previously published work (Fan et al., 2006a, b).

2.4.8. 511 keV photon scanner

PEPT studies at the Birmingham Positron Imaging Centre use a Forte 511 keV photon scanner manufactured by ADAC Laboratories, California. For detailed discussion of the camera's characteristics and capabilities please refer to the papers written by A. Sadrmomtaz et al. and D. J. Parker et al. (Parker et al., 2002; Sadrmomtaz et al., 2007).

2.5. Conclusions

PEPT allows non-invasive real time tracking of tracer particles inside the hydrocyclone to help resolve the flow patterns. The information that can be derived from PEPT data is the motion of the particle, the fraction of time spent by the tracer at each point in the system, the average velocity of the

tracer at each point, the history of the tracer inside a target volume and the residence time distribution of the tracer particle. There is a need to develop a method by which the hydrocyclone flow patterns can be quantified under industrial conditions. This thesis project presents data on the motion of particles in a two-inch hydrocyclones using the PEPT technique.

3. Methodology

Two studies were undertaken to investigate the visualization of particle flow inside small diameter hydrocyclones using the PEPT technique. One study was in a water system while the other was in a silica slurry system.

3.1. Water system study

3.1.1. Tracer particles

The tracer particles used are Dowex Chemicals SBR anion exchange resin beads (Sigma-Aldrich) and are activated using the ion-exchange technique. The resin beads are -700+500 μm in size. ^{18}F was produced from irradiating deionized water via the reaction of $^{16}O(^{3}He,p)^{18}F$ that occurs under direct bombardment using a 33 MeV ^{3}He beam in the Birmingham Scanditronix MC40 variable energy cyclotron (Fan et al., 2006b). The SBR anion exchange resin beads are immersed in the irradiated water that has a starting activity of 60 mCi and subsequently coated in a commercially available epoxy resin, Araldite Rapid, to prevent the leaching of the activity when exposed to an aqueous environment.

3.1.2. Apparatus and instrumentation

Each test run was in tap water. For each run, 10 liters of water was added into the sump tank. Prior to adding the tracer, the system ran until the pressure stabilized. By re-circulating the tracer, multiple passes over the lifetime of the tracer built up the average flow pattern. In order to verify the general application of PEPT for tracking particle flow in a hydrocyclone for different geometries, two conventional hydrocyclones are selected. These are 50mm (2 inch) hydrocyclone units, C124 standard and C126 stub models respectively, manufactured by Richard Mozely Ltd as shown in Figure 26.

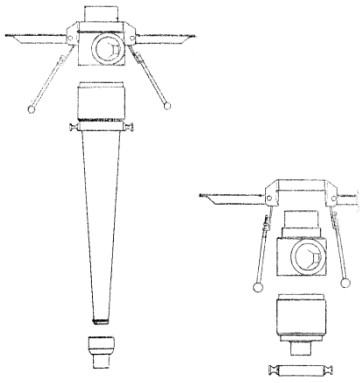

Figure 26: (left) C124 standard hydrocyclone (right) C126 stub hydrocyclone (Richard Mozley Ltd, 1989)

Both hydrocyclone unit moldings are wear resistant polyurethane. Consideration for the choice of these two hydrocyclone units is to offer insight on a wide range of flows and cut points but still

maintain a practical application within the mineral processing industry with respect to small diameter hydrocyclones.

Both hydrocyclone test setups were incorporated in a re-circulating water system. A progressing cavity pump (Mono Merlin CAB12G1B4 series), located downstream in conjunction with a sump tank to form a mobile self-contained testing unit, is used to circulate the feed water to the hydrocyclone inlet. A generalized schematic of the testing system used is illustrated in Figure 27. Both setups enabled the slurry to be re-circulated until the desired pressure was stabilized and then a tracer particle could be added. A summary of the test conditions and variable settings is shown in Table 2.

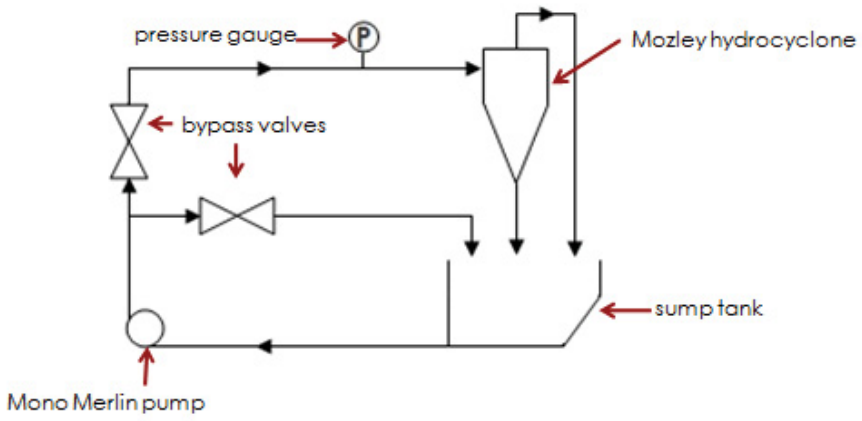

Figure 27: Schematic overview of hydrocyclone setup for water system study

Table 2: Test conditions and variable settings for water system study

Test	Model #	Vortex finder diameter (mm)	Apex diameter (mm)	Pressure (bar)
A	C124	11.1	4.5	1
B	C126	11.1	6.3	1

The University of Birmingham's ADAC Forte with MCD coincidence option positron camera (Figure 28) was used to track the motion trajectory of the tracer particle as it moves between the two detectors of the positron camera inside the hydrocyclone.

Figure 28: ADAC Forte positron camera at Birmingham University

The field of view for each of the camera heads is 50 x 40 cm^2. The positron camera uses these two positron-sensitive detectors, between which the hydrocyclone system under study is mounted, to track the motion of a tracer particle. The camera setup is shown in Figure 28 together with the Cartesian axial coordinates used. The x-y-z motion trajectory of tracer particles in the hydrocyclone is obtained by triangulation of the detected annihilation events and given as an output from the positron camera's software program with respect to time. Figure 29 highlights the experimental test A which is for the standard hydrocyclone model and Figure 30 highlights the experimental test B which is for the stub hydrocyclone model. Tubing is fitted to the overflow and underflow and fed directly to the sump tank to prevent water from damaging the PEPT imaging equipment and the hydrocyclone is set apart from the sump tank/pump system to limit vibrations.

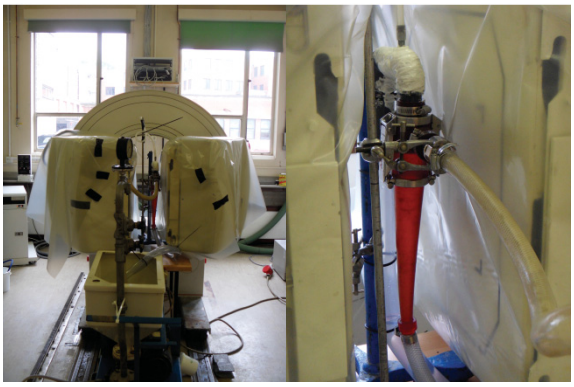

Figure 29: Experimental test A

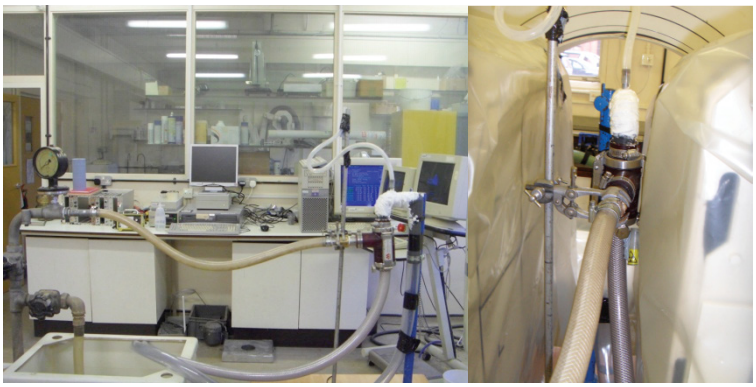

Figure 30: Experimental test B

Measurements were made in the presence of an air core and no particulate phase at standard atmospheric conditions with a liquid water phase. The inlet flow rate and pressure of the feed was adjusted by the bypass valves and both were maintained constantly throughout all the experiments. Numerous runs were done for both setups and each run with a tracer had multiple passes.

3.2. Silica slurry system study

3.2.1. Tracer particles

The tracer particles were two size classes of silica (Table 3) activated using the direct labeling technique (Fan et al., 2006a, b). Initially, a large silica piece was bombarded using a 33 MeV ^{3}He beam from the Birmingham Scanditronix MC40 variable energy cyclotron before crushed and sieved to the desired size classes for testing. Test 1 using the -2000+1700 μm silica tracer particle was designated the 'coarse' test, and test 2 using the -250+150 μm size range was the 'fine' test. The two size classes of silica tracer are above the approximate cut-size of the two-inch hydrocyclone, i.e., under these experimental conditions the tracer particles should report to the underflow (Chandrasekhar and Raghavan, 2004).

Table 3: Test runs

Test	Silica tracer particle size (micrometers)
1 (coarse)	-2000+1700
2 (fine)	-250+150

Each run was in a silica slurry. The silica slurry used for each run had the size distribution shown in Figure 31. For each run, one kilogram of silica was added to the 25 liters of water (3.8% solids) in the sump tank. Prior to adding the tracer, the system was run until the pressure stabilized. By re-circulating the tracer, multiple passes over the lifetime of the tracer built up the average flow pattern.

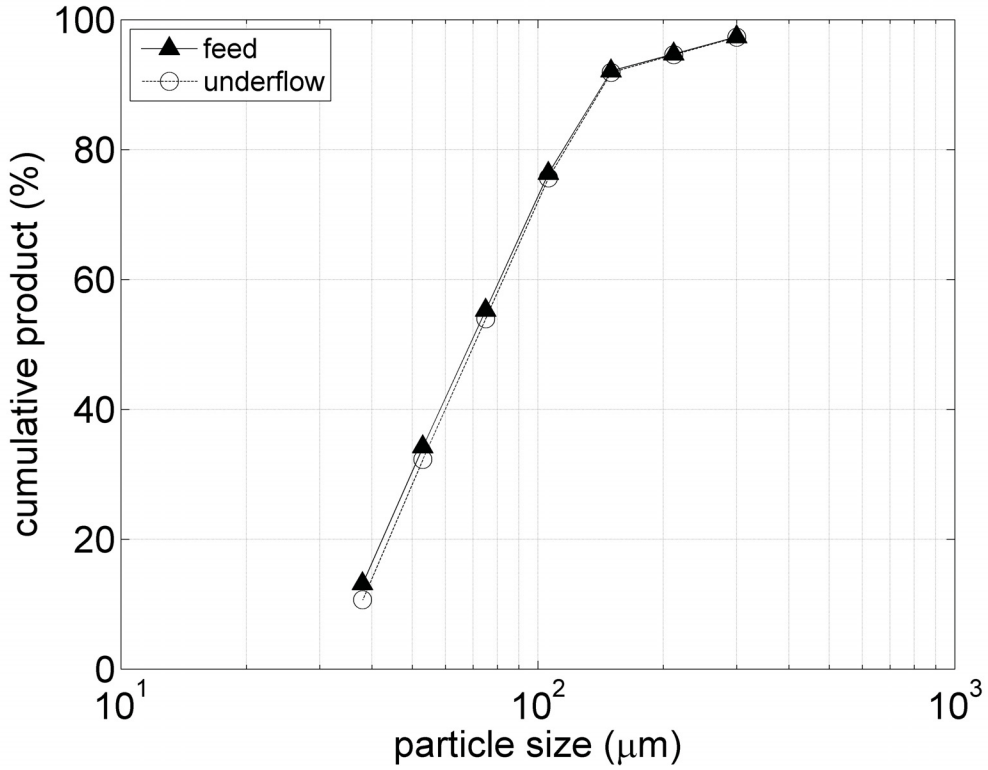

Figure 31: Size distribution of silica slurry

3.2.2. Apparatus and instrumentation

In order to verify the general application of PEPT for tracking particle flow in a hydrocyclone for slurry conditions a conventional small diameter hydrocyclone was selected. The 50 mm (2 inch) hydrocyclone unit, C124 standard model, manufactured by Richard Mozely Ltd, see Figure 32, was used.

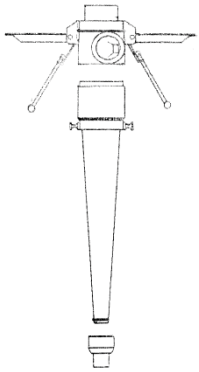

Figure 32: C124 standard hydrocyclone (Richard Mozley Ltd, 1989)

It was observed in the water system study that this hydrocyclone unit offered insight on a wide range of flows and cut points but still maintain a practical application within the mineral processing industry with respect to small diameter hydrocyclones. A progressing cavity pump with a sump tank was

used to circulate the slurry. The hydrocyclone was placed between the two PEPT detectors with the y-axis corresponding to the height of the hydrocyclone (Figure 33). The slurry was re-circulated until the desired pressure was stabilized. The silica tracer particles were thus introduced slowly into the sump tank. A summary of the test conditions and settings is shown in Table 4. Measurements were made in the presence of an air core at ambient atmospheric conditions. The inlet flow rate was adjusted by the bypass valves. The same apparatus setup as in the water system study was used, see Figure 27, for the silica slurry system. The experiment runs for a sufficient length of time to generate the required statistics. The tracer is then removed from the system and another silica particle is labeled with the system running under the same conditions as before.

Table 4: Test conditions and settings

Vortex finder diameter (mm)	Apex diameter (mm)	Sump tank volume (L)	Pressure (psi)
14	4.7	25	20-35

The University of Birmingham's ADAC Forte positron camera was used to track the trajectory of the tracer particles (Parker et al., 1993), see Figure 28. The PEPT geometry with respect to the camera detectors is that the x-axis is from the back of the detector to the front, the y-axis is the vertical and the z-axis is across the front, from left to right. The 3D trajectory is obtained by triangulation and given as an output from the software. The processed data provide the x-y-z coordinates at discrete time intervals. Optimal tracking occurs at kilohertz rates (i.e. up to 1000 particle locations per second), with measurement precision of around 0.5 mm in three dimensions. Details on the data acquisition algorithm can be found in Leadbeater et al. (Leadbeater and Parker, 2009; Leadbeater et al., 2012). Figure 33 highlights the experimental setup for the silica slurry study.

Figure 33: Overview of testing setup with PEPT camera

3.3. Trajectory analysis

The results from a PEPT run consist of a set of a single particle locations made in x,y and z on a frequent time basis. Locations are made on a frequent basis, but with random period due to the random nature of the radioactive decay of fluorine-18. These locations are analyzed with the PEPT algorithm from the University of Birmingham and is outputted as raw data locations with respective to the camera's field of view. Manipulation of the raw data is performed using MATLAB for custom analysis of the data by the author to find passes through the hydrocyclone. The code written to find a pass through the hydrocyclone is found in Appendix A. A pass must enter and exit the hydrocyclone to be considered a valid pass in the run. The instantaneous Lagrangian velocities along the trajectory of the tracer were directly determined using the 6-point method (Stewart et al., 2001). The 6-point method introduces a small amount of smoothing to the velocity data, but is preferred as the effects of PEPT measurement error are greatly reduced. Significant time was spent analyzing each run's raw data to find valid passes and characterize them.

4. Results

Two studies with PEPT were undertaken in this project. The first was a water system study with resin tracer particles and the second was a silica slurry study with silica tracer particles. The silica slurry was a percent solid of approximately 3.8%. Results for both studies are shown in this section. In both studies, the particles entered the system via the sump tank and entered the field of view of the camera via the feed inlet of the hydrocyclone.

All tracer particles fall between the range of moving tracer particle from previous studies where 50 μm tracer particles moving with speeds with an upper limit of 2 m/s had uncertainties in the measured locations of the order of 2.6 mm (Cole et al., 2012) and 1 mm tracer particles moving with speeds up to 10 m/s had uncertainties in precision of the order of 0.5 mm (Leadbeater et al., 2012). For the resin bead tracer particles, the particle range is -700+500 μm and they were moving at a speed of 1.5 m/s. The particle range for the silica tracer particles was -2000+150 μm and it was calculated that they were moving at a speed of 2 m/s. Thus, the frame of reference of the uncertainty of the measured results from these studies is between 0.5 mm-2.6 mm. In this case non-optimal conditions occurred (due to tracer particle activation considerations), but particles were located around 250 times per second on average.

4.1. Water system study results

The results from a PEPT experimental run consists of a set of single particle locations made in 3D on a frequent time basis. The first study was comprised of two tests with resin bead tracer particles in a water system passing through either a standard and stub hydrocyclone model respectively to examine the motion of a particle inside a hydrocyclone.

4.1.1. Standard hydrocyclone

4.1.1.1. Trajectory

A typical run inside a C124 hydrocyclone, standard model hydrocyclone, is shown in Figure 34 where each color represents a separate pass. There were 47 passes through the field of view which are shown in the full data set in Figure 34. The tracer particle then broke and the activity leached into the surrounding water system due to abrasion from the pump on the particle coating. The leaching of the activity into the system was a problem for every test run as the abrasion of the pump on the epoxy coating was faster than the half-life of the tracer thereby shortening the experimental run significantly and even corrupting all run data if the particle leached activity before passes could be recorded by the camera. The position in the hydrocyclone can be defined as the time the particle takes to complete its trajectory to

either the apex or overflow pipe. For this test, all tracer particles reported to the underflow and exited through the apex. For each pass, the particle entered via the feed inlet and progressed downwards in a clockwise vortex.

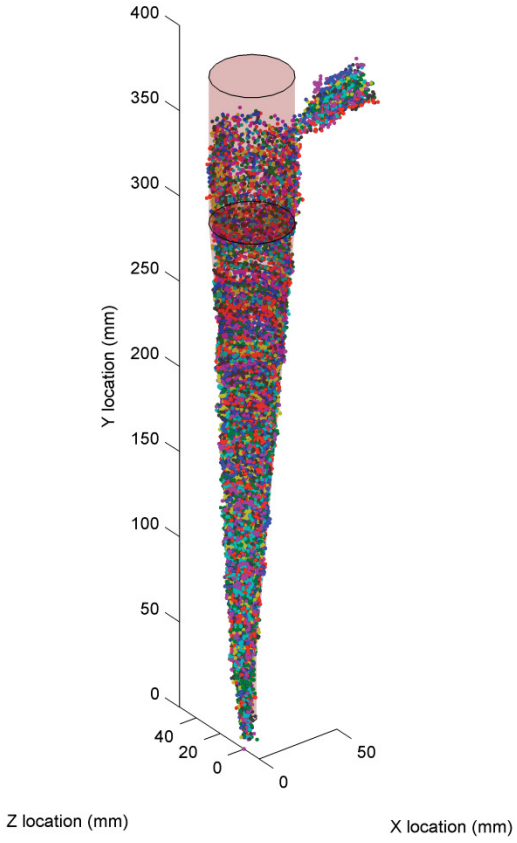

Figure 34: 47 trajectory passes for run 1 for test A

Figure 35 shows a typical pass for the resin tracer particle inside the standard two inch hydrocyclone reporting to the underflow, the color gradient shows the time from the particle entering the field of view and exits.

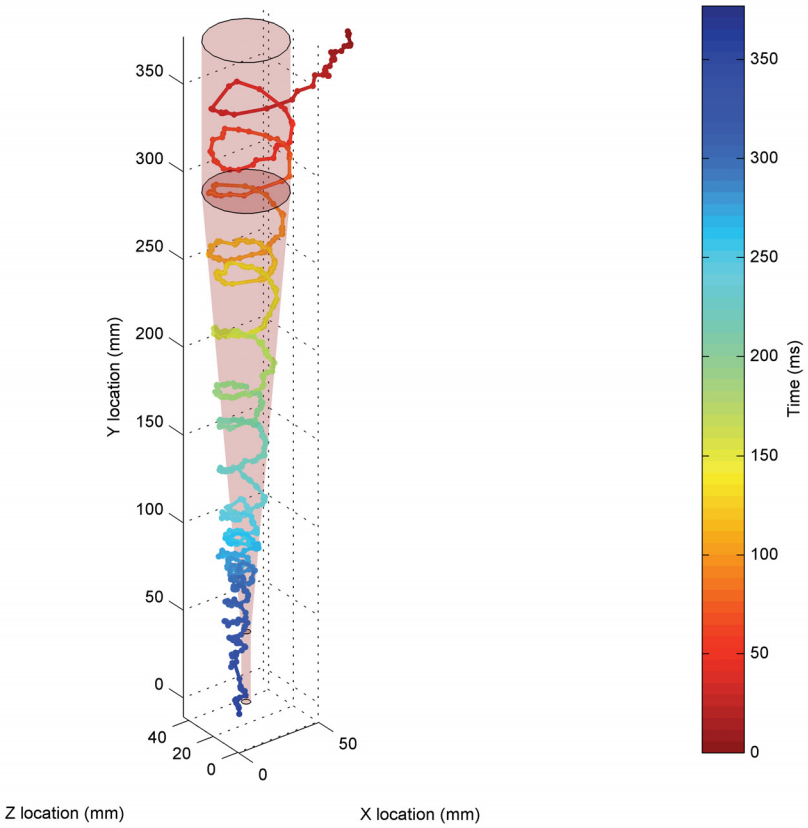

Figure 35: Trajectory for pass 1 in run 1 of test A

Figure 36 is a piecewise breakdown of pass 1 in run 1 of test A between y=50 and y=110 in the conical section.

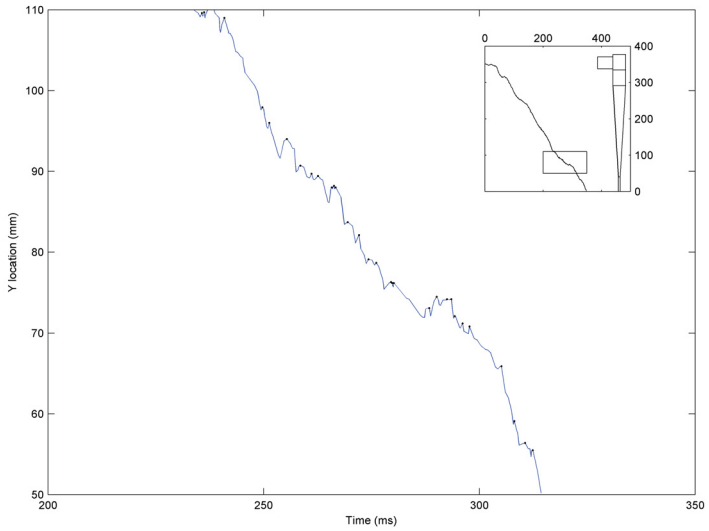

Figure 36: Trajectory for pass 1 in run 1 of test A in the y-direction highlighting local maxima

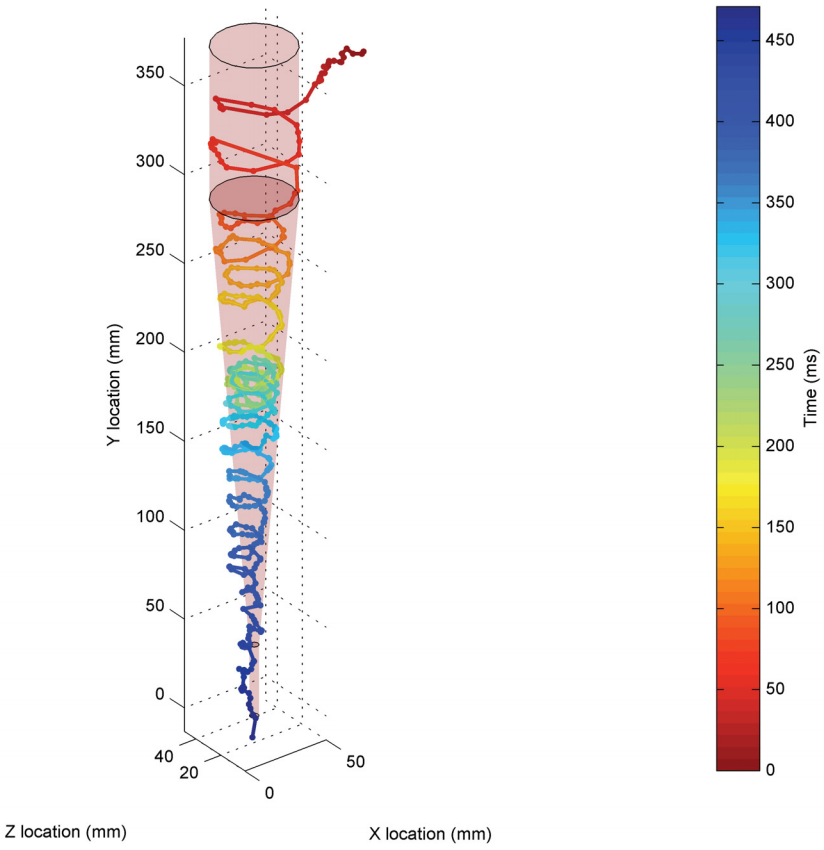

Figure 37: Trajectory for pass 14 in run 1 of test A

Figure 37 shows another typical pass for a the resin tracer particle inside the standard two inch hydrocyclone reporting to the underflow, the color gradient shows the time from the particle entering the field of view and exiting.

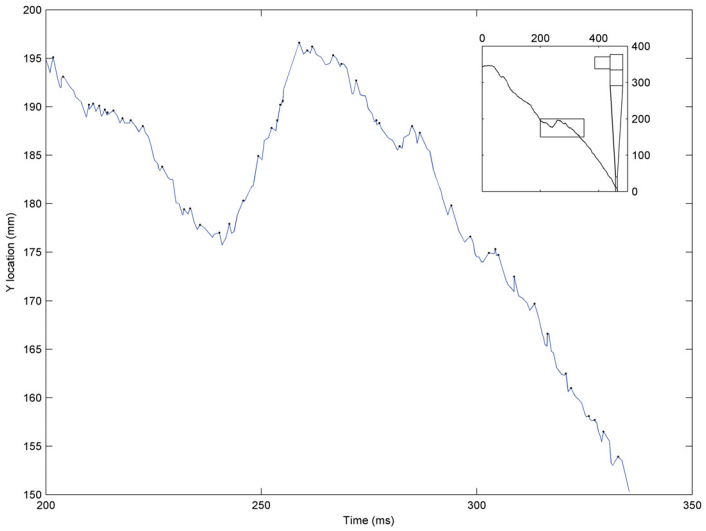

Figure 38: Trajectory for pass 14 in run 1 of test A in the y-direction highlighting local maxima

Figure 38 is a breakdown of pass 14 in run 1 of test A between y=150 and y=200 in the conical section.

4.1.1.2. Frequency

The frequency of resin tracer particle's appearance in different sections of the hydrocyclone through its progression through the hydrocyclone for one run is shown in Figure 39. A, B and C denote the three main sections of the hydrocyclone:

- A represents the feed inlet and vortex finder section;
- B is the cylindrical and conical section;
- C is the apex section.

A spike in count frequency between [225,350] in section B displays a prolonged residence time in the conical section as opposed to the rest of the hydrocyclone. This behaviour is consistent in the subsequent runs. The resin tracer particles spend the bulk of their time in section B.

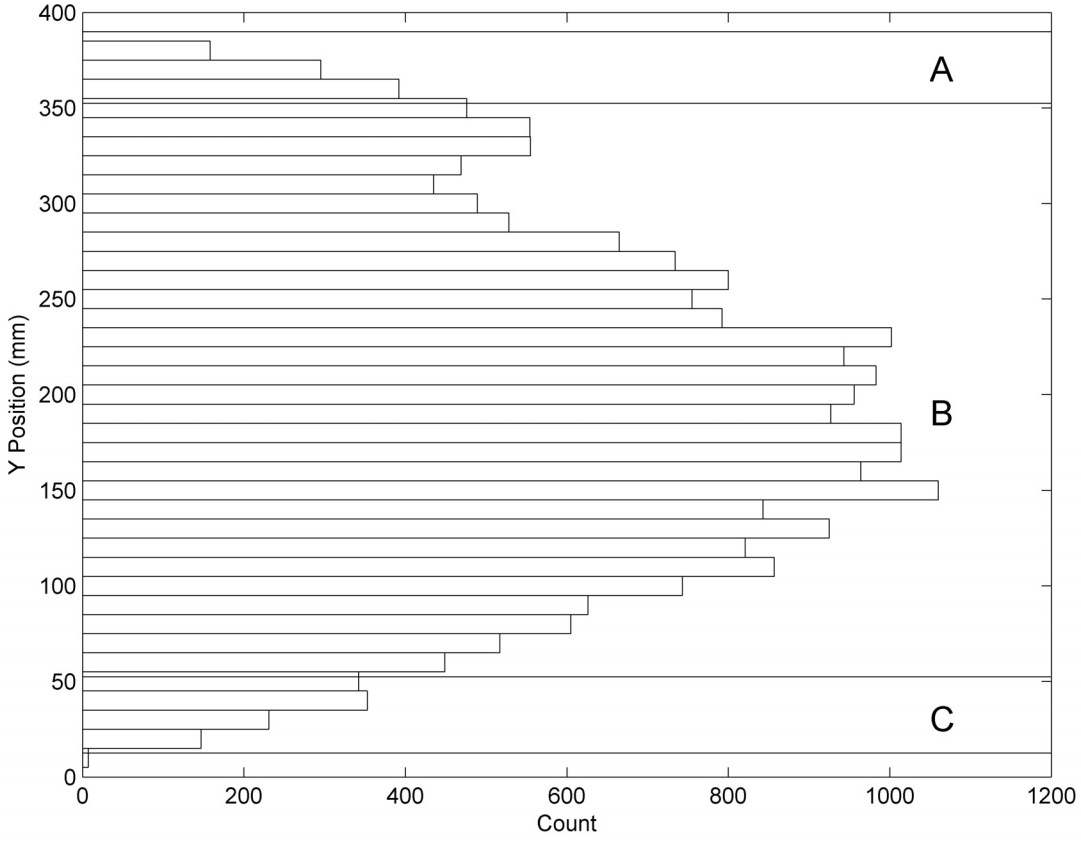

Figure 39: Frequency of particle appearance in different sections of the hydrocyclone in run 1 of test A

4.1.1.3. Residence Time

Table 5 summarizes the average residence time of the resin tracer particle inside the standard hydrocyclone starting from the feed inlet and ending at the apex. The average residence time range is between 315.0 to 465.7 ms for the tracer particle inside the hydrocyclone for all the test runs. This range falls within the 90% confidence level interval. Each run ended with the leaching of the tracer particle into the system.

Table 5: Residence time for standard hydrocyclone underflow passes (from feed inlet)

test run	Underflow				
	contributing passes	average residence time (ms)	standard deviation (ms)	90% confidence level interval	
1	47	384.0	45.2	373.1	394.9
2	24	409.7	58.9	389.9	429.4
3	11	386.4	40.0	366.6	406.2
4	18	465.7	75.6	436.4	495.0
5	11	416.2	54.2	389.3	443.1
6	15	315.0	50.4	293.6	336.4

4.1.1.4. *Velocity map*

The Eulerian velocity maps, Figure 40, were obtained for run 1 of the standard hydrocyclone by averaging the calculated instantaneous Lagrangian velocities along the trajectory of each new tracer pass over a three dimensional grid using the 6-point method described by Leadbeater et al. (Leadbeater et al., 2012).

[a]

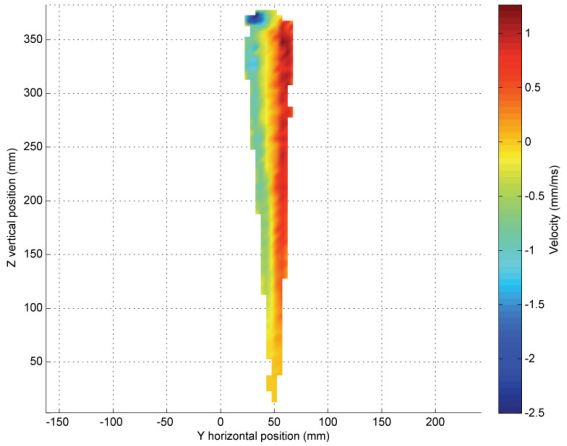

[b]

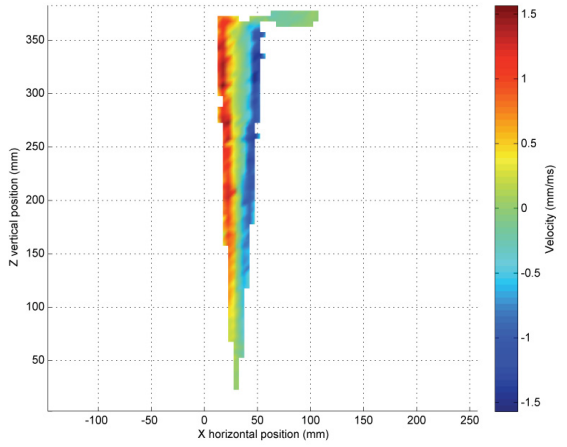

[c]

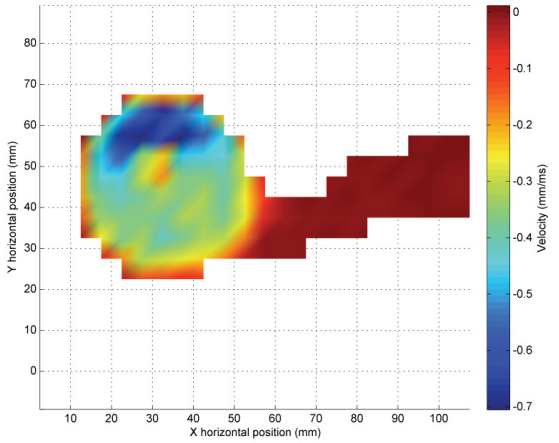

Figure 40: Eulerian velocity maps for run 1 in test A; [a] x-axis, [b] y-axis and [c] z-axis

4.1.2. Stub hydrocyclone

4.1.2.1. Trajectory

A typical run inside a C126 hydrocyclone, stub model hydrocyclone, is shown in Figure 41 where each color represents a separate pass. There were 11 passes through the field of view which are shown in the full data set in Figure 41. The tracer particle then broke and the activity leached into the surrounding system due to abrasion from the pump on the particle coating. The leaching of the activity into the system was a problem for every test run as the abrasion of the pump on the epoxy coating was faster than the half-life of the tracer thereby shortening the experimental run significantly. The position in the hydrocyclone can be defined as the time the particle takes to complete its trajectory to either the apex or overflow pipe. For this test, all tracer particles reported to the underflow and exited through the apex. For each pass, the particle entered via the feed inlet and progressed downwards in a clockwise vortex.

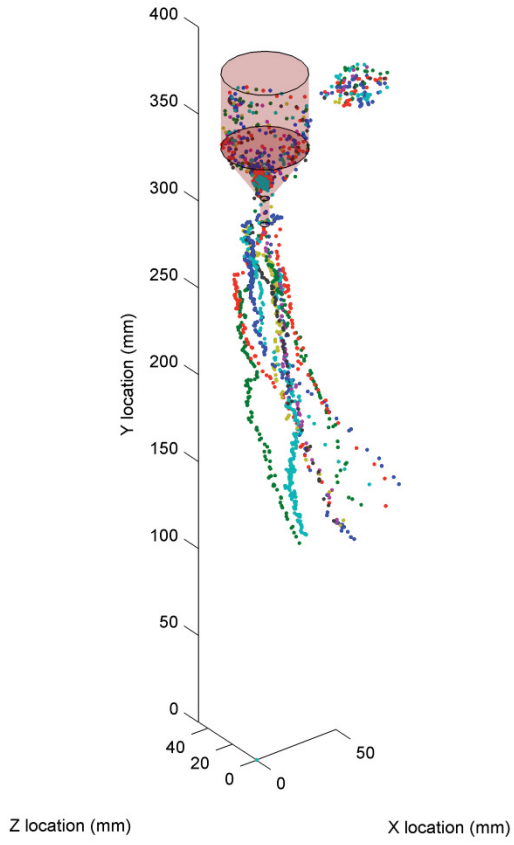

Figure 41: 11 trajectory passes for run 1 of test B

Figure 42 shows a typical pass for a the resin tracer particle inside the stub two inch hydrocyclone reporting to the underflow, the color gradient shows the time from the particle entering the field of view

and exits. The particle enters through the feed inlet at t=0 and rotates downwards along the hydrocyclone wall in a clockwise direction.

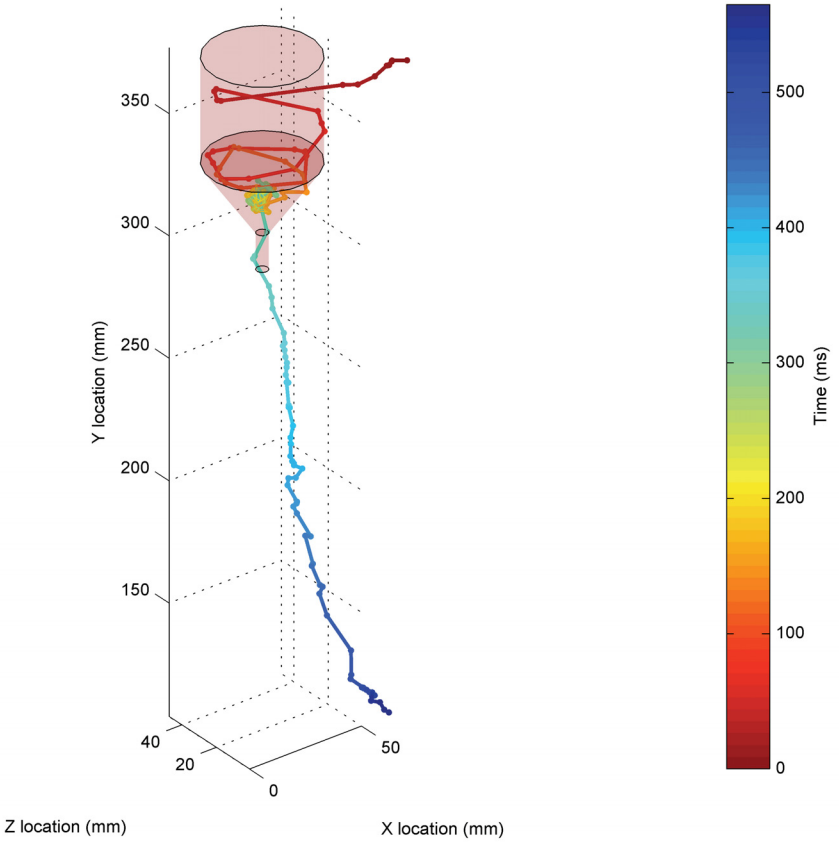

Figure 42: Trajectory of particle for pass 1 in run 1 of test B

Figure 43 shows in a breakdown of pass 1 in run 1 of test B between y=300 and y=350 in the conical section. This is consistent with subsequent passés to the underflow within run 1.

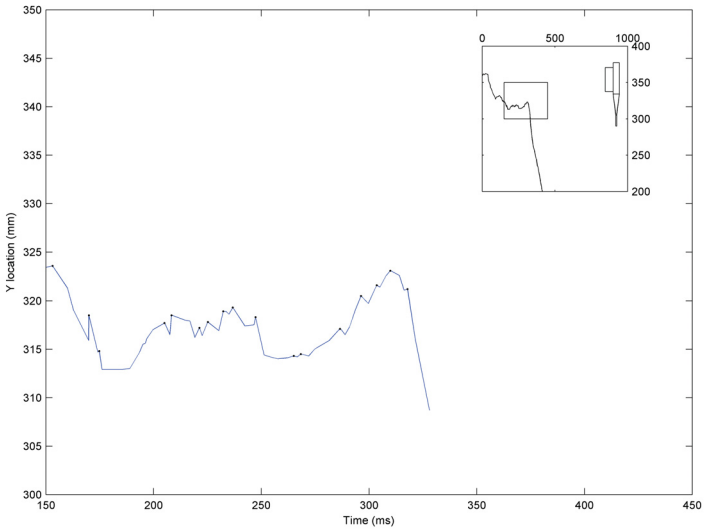

Figure 43: Trajectory of particle for pass 1 in run 1 of test B in the y-direction highlighting local maxima

Subsequent runs with the stub hydrocyclone yielded tracer particles reporting to the overflow as shown in Figure 44 where each color represents a separate pass. There were 7 passes through the field of view which are shown in the full data set in Figure 44. The tracer particle then broke and the activity leached into the surrounding system due to abrasion from the pump on the particle coating. The position in the hydrocyclone can be defined as the time the particle takes to complete its trajectory to either the apex or overflow pipe.

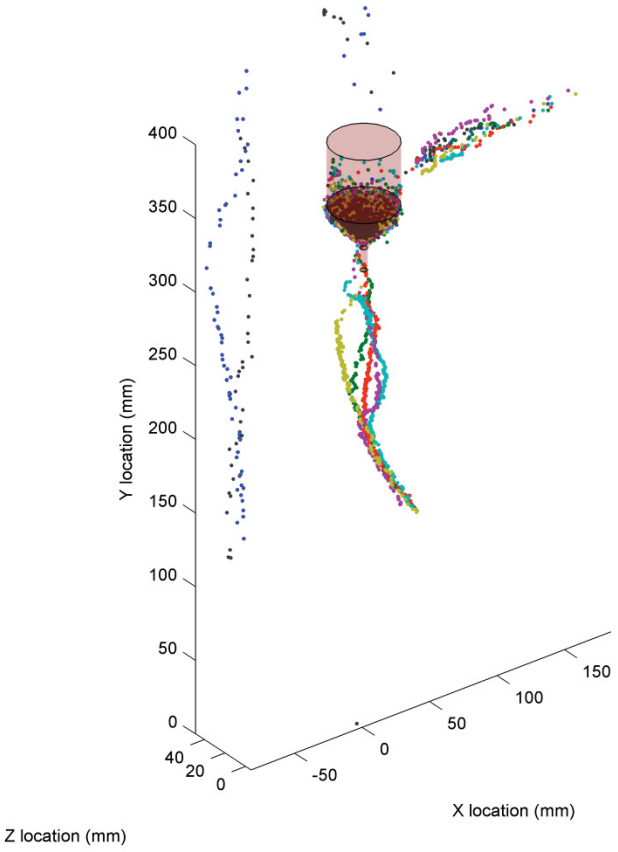

Figure 44: 7 trajectory passes for run 2 of test B

Figure 45 shows a pass for a tracer particle inside the stub two inch hydrocyclone reporting to the overflow. The residence time for the tracer particle reporting to the overflow inside the hydrocyclone increases by an order of magnitude. This is consistent with subsequent passes to the overflow within the stub hydrocyclone.

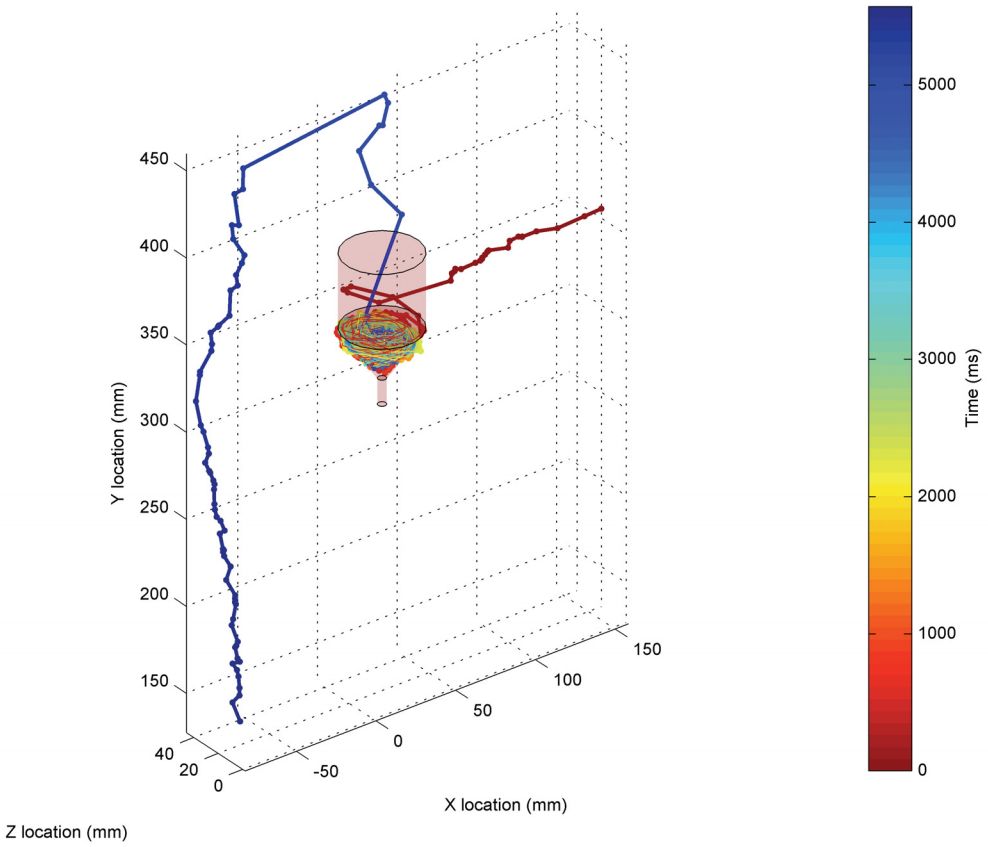

Figure 45: Trajectory of particle for pass 2 in run 2 of test B

Figure 46 shows a pass for run 2 of test B where the resin tracer particle exits via the apex through the underflow with a residence time with an order of magnitude higher seen in run 1 of test B.

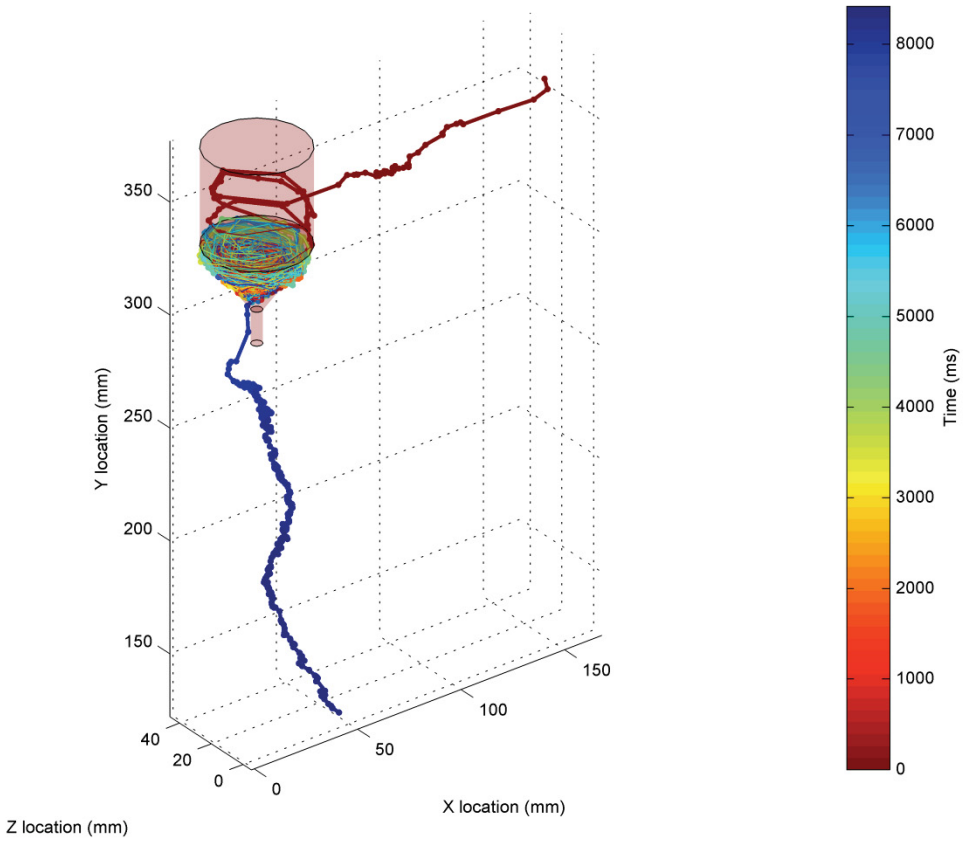

Figure 46: Trajectory of particle for pass 3 in run 2 of test B

4.1.2.2. Frequency

The frequency of resin tracer particle's appearance in different sections of the stub hydrocyclone through its progression through the hydrocyclone for one run is shown in

Figure 47. A, B and C denote the three main sections of the hydrocyclone:

- A represents the feed inlet and vortex finder section;
- B is the conical section;
- C is the apex section.

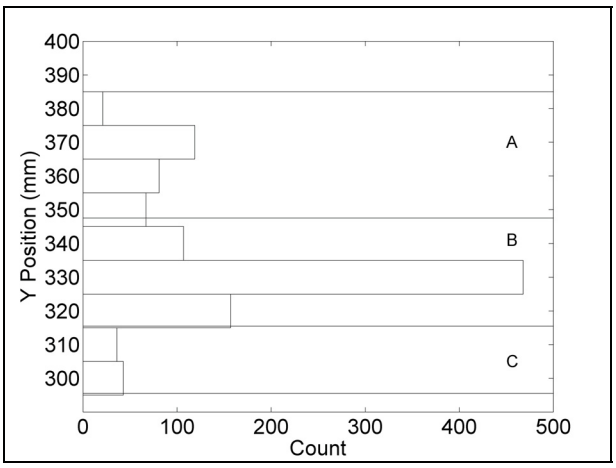

Figure 47: Frequency of particle appearance in different sections of the hydrocyclone in run 1 of test B

4.1.2.3. Residence Time

Table 6 summarizes the average residence time of the resin tracer particle inside the stub hydrocyclone starting from the feed inlet and ending at the apex. Each run ended with the leaching of the tracer particle into the system.

Table 6: Residence time for stub hydrocyclone underflow passes (from feed inlet)

test run	Underflow				
	contributing passes	average residence time (ms)	standard deviation (ms)	90% confidence level interval	
1	11	294.0	157.3	216.0	372.0
2	5	7613.3	5760.3	3376.0	11850.6
3	1	144.5	-	-	-
4	4	2515.3	2280.0	640.1	4390.4

Table 7 summarizes the average residence time of the tracer particle inside the stub hydrocyclone starting from the feed inlet and ending at the overflow.

Table 7: Residence time for stub hydrocyclone overflow passes (from feed inlet)

test run	Overflow				
	contributing passes	average residence time (ms)	standard deviation (ms)	90% confidence level interval	
1	0	-	-	-	-
2	2	10982.1	8478.1	1121.4	20842.8
3	3	1433.4	792.4	681.0	2185.9
4	1	1058.8	-	-	-

4.2. Silica slurry system study results

The second study was comprised of two tests with silica tracer particles, coarse and fine, in a silica slurry system passing through a standard hydrocyclone model respectively to examine the motion of a particle inside a hydrocyclone. The two size classes of silica tracer are above the approximate cut-size of the two-inch hydrocyclone (20-50 μm), i.e., under the experimental conditions the tracer particles should report to the underflow (Chandrasekhar and Raghavan, 2004). Gross-oversize particles are defined as solid particles whose size are above the coarse shoulder of the particle size distribution curve and are statistical outliers from the rest of the population. Gross-oversize particles can be 2 to 5 times greater than the median size (Dumm, 2005). The size of the tracer particles used were to maximize activity as previous PEPT testing have had difficulties with small particle sizes with direct activation (Fan et al., 2006b). The effect of shielding near the vortex finder was not considered as the air core area is under 10% even at high slurry concentration (Gutiérrez et al., 2000).

4.2.1. Coarse tracer particle

Throughout the experiment, the coarse (-2000+1700 μm) silica tracer particles passed through the detector field of view. This allowed the camera to capture the fast moving particle in the primary vortex. The results of a run consist of a set of single particle locations in 3D with time. The tracer particle decreased in activity as the run progressed. The end of a run was when no discernible activity in the tracer particle could be recorded. The position in the hydrocyclone can be defined as the time the particle takes to complete its trajectory to either the apex or overflow pipe. For this test, all tracer particles reported to the underflow and exited through the apex. For each pass, the particle entered via the feed inlet and progressed downwards in a counterclockwise vortex.

4.2.1.1. Trajectory

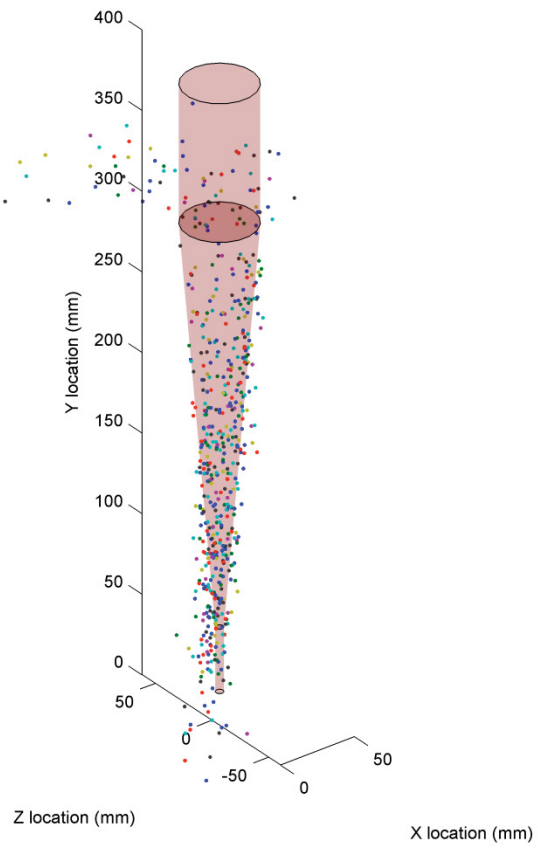

Figure 48: Trajectory of all 25 passes for test 1

All passes for test 1 are shown in Figure 48 where each color represents a pass. There are 25 passes. A typical pass for test 1 is shown in Figure 49, the coarse silica tracer particle inside the standard two inch hydrocyclone reporting to the underflow, the color gradient shows the time from the particle entering the field of view and exits. The particle enters through the feed inlet at t=0 and rotates downwards along the hydrocyclone wall in a counterclockwise direction. Figure 50 highlights the vortex breakdown for pass 1 in test 1.

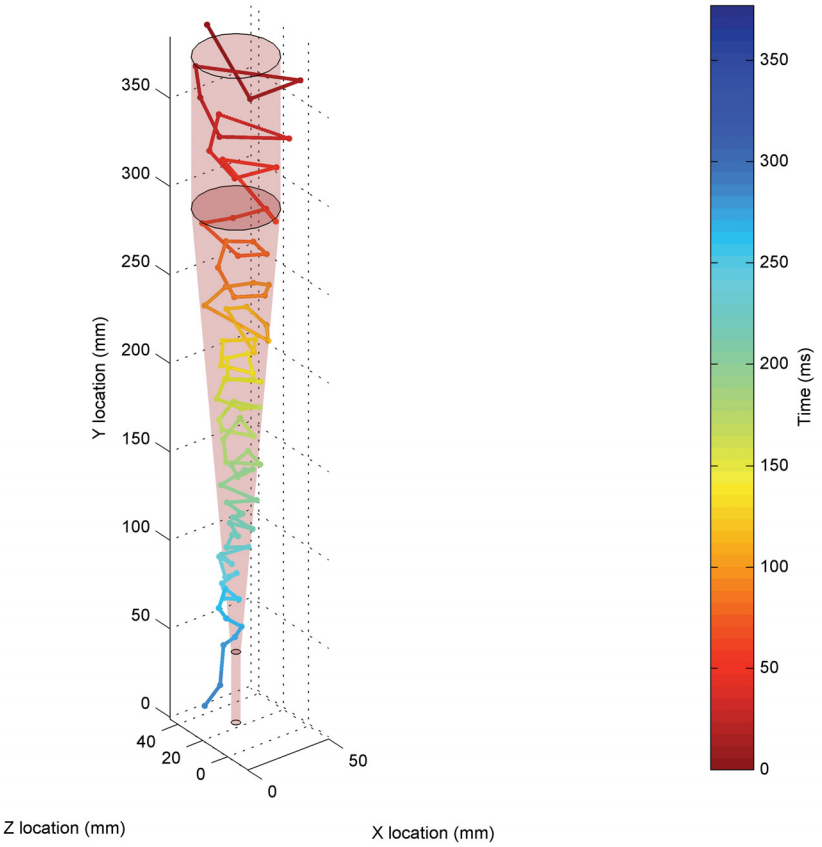

Figure 49: Trajectory of particle for pass 1 in test 1

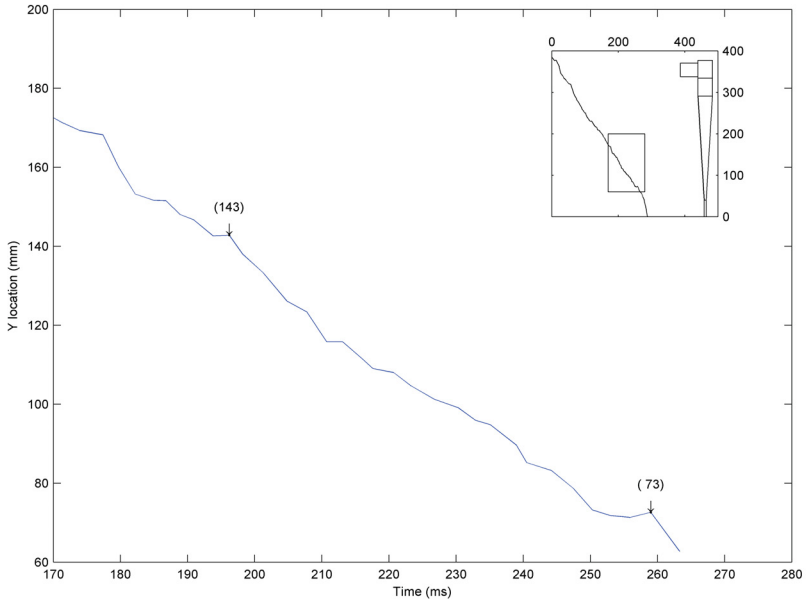

Figure 50: Trajectory of particle for pass 1 in test 1 in the y-direction highlighting local maxima

4.2.1.2. Frequency

The frequency of coarse silica tracer particle's appearance in different sections of the standard hydrocyclone through its progression through the hydrocyclone for one run is shown in Figure 51. A, B and C denote the three main sections of the hydrocyclone:

- A represents the feed inlet and vortex finder section;
- B is the conical section;
- C is the apex section.

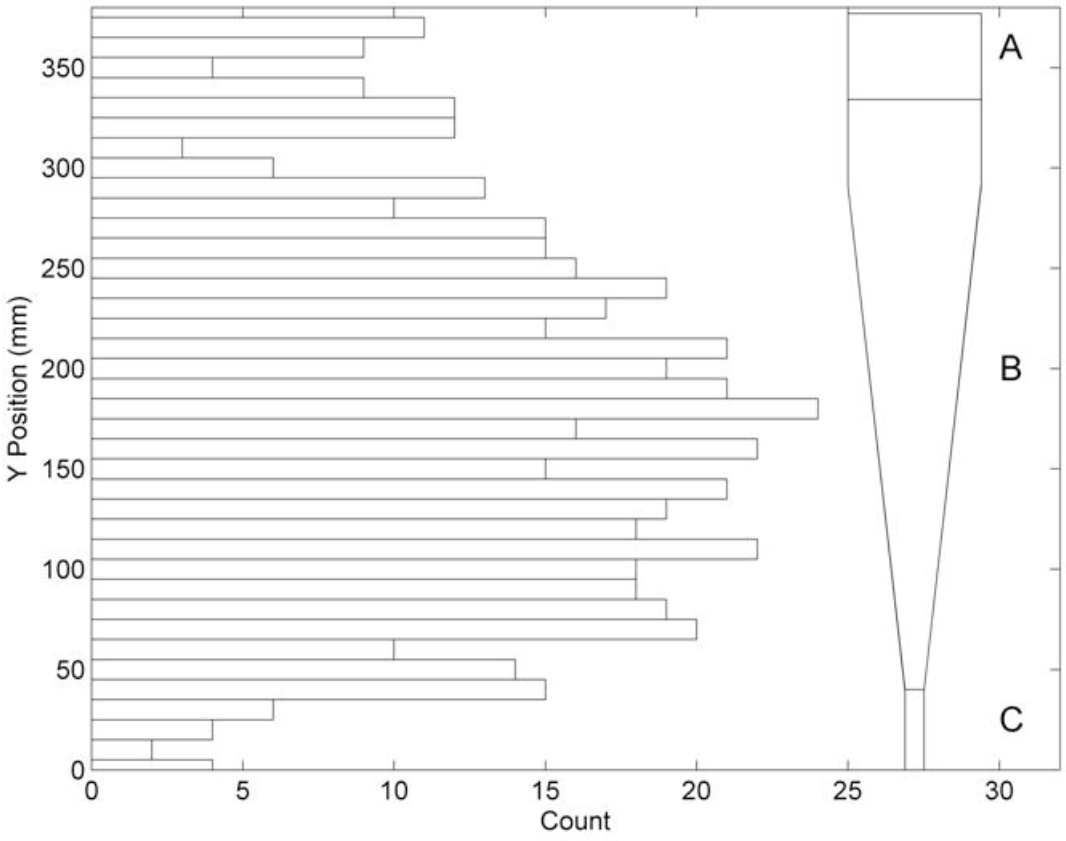

Figure 51: Frequency of particle appearance in different sections of the hydrocyclone in test 1

4.2.2. Fine tracer particle

Throughout the experiment, the fine (-250+150 μm) silica tracer particles passed through the detector field of view. This allowed the camera to capture the fast moving particle in the primary vortex. The results of a run consist of a set of single particle locations in 3D with time. The tracer particle decreased in activity as the run progressed. The end of a run was when no discernible activity in the tracer particle could be recorded. The position in the hydrocyclone can be defined as the time the particle takes to complete its trajectory to either the apex or overflow pipe. For this test, all tracer particles reported to

the underflow and exited through the apex. For each pass, the particle entered via the feed inlet and progressed downwards in a counterclockwise vortex.

4.2.2.1. Trajectory

All 25 passes for test 2 is shown in Figure 52, where each color represents a different pass.

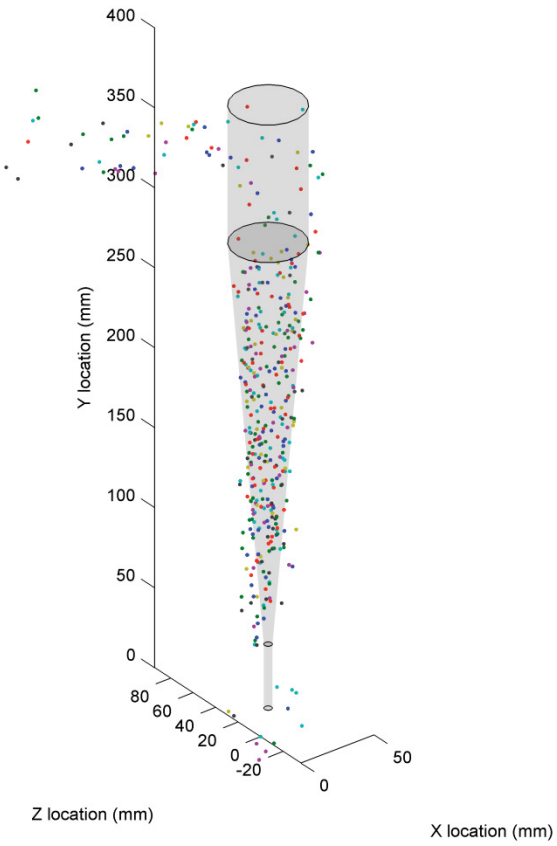

Figure 52: Trajectory of all 25 passes for test 2

A typical pass for test 2 is shown in Figure 53 the fine silica tracer particle inside the standard two inch hydrocyclone reporting to the underflow, the color gradient shows the time from the particle entering the field of view and exits. The particle enters through the feed inlet at t=0 and rotates downwards along the hydrocyclone wall in a clockwise direction. There are less data points for the fine tracer as the smaller particle has a lower activity. All passes for the run were similar in behavior.

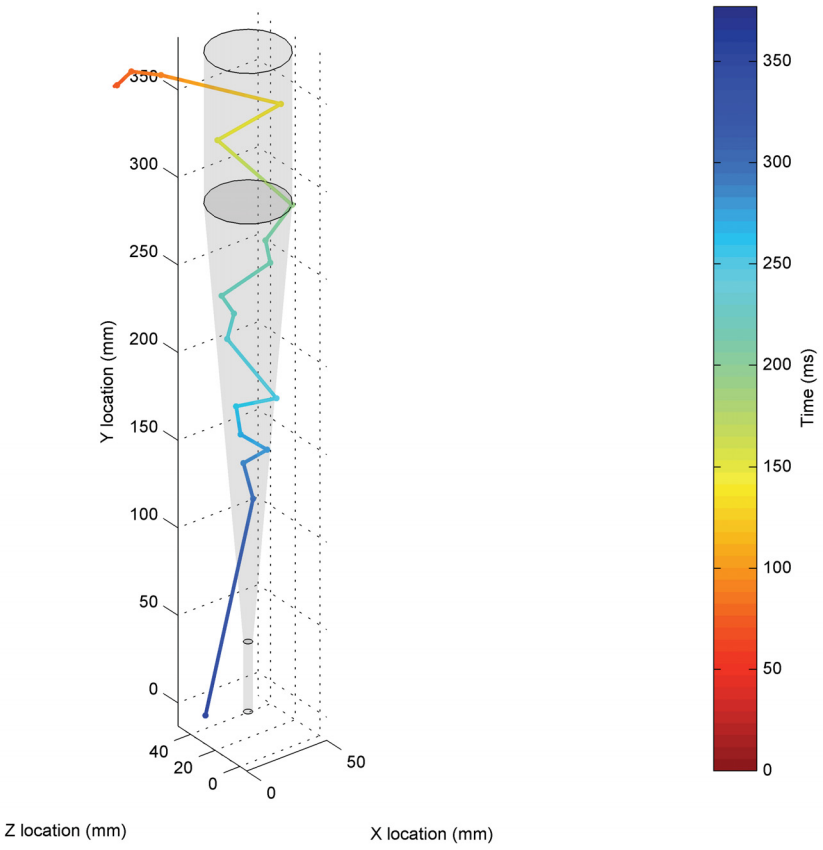

Figure 53: Trajectory of particle for pass 20 in test 2

4.2.2.2. Frequency

The frequency of fine silica tracer particle's appearance in different sections of the standard hydrocyclone through its progression through the hydrocyclone for one run is shown in Figure 54. A, B and C denote the three main sections of the hydrocyclone:

- A represents the feed inlet and vortex finder section;
- B is the conical section;
- C is the apex section.

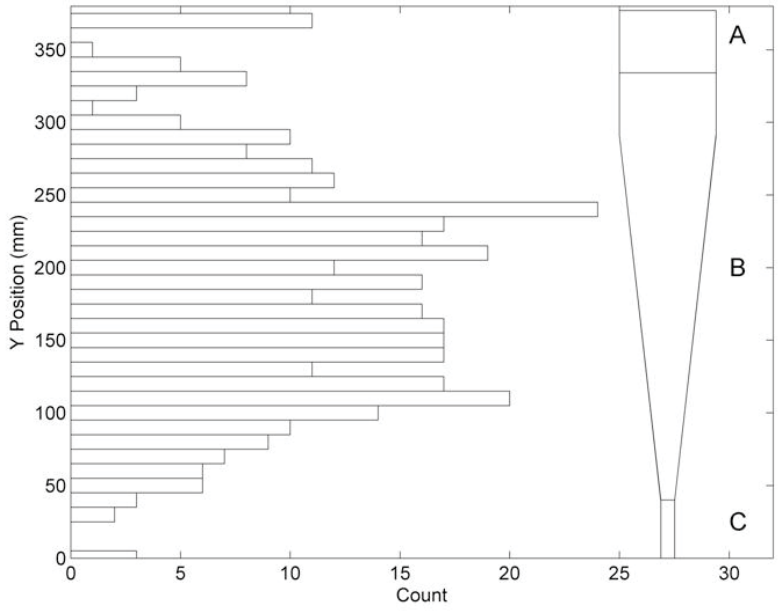

Figure 54: Frequency of particle appearance in different sections of the hydrocyclone in test 2

4.2.3. Residence time

Figure 55 summarizes the residence time for both coarse and fine runs.

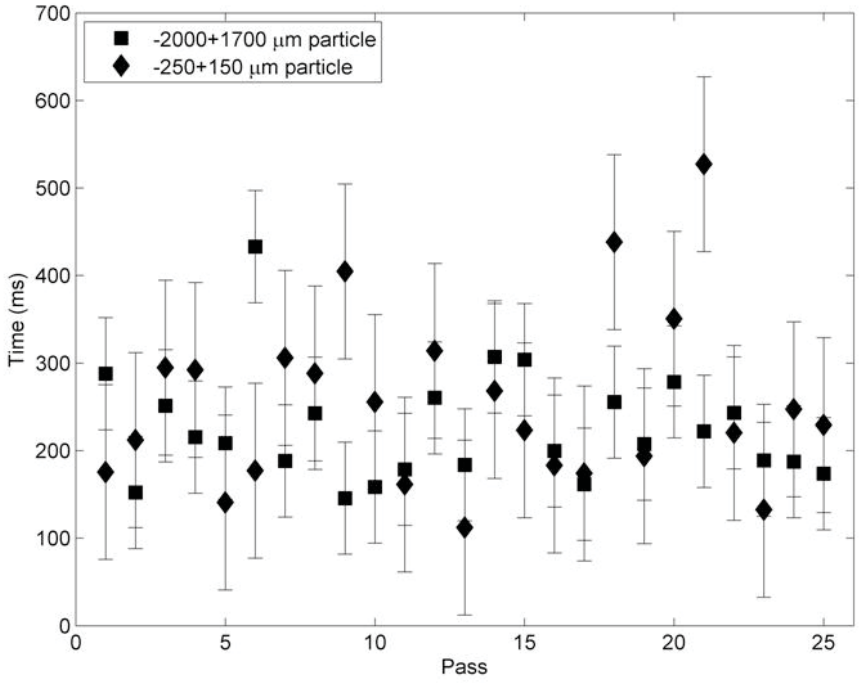

Figure 55: Residence time of coarse and fine silica particles inside hydrocyclone

5. Discussion

The results from the water system study and silica slurry study both show that PEPT is a valid technique for visualizing in situ the particle flow in hydrocyclones. It is the first time that an individual particle is tracked inside a hydrocyclone without altering the flow or simplifying the system to suit an imaging technique. Chang *et al.* injected a tracer particle into the inlet feed pipe rather than let the tracer particle re-circulate inside the system under normal operating conditions and enter the hydrocyclone at random (Chang et al., 2011). Previous studies have not attempted to track individual particles inside a hydrocyclone system in slurry either from the perspective of the feed particles (Section 2.3) due to the limitations of previous tracking techniques. With PEPT, particles inside small diameter two inch hydrocyclones are visualized without altering the system. It brings a unique perspective of particle flow and extends the understanding of flow in hydrocyclone theory.

5.1. Water system study

The water system study was conducted with irradiated resin beads using the ion exchange labeling technique that were coated in an epoxy resin to prevent leaching into the system. The epoxy resin coating was rapidly abraded by the pump as the particle re-circulated in the system. This was the first time in PEPT testing that the epoxy resin coating wore off and the activity leached into the system. The pump was a typical lab scale pump for the hydrocyclone but the epoxy resin coating wore off before even tracer activity reduced due to the short half-life of the radioisotope used. The study looked at two small diameter hydrocyclones, the standard two inch diameter hydrocyclone and the stub two inch diameter hydrocyclone. The size of the hydrocyclones tested was chosen as the entire hydrocyclone could be visualized in the field of view of the PEPT camera. With respect to the cut-size of the two-inch hydrocyclone models, which is under 50 μm, the size range of the resin beads used as tracer particles was between 500 and 700 μm therefore the resin beads were hypothesized to report only to the underflow as the first study was also testing the feasibility of PEPT tracking particles inside a hydrocyclone with adequate resolution of particle locations. A large tracer particle was used to have a substantial activity throughout the course of the experimental testing.

5.1.1. Standard hydrocyclone

Test A was with the standard hydrocyclone setup. For one run, Figure 34 shows 47 passes through the field of view. The position in the hydrocyclone can be defined as the time the particle takes to complete its trajectory to either the apex or overflow pipe. For this test, all tracer particles reported to the underflow and exited through the apex. For each pass, the particle entered via the feed inlet and

progressed downwards in a clockwise vortex. The pitch of the vortex becomes smaller before moving to the right cone wall. There is the characteristic end of the vortex observed, highlighted in Section 2.2.3.6. As the end of vortex is seen in all 47 passes in run 1, in the lower part of the cone section, it shows that the natural vortex length is shorter than the designed hydrocyclone. The natural length is characterized from the beginning of the entrance of the vortex finder to where the vortex breaks down.

As the hydrocyclone flow is turbulent, the end of the vortex is seen to attach to the side wall of the cone. The vortex core is bent but does not precess around the wall for long before it resumes a vortex and exits through the apex. The particle also moves up in the conical section. There are two explanations in theory to the end of vortex phenomenon but actually vortex precession and vortex breakdown are both seen in every pass. Both types of phenomenon are both visualized for the first time in this study. This is also highlighted in Figure 37, followed by its highlighted breakdown in Figure 38. The vortex breakdown and vortex precession is consistently in the lower conical section between the range of y=200 mm and y=150 mm. Such that the vortex end is characteristic in this hydrocyclone. So the natural length is a measurable design factor.

The vortex motion does not completely cease in the axial direction at the point of vortex breakdown but a secondary vortex towards the apex is induced downstream. As stated in Section 2.2.3.6, this is a type of fluid coupling. It had been previously hypothesized that the induction of the secondary vortex is related to the precession of the primary vortex but precession and vortex breakdown occurs at the same time and as the vortex is drawn towards the cone wall the particle also moves upwards before resuming a new induced vortex before exiting through the apex. The same rotational sense is always observed between the primary vortex and the induced vortex.

Section 2.2.3.5 hypothesizes that there would be a stagnant zone between the end of vortex and the apex. This was not observed as the particle continued to move and was moving in a vortex before exiting through the apex after the end of vortex in the lower part of the conical section. This brings a new insight on the natural length of the vortex and hydrocyclone design as it was previously noted that longer hydrocyclone designs are prone to random short circuiting (Alexander, 1949). This end of the natural vortex in the conical section shortens the effective separation space to an extent such that it has an undesirable effect on separation performance as well as re-entrainment of previously separated particles. The end of the natural vortex in the hydrocyclone also is a source of wear on the hydrocyclone as the vortex precession causes particles to rotate closer to the hydrocyclone wall. Understanding the dynamics of the end of vortex can improve hydrocyclone design and performance.

The frequency of resin tracer particle's appearance in different sections of the hydrocyclone through its progression through the hydrocyclone for one run is shown in Figure 39. This behavior is consistent in the subsequent runs. The resin tracer particles spend the bulk of their time in section B. This is proof that the natural length of the vortex breakdown increases the residence time of the particle as it is moving upwards before the induced vortex bring the particle to the apex. Although previous literature spoke of particle stagnation, the particle is moving but just in the opposite direction before the secondary vortex is induced.

Table 5 summarizes the average residence time of the resin tracer particle inside the standard hydrocyclone starting from the feed inlet and ending at the apex. The average residence time range is between 315.0 to 465.7 ms for the tracer particle inside the hydrocyclone for all the test runs. This range falls within the 90% confidence level interval. The tracer particles spent the longest amount of time in the conical section due to the vortex precession and vortex breakdown.

The Eulerian velocity maps in Figure 40, were obtained for run 1 of the standard hydrocyclone by averaging the calculated instantaneous Lagrangian velocities along the trajectory of each new tracer pass over a three dimensional grid using the 6-point method described by Leadbeater *et al.* (Leadbeater et al., 2012). These velocity maps are unsmoothed and lack interpolation to compensate for unvisited areas of the hydrocyclone by the tracer particle, for those reason velocity maps of subsequent runs offer no qualitative insight due to the limited number of passes for each run before the tracer particle's coating leached into the system. The particle velocity is mapped as a function of position. The average velocities along the axis out of the page are shown for a particle moving with approximately circular motion in the standard hydrocyclone. Particles are moving into the page (negative velocity) on the left and out of the page (positive velocity) on the right with the color gradient shows the velocity. The maximum axial velocity in the x-axis and y-axis respectively in Figure 40 [a] and Figure 40 [b] is approximately 1.5 m/s while the maximum axial velocity in the z-axis in Figure 40 [c] is 0.7 m/s. There is evidence of a LZVV towards the hydrocyclone's vertical axis. The particles lying on the locus will be subjected to equal and opposing centrifugal and drag forces leading to an equal chance of reporting either to the underflow or overflow. In the case of the standard hydrocyclone, all tracer particles reported to the underflow such that there is a zero velocity along the center vertical axis of the hydrocyclone. Despite these velocity maps only representing one test run, they are the first results highlighting measured particle velocity, which could not have been visualized by other imaging techniques.

5.1.2. Stub hydrocyclone

Test B was with the stub hydrocyclone setup. For one run, Figure 41 shows 11 passes through the field of view. The position in the hydrocyclone can be defined as the time the particle takes to complete

its trajectory to either the apex or overflow pipe. For this run, all tracer particles reported to the underflow and exited through the apex. For each pass, the particle entered via the feed inlet and progressed downwards in a clockwise vortex. Figure 42 shows a typical pass for a the resin tracer particle inside the stub two inch hydrocyclone reporting to the underflow, the color gradient shows the time from the particle entering the field of view and exits. The particle enters through the feed inlet at t=0 and rotates downwards along the hydrocyclone wall in a clockwise direction. The tracer particle then broke and the activity leached into the surrounding system due to abrasion from the pump on the particle coating. The leaching of the activity into the system was a problem for every test run as the abrasion of the pump on the epoxy coating was faster than the half-life of the tracer thereby shortening the experimental run significantly. This was mitigated in silica slurry system testing by using the direct activation labeling technique rather than the ion exchange labeling technique as it did not require an epoxy coating. The ^{18}F in the particle exists as a structural element within a layer approximately 0.3 mm from the particle's surface which mitigates abrasion compared to the ion exchange labeling technique. Another alternative to the abrasion wear of the epoxy coating would be to not recirculate though this limits the number of successful runs to just one per particle. The diameter of the vortex decreases as the particle moves into the conical section of the hydrocyclone and the pitch also decreases within the conical section of the hydrocyclone in its downward progression towards the apex. Right before the apex, the vortex motion seems to deteriorate and becomes more irregular in its movement, as if the particle is trapped axially in a turbulent flow upwards towards the vortex finder, as shown in greater detail in Figure 43. This is consistent with all subsequent passes. This extends the particle's residence time inside the conical section. This is characteristic of the end of the vortex phenomenon highlighted in Section 2.2.3.6. The natural length is characterized from the beginning of the entrance of the vortex finder to where the vortex breaks down is significantly shorter in the stub hydrocyclone. Figure 42 shows the characteristic of vortex breakdown as the particle moves up and down in its downwards flow to the apex rather than vortex precession in the case of end of vortex phenomenon. Such that end of vortex occurs in both hydrocyclone models regardless of cone length.

Subsequent runs with the stub hydrocyclone yielded tracer particles reporting to the overflow as shown in Figure 44 for run 2 where each color represents a separate pass. Test runs 2-4 recorded particles reporting to both the underflow and overflow which accounting the increased residence time for the particles reporting to the underflow as some display the trajectory shown in Figure 42 while others display the trajectory shown in Figure 46. Test run 3 only had one contributing pass before the particle's activity was leached into the system due to the coating degradation due to the abrasion from the pump. Further runs are required to get better statistical variance. For run 2 there were 7 passes through the field

of view which are shown in the full data set in Figure 44. The tracer particle then broke and the activity leached into the surrounding system due to abrasion from the pump on the particle coating. The position in the hydrocyclone can be defined as the time the particle takes to complete its trajectory to either the apex or overflow pipe. Although the cut-size of the stub hydrocyclone is higher than the standard hydrocyclone, it was still an order of magnitude below the size of the resin tracer particles used for the study. Figure 45 shows a pass for a tracer particle inside the stub two inch hydrocyclone reporting to the overflow. The residence time for the tracer particle reporting to the overflow inside the hydrocyclone increased by an order of magnitude opposed to particles reporting to the underflow. The particle enters the hydrocyclone tangentially via the inlet and sets up a primary outer vortex which flows downwards towards the apex before becoming trapped in a turbulent re-circulating eddy flow at the outer radius of the vortex finder wall before exiting in the overflow. This is consistent with subsequent passes to the overflow within the stub hydrocyclone. This is characteristic of short circuiting of particles. The particles that reported to the overflow were random as the particles had a prevalent disposition to report to the underflow. Figure 46 shows a pass for run 2 of test B where the resin tracer particle exits via the apex through the underflow. The resin particle primary clockwise vortex breaks down in the conical section of the stub hydrocyclone and spends a significant time there before exiting through the apex. It could have reported to the overflow but still it exited via the apex. Such behavior in particles in hydrocyclones is difficult to predict but it is interesting that in stub hydrocyclones the effect of the eddy currents around the vortex finder are stronger and have a direct impact on the particle's trajectory. The end of vortex phenomenon is seen, though there is also an effect of re-circulating eddy flows in play for run 2, highlighted by Figure 44. Re-circulating eddy currents have a direct impact on hydrocyclone efficiency. Even with the cut-size being an order of magnitude lower than the resin tracer particles, short circuiting still occurred. This with the end of vortex phenomenon extended the particle's residence in the hydrocyclone such that it had an adverse effect on hydrocyclone performance. It is important to make note of the natural vortex length when designing hydrocyclones.

The frequency of resin tracer particle's appearance in different sections of the stub hydrocyclone through its progression through the hydrocyclone for one run where the particle only exits through the apex is shown in

Figure 47. The resin tracer particles spend the bulk of their time in section B. The stub hydrocyclone has a shorter conical section and with the prolonged residence it increases the likelihood of particles being taken up by re-circulating eddy flows near the top plate of the hydrocyclone and near the vortex finder. A closer examination is needed to see if vortex precession occurs although it is difficult to tell as re-circulating eddy currents make it difficult to see if the vortex is bending towards the cone wall.

The presence of a stagnant area may also account for the order of magnitude difference in residence time. The particles are moving but at a localized height.

Table 6 summarizes the average residence time of the resin tracer particle inside the stub hydrocyclone starting from the feed inlet and ending at the apex, i.e. reporting to the underflow. Each run ended with the leaching of the tracer particle into the system. Test 1 had passes that reported only to the underflow and the 90% confidence interval was between 216.0 ms and 372.0 ms with an average residence time of 294.0 ms. Runs where both particles went to either the overflow or underflow has an order of magnitude higher residence time. This can be attributed to re-circulating eddy flow effect on particles. Table 7 summarizes the average residence time of the tracer particle inside the stub hydrocyclone starting from the feed inlet and ending at the overflow. All average residence times fall inside the 90% confidence interval. Further runs are needed to get better statistical variance as 30% of the passes in the stub hydrocyclone runs report to the overflow. They differ from the residence time of particles reporting to the underflow by a magnitude higher which suggests that particles that short circuit spend a longer time inside the hydrocyclone before short circuiting through the vortex finder. Such that increasing a particle's residence time in a hydrocyclone has adverse effects on separation efficiency. Further runs are needed to get better statistical variance as 30% of the passes in the stub hydrocyclone runs report to the overflow.

5.2. Silica slurry system study

The silica slurry system study was done with irradiated silica using the direct activation labeling technique to prevent leaching into the system. This was the first time in hydrocyclone visualization that dense slurry was used as the medium. Testing before hand was in lightly seeding mediums. In the silica slurry study here the silica slurry was used with a percent solid of approximately 3.8%. The runs were stopped when tracer activity was too low to register detections on the PEPT camera. The study looked at two tracer particle sizes, -2000+1700 μm (coarse) silica tracer particle and the -250+150 μm (fine) silica tracer particle in the standard two inch diameter hydrocyclone. This study was to visualize particle flow in slurry and see the difference compared to previous studies in water systems and lightly seeded systems that are the basis of hydrocyclone theory today and to differentiate the behavior difference of particles in underflow.

5.2.1. Coarse particle tracer

Throughout the experiment, the coarse (-2000+1700 μm) silica tracer particles passed through the detector field of view. This allowed the camera to capture the fast moving particle in the primary vortex. The results of a run consist of a set of single particle locations in 3D with time. The tracer particle decreased in activity as the run progressed. The end of a run was when no discernible activity in the tracer

particle could be recorded. Figure 48 shows all 25 passes for test 1. The position in the hydrocyclone can be defined as the time the particle takes to complete its trajectory to either the apex or overflow pipe. For this test, all tracer particles reported to the underflow and exited through the apex. For each pass, the particle entered via the feed inlet and progressed downwards in a counterclockwise vortex. A typical pass for test 1 is shown in Figure 49, where the coarse silica tracer particle inside the standard two inch hydrocyclone reporting to the underflow, the color gradient shows the time from the particle entering the field of view and exits. The particle enters through the feed inlet at t=0 and rotates downwards along the hydrocyclone wall in a counterclockwise direction. The diameter of the vortex decreases as the particle moves into the cylindrical section of the hydrocyclone and tapers within the conical section of the hydrocyclone in its downward progression towards the apex. In the conical section at between y=60 and y=200, the particle no longer has a continuous downward trajectory but the particle moves upwards before continuing downwards. This extends the particle's residence time inside the conical section. The particle is also drawn towards the hydrocyclone left side cone wall in this downward flow and moves upwards before spirally downwards and out the apex. This is characteristic of the end of vortex phenomenon. Both vortex precession and vortex breakdown occur. The silica particle is in a slurry and still exhibits the end of vortex. Figure 50 highlights the vortex breakdown as well has the vortex precession as the particle moves to the left cone wall. Vortex breakdown seems to occur before vortex precession. This behavior is characteristically seen from midpoint of the conical section towards the apex; i.e. the vortex motion seems to deteriorate towards the apex, in all measured data. Compared to the water system study, the vortex breakdown occurs higher in the cyclone which suggests a link in natural vortex length and percent solids of feed. The coarse silica tracer particle's appearance in different sections of the standard hydrocyclone through its progression through the hydrocyclone for one run is shown in Figure 51. The coarse silica tracer particles spend the bulk of their time in the lower of section B.

5.2.2. Fine particle tracer

Throughout the experiment, the fine (-250+150 μm) silica tracer particles passed through the detector field of view. This allowed the camera to capture the fast moving particle in the primary vortex. The results of a run consist of a set of single particle locations in 3D with time. The tracer particle decreased in activity as the run progressed. The end of a run was when no discernible activity in the tracer particle could be recorded. The position in the hydrocyclone can be defined as the time the particle takes to complete its trajectory to either the apex or overflow pipe. For this test, all tracer particles reported to the underflow and exited through the apex. For each pass, the particle entered via the feed inlet and progressed downwards in a counterclockwise vortex. All 25 passes for test 2 are shown in Figure 52. A typical pass for test 2 is shown in Figure 53 where the fine silica tracer particle inside the standard two inch hydrocyclone reporting to the underflow, the color gradient shows the time from the particle entering

the field of view and exits. The particle enters through the feed inlet at t=0 and rotates downwards along the hydrocyclone wall in a clockwise direction. The diameter of the vortex decreases as the particle moves into the cylindrical section of the hydrocyclone and tapers within the conical section of the hydrocyclone in its downward progression towards the apex. In the conical section at between y=100 and y=200, the particle no longer has a continuous downward trajectory but the particle moves upwards before continuing downwards. This extends the particle's residence time inside the conical section. The particle is also drawn towards the hydrocyclone right side cone wall in this downward flow and moves upwards before spirally downwards and out the apex. There are less data points for the fine tracer as the smaller particle has a lower activity. All passes for the run were similar in behavior. Vortex precession is seen as the particle does move to the cone wall and vortex breakdown in the sense that the particle does move axially upwards towards the vortex finder despite the minimal tracking points. The frequency of fine silica tracer particle's appearance in different sections of the standard hydrocyclone through its progression through the hydrocyclone for test 2 is shown in Figure 54. The fine tracer particles spend the bulk of their time in the higher part of section B than the coarse particles. This could be attributed to different selection zones but at the low activity, larger particle sizes are recommended in the future when testing with silica particles to improve precision.

5.2.3. Residence time of coarse and fine tracers

Figure 55 summarizes the residence time for both coarse and fine runs. The average residence time for the -2000+1700 µm silica tracer particle is 225.4 ms with a standard deviation of 64.1 ms. The average residence time for the -250+150 µm silica tracer particle is 252.8 ms with a standard deviation of 99.9 ms. A t-test established there was no statistical different between the residence time indicating that the coarse and fine particles reporting to the underflow spend the same time inside the hydrocyclone. There is no difference in residence in small or larger particles reporting to the underflow.

6. Conclusion & Future Work

PEPT technique can be used to understand the trajectory of particles inside hydrocyclones. PEPT camera have previously shown to be ability to visualize the high speed of the particle passing through small diameter hydrocyclones but previous PEPT studies have not attempted to track individual particles inside a hydrocyclone system in slurry. Previous studies have not attempted to track individual particles inside a hydrocyclone system in slurry either from the perspective of the feed particles due to the limitations of previous tracking techniques. With PEPT, particles inside small diameter two inch hydrocyclones are visualized without altering the system. It brings a unique perspective of particle flow and extends the understanding of flow in hydrocyclone theory. The trajectory of resin bead particles inside two inch stub and standard hydrocyclones has been visualized along with the residence time of the particles in water system. The evidence of a sudden change in the hydrocyclone flow pattern corresponding to the end of the vortex was observed in water and silica slurry systems. The end of vortex phenomenon was observed to have two characteristics, vortex precession and vortex breakdown and happen in unison and occurred in the neighborhood of the conical section.

The trajectory of silica particles inside two inch standard hydrocyclone has been visualized along with the residence time of the particles in water-particulate system (3.8% solids silica). The evidence of a sudden change in the hydrocyclone flow pattern corresponding to the end of the vortex was observed in a water-particulate system as well as the turbulent motion of the hydrocyclone flow. The end of vortex phenomenon was observed to have two characteristics, vortex precession and vortex breakdown and happen in unison in this study. A thorough understanding of the dynamics of the end of the vortex is essential to improve hydrocyclone performance. The two explanations in theory to the end of vortex phenomenon, vortex precession and vortex breakdown, are both visualized for the first time in this study. The end of the vortex came into the neighborhood of the conical section. This end of the natural vortex in the conical section shortens the effective separation space to an extent such that it has an undesirable effect on separation performance as well as re-entrainment of previously separated particles. Thus, understanding the dynamics of the end of vortex can improve hydrocyclone design and performance. The silica particles reporting to the underflow, the fine and coarse particles spend the same residence time in the hydrocyclone but the fine particle spend it in a region higher in the conical section compared to the coarser particle. This first imaging testing in slurry concentration in the feed has given a new appreciation of hydrocyclone imaging with respect to industrial applications.

This end of the natural vortex in the conical section shortens the effective separation space to an extent such that it has an undesirable effect on separation performance as well as re-entrainment of previously separated particles. The end of the natural vortex in the hydrocyclone also is a source of wear on the hydrocyclone as the vortex precession causes particles to rotate closer to the hydrocyclone wall. Understanding the dynamics of the end of vortex can improve hydrocyclone design and performance. The natural length of the vortex breakdown increases the residence time of the particle as it is moving upwards before the induced vortex brings the particle to the apex. Re-circulating eddy currents have a direct impact on hydrocyclone efficiency. Even with the cut-size being an order of magnitude lower than tracer particles, short circuiting still occurs. The re-circulating eddy flow can cause particles to short-circuit to the overflow has been observed in the stub hydrocyclone, resulting in an increased residence time inside the hydrocyclone of more than a factor of 10. Particles that spend a longer residency in the hydrocyclone have an increased probability to short circuit. The changes in velocity for the standard hydrocyclone have also been observed and highlight the LZVV. Coupled with the end of vortex phenomenon extended the particle's residence in the hydrocyclone such that it had an adverse effect on hydrocyclone performance. It is important to make note of the natural vortex length when designing hydrocyclones.

Future work will be to compare CFD modeling to the PEPT tracked data to test the validity of hydrocyclone models and previous imaging techniques with PEPT data. A thorough understanding of the dynamics of the end of the vortex is essential to improve hydrocyclone performance.

Appendix A

```
clc
clear all
close all

SAVE=1;
yy=[];

%loads individual passes
for A=1:25;
filename = (['outputa_', num2str(A)]);
%loads filename
refinedpass=xlsread(filename);
%converts structure array to cell array
%converts cell array to mat array
pass = refinedpass;
%counts the total amount of locations per pass
locations=length(pass);
%calculates time length of a pass
times=pass(:,1)-pass(1,1);

t=times;
x=pass(:,2);
y=pass(:,3);
z=pass(:,4);

yy=[yy; y];

end

%finds the maximum/minimum y coordinates
C = max(yy)
D = min(yy)

a=1;
%loads individual passes
for A=1:25;
filename = (['outputa_', num2str(A)]);
%loads filename
refinedpass=xlsread(filename);
%converts structure array to cell array
%converts cell array to mat array
pass = refinedpass;
%counts the total amount of locations per pass
locations=length(pass);

%reset y-coordinates to origin by a given factor
a1=124;
%reset x-coordinates to origin by a given factor
a2=302;
```

```
%reset z-coordinates to origin by a given factor
a3=221;
%reset time to start at 0
pass(pass(:,3)<a1,:) = [] ;
times=pass(:,1)-pass(1,1);

t=times;
x=pass(:,2);
z=pass(:,4);

%to fix the offset
for a=1:length(pass)
%y-coordinates
pass(a,3)=(pass(a,3)-a1);
%x-coordinates
pass(a,2)=(pass(a,2)-a2);
%z-coordinates
pass(a,4)=(pass(a,4)-a3);
end

%xyz locations over time - full data set

fig001a = figure
colormap gray;
plot(t,pass(:,2),'k x', 'MarkerSize', 5);
hold on
plot(t,pass(:,3), 'k +', 'MarkerSize', 5);
plot(t,pass(:,4), 'k *', 'MarkerSize', 5);
xlabel('Time (ms)');
ylabel('Position (mm)');
legend('X horizontal', 'Y vertical', 'Z horizontal',0);
grid on;
ylim([0 400]);
[str] = sprintf('fig001a%d', A);
print(fig001a, '-dpng', '-r500', str)
close(fig001a);

end


for A=1:25;

    filename = (['outputa_', num2str(A)]);
    %loads filename
    refinedpass=xlsread(filename);
    %converts structure array to cell array
    %converts cell array to mat array
    pass = refinedpass;

    locations=length(pass);
    %to reset time to start at 0
    %pass(pass(:,3)<a3,:) = [] ;
    times=pass(:,1)-pass(1,1);

    t=times;
```

```
    x=pass(:,2);
    z=pass(:,4);




    %to fix the offset in the y direction
 for a=1:length(pass)
     %y
    pass(a,3)=(pass(a,3)-a1);
    %x
    pass(a,2)=(pass(a,2)-a2);
    %z
    pass(a,4)=(pass(a,4)-a3);
 end

% pass(pass(:,3)<a3,:) = [] ;
y=pass(:,3);
x=pass(:,2);
    z=pass(:,4);

x=pass(:,2);
y=pass(:,3);
z=pass(:,4);

boomi=[x,y,z];
%        [R,t]=AxelRot(deg,u,x0)
[R,tp]=AxelRot(0.45,[0,1,0],[0,0,0]);
boomsa=bsxfun(@plus,boomi*R',tp') ;
x=boomsa(:,1);
y=boomsa(:,2);
z=boomsa(:,3);
figa = figure;
colormap gray;
    % flips color bar order
    colormap(flipud(colormap));
    hold on;
    grid on;
    scatter3(x,z,y,10, t, 'filled') ;


    set(gca, 'FontSize',8);
    %perform linear interpolation on trajectory to draw fitted line
        [tint xint] = inter(t,x,0.1) ;
        [tint yint] = inter(t,y,0.1) ;
        [tint zint] = inter(t,z,0.1) ;
        if i < 5000 color_line3(xint,zint,yint,tint);  end
        view(3);
        cbar_handle=colorbar ;
        set(cbar_handle,'FontSize',8);
        set(get(cbar_handle,'ylabel'),'string','Time (ms)','FontSize',8);
   [str] = sprintf('X, Y, Z locations over time - Pass %d, Locations %d', A,
locations);
   % title(str,'FontSize',20););
        xlabel('X location (mm)','FontSize',8);
```

```
        ylabel('Z location (mm)','FontSize',8);
        zlabel('Y location (mm)','FontSize',8);
   %offses the ylabels
   %set(gca,'YTickLabel',{'120';'140  '});


   argh=(44.5-4.7)/2;
boom=44.5;
X1=[22.25 22.25 40];
X2=[22.25 22.25 291];
r1=4.7/2;
r2=44/2;
r=[r1 r2];
ra=[r2 r2];
X1a=[22.25 22.25 377];
X2a=[22.25 22.25 291];

X1b=[22.25 22.25 40];
X2b=[22.25 22.25 0];
rb= [r1 r1];

n=20;
%cyl_color=[0.545,0,0];
cyl_color=[0.5,0.5,0.5];
closed=1;

lines=0;

[Cylinder EndPlate1 EndPlate2] = cone(X1a,X2a,ra,n,cyl_color,closed,lines)
[Cylinder EndPlate1 EndPlate2] = cone(X1,X2,r,n,cyl_color,closed,lines)
[Cylinder EndPlate1 EndPlate2] = cone(X1b,X2b,rb,n,cyl_color,closed,lines)


   axis equal ;
   xlim([0 50]);
   [str] = sprintf('figa%d', A);
print(figa, '-dpng', '-r500', str);
close(figa);

figcd = figure;
colormap gray;
    % flips color bar order
    colormap(flipud(colormap));
    hold on;
    grid on;
    scatter3(x,z,y,10, t, 'filled') ;


    set(gca, 'FontSize',8);
    %perform linear interpolation on trajectory to draw fitted line
        [tint xint] = inter(t,x,0.1) ;
        [tint yint] = inter(t,y,0.1) ;
        [tint zint] = inter(t,z,0.1) ;
        if i < 5000 color_line3(xint,zint,yint,tint);  end
        view(3);
```

```
        cbar_handle=colorbar ;
        set(cbar_handle,'FontSize',8);
        set(get(cbar_handle,'ylabel'),'string','Time (ms)','FontSize',8);
   [str] = sprintf('X, Y, Z locations over time - Pass %d, Locations %d', A,
locations);
   % title(str,'FontSize',20););
        xlabel('X location (mm)','FontSize',8);
        ylabel('Z location (mm)','FontSize',8);
        zlabel('Y location (mm)','FontSize',8);
   %offses the ylabels
   %set(gca,'YTickLabel',{'120';'140  '});


   argh=(44.5-4.7)/2;
boom=44.5;
X1=[22.25 22.25 40];
X2=[22.25 22.25 291];
r1=4.7/2;
r2=44/2;
r=[r1 r2];
ra=[r2 r2];
X1a=[22.25 22.25 377];
X2a=[22.25 22.25 291];

X1b=[22.25 22.25 40];
X2b=[22.25 22.25 0];
rb= [r1 r1];

n=20;
cyl_color=[0.5,0.5,0.5];
closed=1;

lines=0;

[Cylinder EndPlate1 EndPlate2] = cone(X1a,X2a,ra,n,cyl_color,closed,lines)
[Cylinder EndPlate1 EndPlate2] = cone(X1,X2,r,n,cyl_color,closed,lines)
[Cylinder EndPlate1 EndPlate2] = cone(X1b,X2b,rb,n,cyl_color,closed,lines)


   axis equal ;
 zlim([60 200])
   [str] = sprintf('figcd%d', A);
print(figcd, '-dpng', '-r500', str);
close(figcd);




figb = figure;
colormap gray;
x = t;
left = y;

posBig = [0.1 0.1 0.8 0.8];
```

```
posSmall = [0.64 0.60 0.18 0.24];

%# create axes (big/small)
hAxB = axes('Position',posBig);
hAxS = axes('Position',posSmall);

%# plot

scatter(hAxB, x, y, 'k');
           set(hAxB, 'FontSize',8);

xlims=170;
xlimb=280;

ylims=60;
ylimb=200;

pass(:,1)=times;
%pass 1 is time
pass(pass(:,1)>=xlimb,:) = [] ;
pass(pass(:,3)<ylims,:) = [] ;
%pass 3 is y position
%pass(pass(:,3)<ylims,:) = [] ;

t=pass(:,1);
y=pass(:,3);

[ymax,imax,ymin,imin] = extrema(y);

lol=t(imax);
lmao=ymax;


t1={''};
t2 = cellstr(num2str(lmao(:),'(%3.f)'));
str = strcat(t1, t2);


plot(hAxB,t,y,t(imax),ymax,'k.', 'MarkerSize', 5);
          set(hAxB, 'FontSize',8);

text(lol,lmao+6,str, 'FontSize',
8,'BackgroundColor',[1,1,1],'Margin',1,'HorizontalAlignment','center','Vertic
alAlignment','Baseline','Parent', hAxB);
text(lol,lmao,'\downarrow','Color','k','fontsize',8,'HorizontalAlignment','ce
nter','VerticalAlignment','Baseline', 'Parent', hAxB);

plot(hAxS, x, left, 'k');
 set(hAxS, 'FontSize',8);
            ylim([0 400]);
%# set axes properties

set(hAxB, 'XLim',[xlims xlimb], 'YLim',[ylims ylimb]);
```

```
set(hAxS , 'Color','none', 'XAxisLocation','top',
'YAxisLocation','right','XLim',[0 500]);

xlabel(hAxB,'Time (ms)','FontSize',8);
ylabel(hAxB,'Y location (mm)','FontSize',8);

c=440;
%c=53
d=0;

hold on;

plot([c+0 c+44],[d+334 d+334],'k-');
line([c+44 c+44],[d+334 d+377],'color',[0,0,0]);
line([c+0 c+0],[d+334 d+377],'color',[0,0,0]);
plot([c+0 c+44],[d+377 d+377],'k-');
line([c+44 c+44],[d+334 d+370.5],'color',[0,0,0]);
line([c+0 c+0],[d+334 d+370.5],'color',[0,0,0]);
plot([c+0 c+(-53)],[d+370.5 d+370.5],'k-');
line([c+44 c+44],[d+291 d+334],'color',[0,0,0]);
line([c+0 c+0],[d+291 d+334],'color',[0,0,0]);
plot([c+0 c+44],[d+291 d+291],'k-');
plot([c+0 c+(-53)],[d+337.5 d+337.5],'k-');
line([c+(-53) c+(-53)],[d+337.5 d+370.5],'color',[0,0,0]);
plot([c+5.5 c+38.5],[d+377 d+377],'k-');
line([c+25.15 c+44],[d+40 d+291],'color',[0,0,0]);
line([c+0 c+18.85],[d+291 d+40],'color',[0,0,0]);
plot([c+18.85 c+25.15],[d+0 d+0],'k-')
plot([c+18.85 c+25.15],[d+40 d+40],'k-')
line([c+18.85 c+18.85],[d+0 d+40],'color',[0,0,0]);
line([c+25.15 c+25.15],[d+0 d+40],'color',[0,0,0]);

plot([xlims xlimb],[ylims ylims],'k-');
plot([xlims xlimb],[ylimb ylimb],'k-');
line([xlims xlims],[ylims ylimb],'color',[0,0,0]);
line([xlimb xlimb],[ylims ylimb],'color',[0,0,0]);


[str] = sprintf('figb%d', A);
print(figb, '-dpng', '-r500', str);
close(figb);


end


   %y
   %y
  %y
  %y
    a1=124;
    %x
```

```
a2=272+50-9+14-20-5-5+5;
%z
a3=182+30-11+20+5-5;

for A=1:25;

    filename = (['outputa_', num2str(A)]);
    %loads filename
    refinedpass=xlsread(filename);
    %converts structure array to cell array
    %converts cell array to mat array
    pass = refinedpass;

    locations=length(pass);
    %to reset time to start at 0
   % pass(pass(:,3)<a3,:) = [] ;
    times=pass(:,1)-pass(1,1);

    t=times;




    %to fix the offset in the y direction
 for a=1:length(pass)
     %y
    pass(a,3)=(pass(a,3)-a1);
    %x
    pass(a,2)=(pass(a,2)-a2);
    %z
    pass(a,4)=(pass(a,4)-a3);
 end


x=pass(:,2);
y=pass(:,3);
z=pass(:,4);

j=1;
     for j=1:length(t)
            ts(j,A) = t(j) ;
            xs(j,A) = x(j) ;
            ys(j,A) = y(j) ;
            zs(j,A) = z(j) ;
     end

     fig4=figure('DefaultAxesColorOrder',[0 0 0], ...
'DefaultAxesLineStyleOrder','.|x|+|d|o|s|d|v|^|<|>|p|h')
     colormap gray;
plot3(xs,zs,ys);
           set(gca, 'FontSize',8);

xlabel('X location (mm)','FontSize',8);
ylabel('Z location (mm)','FontSize',8);
```

```
zlabel('Y location (mm)','FontSize',8);

axis equal ;
   zlim([0 400]);
   xlim([0 50]);
[str] = sprintf('fig4%d', A);




argh=(44-4.7)/2;
boom=44;
X1=[22 22 40];
X2=[22 22 291];
r1=4.7/2;
r2=44/2;
r=[r1 r2];
ra=[r2 r2];
X1a=[22 22 377];
X2a=[22 22 291];

X1b=[22 22 40];
X2b=[22 22 0];
rb= [r1 r1];

n=20;
%cyl_color=[0.545,0,0];
cyl_color=[0.5,0.5,0.5];
closed=1;

lines=0;

[Cylinder EndPlate1 EndPlate2] = cone(X1a,X2a,ra,n,cyl_color,closed,lines)
[Cylinder EndPlate1 EndPlate2] = cone(X1,X2,r,n,cyl_color,closed,lines)
[Cylinder EndPlate1 EndPlate2] = cone(X1b,X2b,rb,n,cyl_color,closed,lines)




print(fig4, '-dpng', '-r500', str);
close(fig4);

end




for A=1:25;

    filename = (['outputa_', num2str(A)]);
    %loads filename
    refinedpass=xlsread(filename);
```

```
    %converts structure array to cell array
    %converts cell array to mat array
    pass = refinedpass;

    locations=length(pass);
    %to reset time to start at 0
   % pass(pass(:,3)<a3,:) = [] ;
    times=pass(:,1)-pass(1,1);

    t=times;




    %to fix the offset in the y direction
 for a=1:length(pass)
     %y
    pass(a,3)=(pass(a,3)-a1);
    %x
    pass(a,2)=(pass(a,2)-a2);
    %z
    pass(a,4)=(pass(a,4)-a3);
 end


x=pass(:,2);
y=pass(:,3);
z=pass(:,4);

j=1;
     for j=1:length(t)
            ts(j,A) = t(j) ;
            xs(j,A) = x(j) ;
            ys(j,A) = y(j) ;
            zs(j,A) = z(j) ;
     end

fig4b=figure ('DefaultAxesColorOrder',[0 0 0], ...
'DefaultAxesLineStyleOrder','.|x|+|d|o|s|d|v|^|<|>|p|h')
colormap gray;

subplot(3,1,1); plot(ts,xs);
           set(gca, 'FontSize',8);
hold on
title('X location','FontSize',8)
xlabel('Time (ms)','FontSize',8);
ylabel('Position (mm)','FontSize',8);
grid on;
subplot(3,1,2); plot(ts,ys);
           set(gca, 'FontSize',8);
title('Y location','FontSize',8)
xlabel('Time (ms)','FontSize',8);
ylabel('Position (mm)','FontSize',8);
grid on;
subplot(3,1,3); plot(ts,zs);
```

```
            set(gca, 'FontSize',8);
hold on;
title('Z location','FontSize',8)
xlabel('Time (ms)','FontSize',8);
ylabel('Position (mm)','FontSize',8);
axis equal ;
[str] = sprintf('fig4b%d', A);
print(fig4b, '-dpng', '-r500', str);
close(fig4b);

end


i=1;

for A=1:25;

    filename = (['outputa_', num2str(A)]);
    %loads filename
    refinedpass=xlsread(filename);
    %converts structure array to cell array
    %converts cell array to mat array
    pass = refinedpass;

    locations=length(pass);
    %to reset time to start at 0
   % pass(pass(:,3)<a3,:) = [] ;
    times=pass(:,1)-pass(1,1);

    t=times;




    %to fix the offset in the y direction
 for a=1:length(pass)
     %y
    pass(a,3)=(pass(a,3)-a1);
    %x
    pass(a,2)=(pass(a,2)-a2);
    %z
    pass(a,4)=(pass(a,4)-a3);
 end


X=pass(:,2);
Y=pass(:,3);
Z=pass(:,4);
 tend = 9e9;


for i=11:length(t)-5
    if(t(i)>tend) break; end;
    if(t(i)<1) continue; end;
```

```
%calc 6-point velocities for each location

        velx(i)    =       0.1  * (( X(i+5) - X(i  )) / ( t(i+5) - t(i  )) )
+ ...
                        0.15 * (( X(i+4) - X(i-1)) / ( t(i+4) - t(i-1)) ) +
...
                        0.25 * (( X(i+3) - X(i-2)) / ( t(i+3) - t(i-2)) ) +
...
                        0.25 * (( X(i+2) - X(i-3)) / ( t(i+2) - t(i-3)) ) +
...
                        0.15 * (( X(i+1) - X(i-4)) / ( t(i+1) - t(i-4)) ) +
...
                        0.1  * (( X(i  ) - X(i-5)) / ( t(i  ) - t(i-5)) ) ;


        vely(i)    =       0.1  * (( Y(i+5) - Y(i  )) / ( t(i+5) - t(i  )) )
+ ...
                        0.15 * (( Y(i+4) - Y(i-1)) / ( t(i+4) - t(i-1)) ) +
...
                        0.25 * (( Y(i+3) - Y(i-2)) / ( t(i+3) - t(i-2)) ) +
...
                        0.25 * (( Y(i+2) - Y(i-3)) / ( t(i+2) - t(i-3)) ) +
...
                        0.15 * (( Y(i+1) - Y(i-4)) / ( t(i+1) - t(i-4)) ) +
...
                        0.1  * (( Y(i  ) - Y(i-5)) / ( t(i  ) - t(i-5)) ) ;


        velz(i)     =      0.1  * (( Z(i+5) - Z(i  )) / ( t(i+5) - t(i  )) )
+ ...
                        0.15 * (( Z(i+4) - Z(i-1)) / ( t(i+4) - t(i-1)) ) +
...
                        0.25 * (( Z(i+3) - Z(i-2)) / ( t(i+3) - t(i-2)) ) +
...
                        0.25 * (( Z(i+2) - Z(i-3)) / ( t(i+2) - t(i-3)) ) +
...
                        0.15 * (( Z(i+1) - Z(i-4)) / ( t(i+1) - t(i-4)) ) +
...
                        0.1  * (( Z(i  ) - Z(i-5)) / ( t(i  ) - t(i-5)) ) ;


        speed(i) = sqrt( (velx(i)*velx(i)) + (vely(i)*vely(i)) +
(velz(i)*velz(i))) ;

end
[str] = sprintf('fig015a%d', A);

fig015a = figure;
colormap gray;
[H,B]=hist(velx,50);
bar(B,100.*H./sum(H),1)
title('X (horizontal) velocities');
xlabel('Velocity, m/s');
```

```
ylabel('%');

print(fig015a, '-dpng', '-r500', str);
close(fig015a);
[str] = sprintf('fig015b%d', A);

fig015b = figure;
colormap gray;
[H,B]=hist(vely,50);
bar(B,100.*H./sum(H),1)
title('Y (horizontal) velocities');
xlabel('Velocity, m/s');
ylabel('%');
print(fig015b, '-dpng', '-r500', str);
close(fig015b);
[str] = sprintf('fig015c%d', A);

fig015c = figure;
colormap gray;
[H,B]=hist(velz,50);
bar(B,100.*H./sum(H),1)
title('Z (vertical) velocities');
xlabel('Velocity, m/s');
ylabel('%');
print(fig015c, '-dpng', '-r500', str);
close(fig015c);
[str] = sprintf('fig015d%d', A);
fig015d = figure;
colormap gray;
[H,B]=hist(speed,50);
bar(B,100.*H./sum(H),1);
title('Speed');
xlabel('Speed, m/s');
ylabel('%');
print(fig015d, '-dpng', '-r500', str);
close(fig015d);

end
```

References

Abrahamson, J., Allen, R.W.K., The efficiency of conventional return flow cyclones at high temperatures. AIChE Symposium Series, 1986, **99**, 31-43.

Alexander, R.M., 1949. Fundamentals of cyclone design and operations, In *The Australasian Institute of Mining and Metallurgy Proceedings*. The Australasian Institute of Mining and Metallurgy, pp. 203-228.

Anderson, H., Price, P., What does positron emission tomography offer oncology? European Journal of Cancer, 2000, **36(16)**, 2028-2035.

ASTM Standard, 2009. Standard Guide for X-Ray Compton Scatter Tomography, In *Nondestructive Testing Standards*. ASTM International, West Conshohocken, PA.

Ba, Z.S., Wang, H.L., Numerical Simulation of the Separating Performance of Hydrocyclones. Chemical Engineering & Technology, 2006, **29(10)**, 1161-1166.

Barigou, M., Particle Tracking in Opaque Mixing Systems: An Overview of the Capabilities of PET and PEPT. Chemical Engineering Research and Design, 2004, **82(9)**, 1258-1267.

Bbosa, L.S., Govender, I., Mainza, A.N., Powell, M.S., Power draw estimations in experimental tumbling mills using PEPT. Minerals Engineering, 2011, **24(3–4)**, 319-324.

Bemrose, C.R., Fowles, P., Hawkesworth, M.R., O'Dwyer, M.A., Application of positron emission tomography to particulate flow measurement in chemical engineering processes. Nuclear Instruments and Methods in Physics Research Section A: Accelerators, Spectrometers, Detectors and Associated Equipment, 1988, **273(2-3)**, 874-880.

Bergström, J., Vomhoff, H., Experimental hydrocyclone flow field studies. Separation and Purification Technology, 2007, **53(1)**, 8-20.

Bergström, J., Vomhoff, H., Söderberg, D., Tangential velocity measurements in a conical hydrocyclone operated with a fibre suspension. Minerals Engineering, 2007, **20(4)**, 407-413.

Bradley, D., *The Hydrocyclone*. 1965, Pergamon Press, Oxford, England.

Bradley, D., Pulling, D.J., Flow patterns in the hydraulic cyclone and their interpretation in terms of performance. Transactions of the Institution of Chemical Engineers, 1959, **37**, 34-45.

Bretney, E., 1891. Water purifier, United States of America.

Brookhaven National Laboratory, 2005. National Nuclear Data Center, p. **http://www.nndc.bnl.gov/**.

Chan, C.W., Seville, J.P.K., Fan, X., Baeyens, J., Particle motion in CFB cyclones as observed by positron emission particle tracking. Industrial & Engineering Chemistry Research, 2009, **48**, 253-261.

Chandrasekhar, S., Raghavan, P., 2004. A Novel Approach to Correlate Brightness of Kaolin with the Iron and Titanium Contents, In *Mineral Processing Technology*, eds. Rao, G.V., Misra, V.N. Allied Publishers Pvt. Ltd., Bhubaneswar, India.

Chang, Y.-F., Ilea, C.G., Aasen, Ø.L., Hoffmann, A.C., Particle flow in hydrocyclone investigated by positron emission particle tracking. Chemical Engineering Science, 2011, **66(18)**, 4203-4211.

Chen, W., Zydek, N., Parma, F., Evaluation of hydrocyclone models for practical applications. Chemical Engineering Journal, 2000, **80(1-3)**, 295-303.

Chiang, S.-H., He, D., Feng, Y., 2003. Liquid-Solids Separation, In *Handbook of Fluidization and Fluid-Particle Systems*. Marcel Dekker Inc., New York City, New York, pp. 811-850.

Chu, K.W., Wang, B., Yu, A.B., Vince, A., CFD-DEM modelling of multiphase flow in dense medium cyclones. Powder Technology, 2009, **193(3)**, 235-247.

Coelho, M.A.Z., Medronho, R.A., 1992. An Evaluation of the Plitt and Lynch & Rao Models for the Hydrocyclones, In *Hydrocyclones*, eds. Svarovsky, L., Thew, M.T. Springer Netherlands, pp. 63-72.

Cole, K.E., Buffler, A., van der Meulen, N.P., Cilliers, J.J., Franzidis, J.P., Govender, I., Liu, C., van Heerden, M.R., Positron emission particle tracking measurements with 50 micron tracers. Chemical Engineering Science, 2012, **75(0)**, 235-242.

Cole, K.E., Waters, K.E., Fan, X., Neethling, S.J., Cilliers, J.J., Combining Positron Emission Particle Tracking and image analysis to interpret particle motion in froths. Minerals Engineering, 2010, **23(11–13)**, 1036-1044.
Concha, F., Flow patterns in hydrocyclones. KONA, 2007, **25**, 97-132.
Dabir, B., Petty, C.A., 1984a. Laser Doppler anemometry measurements of tangential and axial velocities in a hydrocyclone operating without an air core, In *2nd International Conference on Hydrocyclones*, Bath, England, pp. 15-26.
Dabir, B., Petty, C.A., 1984b. Laser doppler anemometry measurements of tangential and axial velocities in a hydrocyclone operating without an air core, In *2nd International Conference on Hydrocyclones*, Bath, England.
Dabir, B., Petty, C.A., Measurements of mean velocity profiles in a hydrocyclone using laser doppler anemometry. Chemical Engineering Communications, 1986, **48(4-6)**, 377-388.
Dickin, F.J., Williams, R.A., Beck, M.S., Determination of composition and motion of multicomponent mixtures in process vessels using electrical impedance tomography-I. Principles and process engineering applications. Chemical Engineering Science, 1993, **48(10)**, 1883-1897.
Fan, X., Parker, D.J., Smith, M.D., Enhancing 18F uptake in a single particle for positron emission particle tracking through modification of solid surface chemistry. Nuclear Instruments and Methods in Physics Research A, 2006a, **558**, 542-546.
Fan, X., Parker, D.J., Smith, M.D., Labelling a single particle for positron emission particle tracking using direct activation and ion-exchange techniques. Nuclear Instruments and Methods in Physics Research A, 2006b, **562**, 345-350.
Fan, X., Waters, K.E., Rowson, N.A., Parker, D.J., Modification of ilmenite surface chemistry for enhancing surfactants adsorption and bubble attachment. Journal of Colloid and Interface Science, 2009, **329(1)**, 167-172.
Fanglu, G., Wenzhen, L., 1987. Measurement and study of velocity field in various cyclones by use of laser doppler anemometry, In *3rd International Conference on Hydrocylones*, ed. Wood, P. Elsevier Applied Science, Oxford, England.
Fisher, M.J., Flack, R.D., Velocity distributions in a hydrocyclone separator. Experiments in Fluids, 2002, **32**, 302-312.
Galvin, K.P., Smitham, J.B., Use of X-rays to determine the distribution of particles in an operating cyclone. Minerals Engineering, 1994, **7(10)**, 1269-1280.
Gutiérrez, J.A., Dyakowski, T., Beck, M.S., Williams, R.A., Using electrical impedance tomography for controlling hydrocyclone underflow discharge. Powder Technology, 2000, **108(2–3)**, 180-184.
Hawkesworth, M.R., O'Dwyer, M.A., Walker, J., A positron camera for industrial application. Nuclear Instruments and Methods in Physics Research A, 1986, **253**, 145-157.
Hoffmann, A.C., Stein, L.E., *Gas Cyclones and Swirl Tubes*. 2nd edn. 2008, Springer.
Holdich, R.G., *Fundamentals of Particle Technology* 2002, Midland Information Technology and Publishing, Shepshed, England.
Hsieh, K.T., Rajamani, K., Phenomenological model of the hydrocyclone: Model development and verification for single-phase flow. International Journal of Mineral Processing, 1988a, **22(1-4)**, 223–237.
Hsieh, K.T., Rajamani, K., Phenomenological model of the hydrocyclone: Model development and verification for single-phase flow. International Journal of Mineral Processing, 1988b, **22(1–4)**, 223-237.
Hwang, K.-J., Wu, W.-H., Qian, S., Nagase, Y., CFD Study on the Effect of Hydrocyclone Structure on the Separation Efficiency of Fine Particles. Separation Science and Technology, 2008, **43(15)**, 3777-3797.
Jiang, M., Zhao, L., He, J., Pressure Drop Ratio — An Important Performance Parameter in Liquid-Liquid Hydrocyclone Separation. Proceedings of the Eighth International Offshore and Polar Engineering Conference, 1998, **2**.
Jirun, X., Qian, L., Jicun, Q., Studying the flow field in a hydrocyclone with no forced vortex: Part I: average velocity. Filtration & Separation, 1990, **27(4)**, 276-278.

Kelsall, D.F., A study of the motion of solid particles in a hydraulic cyclone. Transactions of the Institution of Chemical Engineers, 1952, **30**, 87-108.
Knowles, S.R., Woods, D.R., Feuerstein, I.A., The velocity distribution within a hydrocyclone operating without an air core. The Canadian Journal of Chemical Engineering, 1973, **51**, 263-271.
Kraipech, W., Chen, W., Dyakowski, T., Nowakowski, A., The performance of the empirical models on industrial hydrocyclone design. International Journal of Mineral Processing, 2006, **80(2-4)**, 100-115.
Leadbeater, T.W., Parker, D.J., A high speed PC-based data acquisition and control system for positron imaging. Nuclear Instruments and Methods in Physics Research Section A: Accelerators, Spectrometers, Detectors and Associated Equipment, 2009, **604(1–2)**, 355-358.
Leadbeater, T.W., Parker, D.J., Gargiuli, J., Positron imaging systems for studying particulate, granular and multiphase flows. Particuology, 2012, **10(2)**, 146-153.
Lim, E.W.C., Chen, Y.-R., Wang, C.-H., Wu, R.-M., Experimental and computational studies of multiphase hydrodynamics in a hydrocyclone separator system. Chemical Engineering Science, 2010a, **65**, 6415–6424.
Lim, E.W.C., Chen, Y.-R., Wang, C.-H., Wu, R.-M., Experimental and computational studies of multiphase hydrodynamics in a hydrocyclone separator system. Chemical Engineering Science, 2010b, **65(24)**, 6415-6424.
Lynch, A.J., Rowland, C.A., *The History of Grinding*. 2005, Society for Mining, Metallurgy and Exploration Inc., Littleton, Colorado.
Marigo, M., Davies, M., Leadbeater, T., Cairns, D.L., Ingram, A., Stitt, E.H., Application of Positron Emission Particle Tracking (PEPT) to validate a Discrete Element Method (DEM) model of granular flow and mixing in the Turbula mixer. International Journal of Pharmaceutics, 2013, **446(1–2)**, 46-58.
Marins, L.P.M., Duarte, D.G., Loureiro, J.B.R., Moraes, C.A.C., Silva Freire, A.P., LDA and PIV characterization of the flow in a hydrocyclone without an air-core. Journal of Petroleum Science and Engineering, 2010, **70**, 168–176.
Mavros, P., Flow Visualization in Stirred Vessels: A Review of Experimental Techniques. Chemical Engineering Research and Design, 2001, **79(2)**, 113-127.
Miller, J.D., Das, A., Lelinski, D., Chamblee, J.W., 1993. Multiphase flow characteristics of gas sparged hydrocyclone flotation deinking, In *TAPPI Engineering Conference*. Technical Association of the Pulp and Paper Industry, Orlando, Florida, pp. 417-428.
Monredon, T.C., Hsieh, K.T., Rajamani, R.K., Fluid flow model of the hydrocyclone: an investigation of device dimensions. International Journal of Mineral Processing, 1992, **35(1–2)**, 65-83.
Napier-Munn, T.J., Morrell, S., Morrison, R.D., Kojovic, T., *Mineral Comminution Circuits: Their Operation and Optimisation*. 1996, Julius Kruttschnitt Mineral Research Centre, Brisbane, Australia.
Ortega-Rivas, E., *Hydrocyclones*. 2000, Wiley.
Parker, D.J., Allen, D.A., Benton, D.M., Fowles, P., McNeil, P.A., Tan, M., Beynon, T.D., Developments in particle tracking using the Birmingham Positron Camera. Nuclear Instruments and Methods in Physics Research Section A: Accelerators, Spectrometers, Detectors and Associated Equipment, 1997, **392(1–3)**, 421-426.
Parker, D.J., Broadbent, C.J., Fowles, P., Hawkesworth, M.R., McNeil, P., Positron emission particle tracking - a technique for studying flow within engineering equipement. Nuclear Instruments and Methods in Physics Research Section A: Accelerators, Spectrometers, Detectors and Associated Equipement, 1993, **326**, 592-607.
Parker, D.J., Forster, R.N., Fowles, P., Takhar, P.S., Positron emission particle tracking using the new Birmingham positron camera. Nuclear Instruments and Methods in Physics Research A, 2002, **477**, 540-545.
Parker, D.J., Hawkesworth, M.R., Broadbent, C.J., Fowles, P., Fryer, T.D., McNeil, P.A., Industrial positron-based imaging: Principles and applications. Nuclear Instruments and Methods in Physics Research Section A: Accelerators, Spectrometers, Detectors and Associated Equipment, 1994, **348(2-3)**, 583-592.
Phelps, M.E., *PET : molecular imaging and its biological applications*. 2004, Springer, New York.

Plitt, L.R., A mathematical model of the hydrocyclone. CIM Bulletin, 1976, **69(776)**, 114-123.
Qian, F., Zhang, M., Study of the natural vortex length of a cyclone with response surface methodology. Computers & Chemical Engineering, 2005, **29(10)**, 2155-2162.
Rajamani, R.K., Milin, L., 1992. Fluid flow model of a hydrocyclone for concentrated slurry classification, In *Hydrocyclones. Analysis and Applications. Series in Fluid Mechanics and its Applications*, eds. Svarovsky, L., Thew, M.T. Kluwer, London, pp. 95-108.
Richard Mozley Ltd, 1989. Mozley Two Inch Hydrocyclones.
Romero, J., Sampaio, R., Gama, R.S.d., Numerical simulation of flow in a hydrocyclone. Latin American Applied Research, 2004, **34(1)**.
Sadrmomtaz, A., Parker, D.J., Byars, L.G., Modification of a medical PET scanner for PEPT studies. Nuclear Instruments and Methods in Physics Research Section A: Accelerators, Spectrometers, Detectors and Associated Equipment, 2007, **573(1-2)**, 91-94.
Schlaberg, H.I., Podd, F.J.W., Hoyle, B.S., Ultrasound process tomography system for hydrocyclones. Ultrasonics, 2000, **38(1–8)**, 813-816.
Schubert, H., Which demands should and can meet a separation model for hydrocyclone classification? International Journal of Mineral Processing, 2010, **96(1–4)**, 14-26.
Serway, R.A., Beichner, R.J., *Physics for Scientists and Engineers*. 5th edn. 1999, Brooks/Cole Publishing Company.
Seville, J.P.K., Ingram, A., Fan, X., Parker, D.J., Jinghai, L., 2009. Chapter 4: Positron Emission Imaging in Chemical Engineering, In *Advances in Chemical Engineering*. Academic Press, pp. 149-178.
Silva, C.L.Q., Penna, W., Araújo, A.C.B., Brito, R.P., Vasconcelos, L.G.S., Alves, J.J.N., Model fine tuning for prediction of hydrocyclone performance - An industrial case study. International Journal of Mineral Processing, 2009, **92**, 34-41.
Spelter, L.E., Nirschl, H., Classification of Fine Particles in High-Speed Centrifuges. Chemical Engineering & Technology, 2010, **33(8)**, 1276-1282.
Stairmand, C.J., The design and performance of cyclones. Transactions of the Institution of Chemical Engineering, 1951, **29**, 357-383.
Stewart, R.L., Bridgwater, J., Parker, D.J., Granular flow over a flat-bladed stirrer. Chemical Engineering Science, 2001, **56(14)**, 4257-4271.
Svarovsky, J., 1992. A new method of testing hydrocyclone grade efficiencies, In *Hydrocyclones. Analysis and Applications. Series in Fluid Mechanics and its Applications*, eds. Svarovsky, L., Thew, M.T. Kluwer, London, pp. 135-145.
Svarovsky, L., *Solid-Liquid Separation*. 4th edn. 2001, Butterworth-Heinemann.
Ter-Pogossian, M.M., The origins of positron emission tomography. Seminars in Nuclear Medicine, 1992, **22(3)**, 140-149.
Trawinski, H.F., 1984. About the practice of hydrocyclone operation, In *2nd International Conference on Hydrocyclones*, Bath, England.
Van de Velden, M., Baeyens, J., Seville, J.P.K., Fan, X., The solids flow in the riser of a Circulating Fluidised Bed (CFB) viewed by Positron Emission Particle Tracking (PEPT). Powder Technology, 2008, **183(2)**, 290-296.
van Esch, F., The Efficiency of Hydrocyclones for the Separation of Different Starches. Starch - Stärke, 1991, **43(11)**, 427-431.
Volkwyn, T.S., Buffler, A., Govender, I., Franzidis, J.P., Morrison, A.J., Odo, A., van der Meulen, N.P., Vermeulen, C., Studies of the effect of tracer activity on time-averaged positron emission particle tracking measurements on tumbling mills at PEPT Cape Town. Minerals Engineering, 2011, **24(3–4)**, 261-266.
Wang, B., Zhang, J., He, Y., An, S., Investigation on Eccentric Agitation in the Stirred Vessel Using 3D-Laser Doppler Velocimeter. Chinese Journal of Chemical Engineering, 2006, **14(5)**, 618-625.
Waters, K., Langlois, R., Leadbeater, T., 2012. Using positron emission particle tracking to understand spiral concentrators, In *9th International Mineral Processing Conference – Procemin 2012*, eds. Doll, A., Kracht, W., Kuyvenhoven, R. Gecamin, Santiago, Chile.

Waters, K., Rowson, N.A., Fan, X., Parker, D.J., Cilliers, J.J., Positron emission particle tracking as a method to map the movement of particles in the pulp and froth phases. Minerals Engineering, 2008, **21**, 877-882.
Williams, R.A., Jia, X., West, R.M., Wang, M., Cullivan, J.C., Bond, J., Faulks, I., Dyakowski, T., Wang, S.J., Climpson, N., Kostuch, J.A., Payton, D., Industrial monitoring of hydrocyclone operation using electrical resistance tomography. Minerals Engineering, 1999, **12(10)**, 1245-1252.
Wills, B.A., Napier-Munn, T., *Wills' Mineral Processing Technology: An Introduction to the Practical Aspects of Ore Treatment and Mineral Recovery*. 2006, Elsevier Science & Technology Books, Oxford, England.
Zagorodni, A.A., *Ion Exchange Materials: Properties And Applications*. 2007, Elsevier Ltd.